DEVELOPMENT OF AN OPTIMAL IMPACT ENERGY ABSORBER FOR HIGHWAY CRASH CUSHIONS

A Thesis

by

CHRISTOPHER RYAN MICHALEC

Submitted to the Office of Graduate Studies of
Texas A&M University
in partial fulfillment of the requirements for the degree of

MASTER OF SCIENCE

August 2005

Major Subject: Mechanical Engineering

DEVELOPMENT OF AN OPTIMAL IMPACT ENERGY ABSORBER FOR HIGHWAY CRASH CUSHIONS

A Thesis

by

CHRISTOPHER RYAN MICHALEC

Submitted to the Office of Graduate Studies of
Texas A&M University
in partial fulfillment of the requirements for the degree of

MASTER OF SCIENCE

Approved by:

Chair of Committee,	Steve Suh
Committee Members,	Harry Hogan
	Lynn Beason
Head of Department,	Dennis O'Neal

August 2005

Major Subject: Mechanical Engineering

ABSTRACT

Development of an Optimal Impact Energy Absorber for
Highway Crash Cushions. (August 2005)
Christopher Ryan Michalec, B.S., Texas A&M University
Chair of Advisory Committee: Dr. Steve Suh

The objective of this research is to develop a new and efficient method of absorbing a vehicle's kinetic energy for highway safety crash cushions. A vehicle that makes a direct impact with a rigid highway structure traveling at highway speeds can be fatal for its occupants. Crash cushions are implemented on roadways in front of these rigid structures with the intent to "soften" the impact. The cushion will bring a vehicle to a stop at safe rates before it impacts the rigid structure. The energy absorbing component of the crash cushion must meet four main requirements. The cushion must reduce the vehicles speed at a rate that does not allow the occupant to impact the vehicle interior at velocities greater than 12 m/s. The cushion must then bring the vehicle to a complete stop with deceleration rates below 20 g's. A crash cushion must satisfy these requirements for an 820 kg vehicle and a 2000 kg vehicle traveling at 100 km/hr.

Advanced design methodologies were applied to enable multiple, innovative design concepts. These concepts made use of the deformation of steel in structural pipe, structural angle, and structural plate to reduce the velocity of a vehicle at a safe rate. Critical design parameters were identified which allowed for efficient and effective numerical experiments to be conducted. The data collected from these experiments were then validated when compared to physical test data. After the data had been collected, each of the designs was compared to one another in order to decide upon the best design. The design selected was the deforming plate concept which makes use of steel plate mounted in a fashion that created two arms that acted similar to two cantilever beams. A wedge was forced beneath these arms deforming them upward. This

design is effective because the deformation can be easily controlled by the thickness of the plate, the moment arm created by the wedge, and the geometry of the wedge. Steel plate is a readily available material that requires minimal manufacturing for installation preparation making it cost-effective, and easy to install. In the event of impact with the cushion, new parts will be inexpensive and readily available. Being reusable, easy to repair and low in cost, the energy absorbing concept presented herein is a cost effective alternative to existing energy absorbing technology. Due to replaceable parts being readily available, repair time and cost will be reduced compared to other designs that require new parts to be fabricated for replacement. This will make for a competitive design.

DEDICATION

I would like to dedicate this thesis to the late Otto Michalec who taught me that with a little creativity, one can have anything they want. Why buy it at the store if you can make your own. This lesson was made very clear to me when I was very young mowing his lawn with a lawnmower that had a muffler made from coffee cans, a seat made from an office chair, and several other custom additions. He could make anything out of virtually nothing and make it work just as well as if you were to have gone to the store to buy it. The summers that I spent in his shed inventing and tinkering with what most would call junk helped me discover my passion for creative design at an early age.

ACKNOWLEDGEMENTS

I would like to thank D. Lance Bullard and Dean Alberson for their support and inspiration. I have learned so much from working with them over the years at Texas Transportation Institute and Safety Quest. I have gained much valuable experience from the opportunities that they have made available to me. They have taught me so many lessons not just in engineering but life too. It was their influence that convinced me to make that extra push to pursue a master's degree.

I would also like to thank Dr. Suh, for telling me that I would never regret any efforts put into acquiring a master's degree. This has proven to be very true. There were many times when I would knock on his door asking for a minute knowing he was very busy. I was never turned away. He would always drop what he was doing to take as much time as needed to help me. His patience and support are greatly appreciated and not forgotten.

TABLE OF CONTENTS

Page

Page

Page

LIST OF FIGURES

FIGURE Page

FIGURE Page

FIGURE Page

FIGURE Page

FIGURE Page

FIGURE Page

FIGURE Page

LIST OF TABLES

CHAPTER I

INTRODUCTION

Background

General

Millions of vehicles make use of our roadways every single day. With usage of this magnitude, accidents are highly likely. Motor vehicle crashes are the leading cause of death for persons between 2 and 33 years old. In 2003 alone, 42,643 people were killed in an estimated 6,328,000 reported motor vehicle crashes in the United States, District of Columbia, and Puerto Rico combined (National Center for Statistics & Analysis 2004). It is estimated that more than 30% of the deaths result from single vehicle impacts with roadside structures (Ross 1995). These roadside structures vary from utility poles and mailboxes to trees and bridge supports. Many lives can be saved with the implementation of a device designed to absorb the energy of the vehicle and cushion its impact with these rigid structures. Figure 1 illustrates a crash cushion use for highway safety. The cushion is placed at the end of a concrete barrier with the intent to “soften” impact with the rigid structure.

Roadside Safety Engineering

In the 1960’s more attention was paid to the potential for roadside structures to cause occupant death upon impact from a vehicle. Even though a structure looked weak and forgiving, crash tests were able to prove otherwise.

This thesis follows the style of *Journal of Performance of Constructed Facilities,* ASCE.

Figure 1. Crash Cushion Installation

With the number of yearly fatalities increasing, it was clear that “forgiving” roadside structures needed to be developed to ensure the safety of the driving public. The design of highway structures needed to not only take the devices function into consideration but also take the safety of vehicle occupants into consideration. Roadside safety structures are evolving into safer designs as time goes on. Even though there are many designs currently in use that work well, more efficient and cost effective designs are still a must. This is where roadside safety engineering comes into play.

Crash Cushion Components

A crash cushion has several jobs to perform and separate components to aid in each job. A crash cushion must be able to redirect a vehicle upon a side impact. To do this, a wide variety of materials can be used to prevent the vehicle from penetrating the cushion. One example of this is seen in Figure 1 where the cushion makes use of steel thrie beam. In order to support the deflecting material, internal supports are used. In the event of a head on impact, these intermediate supports must not be fixed to allow for the vehicle to travel the length of the cushion.

The energy absorbing component can be installed anywhere within the cushion. For the focus of this research, the energy absorbing component will be mounted to the ground. Figure 2 illustrates a front sled that will be impacted by the vehicle. In order for the sled to advance along the cushions length, its base must be forced through the energy absorbing component. It is this component that will make use of steel that must be deformed by mandrels attached to the base of the sled in order to advance.

The figure illustrates a truck impacting the sled. The sled is then pushed along the length of the energy absorbing material. The vehicle is expected to have been brought to a complete stop before making contact with the rigid structure behind the cushion. The stop is also expected to have been made in a safe manner. The intermediate supports and side material have been left out of the illustration to clearly depict the components being used to absorb the vehicle's kinetic energy.

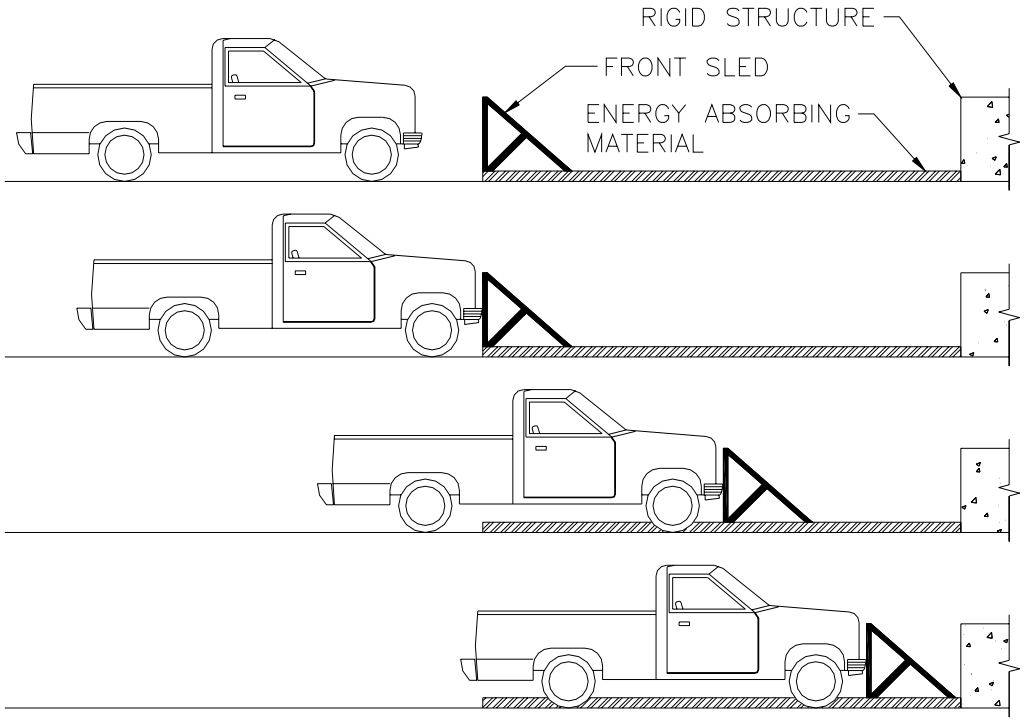

Figure 2. Crash Cushion Sled and Energy Absorbing Component Illustration

Need for Energy Absorbing Devices

There are many different safety devices designed to protect the occupants of vehicles traveling on the roadway. Slip bases are used to release a sign post from the ground by breaking away just above ground level allowing the vehicle to travel through the post causing minimal damage. Guardrails are designed to cushion and redirect an impacting vehicle preventing it from traveling into oncoming lanes of traffic or into unsafe terrain. Concrete barriers are used in construction zones to restrict the flow of traffic to the roadway and away from areas where construction is taking place. Although effective in safely redirecting vehicles in a side impact, when the end barrier of a group of connected barriers is impacted head on the barrier does not absorb energy, it holds its position in a rigid manner. This is an unsafe situation for motorists. Bridge supports are another structure considered very dangerous if left exposed. In the event that a vehicle impacts these rigid structures at high speeds there is a high possibility for serious injury or fatality of the vehicle occupants. Rigid structures on the highways are not an uncommon sight. These structures pose as a threat without a device to absorb the energy of an impacting vehicle at a safe rate before it contacts the structure. This creates a need for the design of effective crash cushions and other energy absorbing devices.

Previous Designs

There have been many different designs of crash cushions tested for highway use. Designs have utilized material from bails of hay to metal barrels as methods for absorbing the energy of a vehicle. Simple ideas are sometimes the best for an effective design. Currently in use is the Inertial System Crash Cushion which makes use of sand filled barrels that have various weights placed together in a group. Upon impact, the breaking of the barrels and displacement of the sand inside absorbs energy (Bullard 1995a). A Polyethylene Narrow Impact Attenuation design makes use of 9 polyethylene cylinders placed in a row. The impacting vehicle will crush these cylinders. Energy is absorbed by

the deformation of the cylinder walls (Alberson 1994). A similar design is the Narrow Connecticut Impact Attenuation System (NCIAS) which makes use of steel cylinders positioned in a row with two wire ropes on each side to hold them in place. The energy is absorbed by the deformation of the cylinders (Buth and Menges 1998). The Trinity Attenuating Crash Cushion (TRACC™) makes use of a steel frame which slides on guide tracks made from two c-channels. Various plates are sheared and torn by the front sled as it travels the length of the crash cushion (Menges and Alberson 2002). Designs currently in use make use of creative methods to absorb the energy of a vehicle traveling at highway speeds. Although effective, there is still room for improvement not just in performance but in cost, production time, installation time, and ease of installation. This is the reason for the variety of crash cushion designs in use today. There are still alternate methods and improvements to current crash cushion technology that can be made.

Steel Deforming Technology

Although the current crash cushions are effective in absorbing energy, issues may arise in the repair and replacement stages after an impact has occurred. Replacement of an entire system can be very costly so it is desired to replace only the part or parts that have been damaged on a system. Using steel pipe that is readily available will reduce the cost of having to manufacture a new energy absorbing component of the design. Most of the energy absorbing components in current designs require a part to be drilled, cut, and shaped in order to be prepared for installation into the crash cushion. The scope of this research focuses on steel pipe, plate, and angle that can be implemented into the crash cushion design in the same form that it is purchased. There are two forms of alterations that must be made on the energy absorbing material. The material must be formed into a shape which is desired to absorb the energy. The material must then have extra modifications made to mount it into a crash cushion. Just as the current designs require a way to mount the energy

absorbing component into the crash cushion, the deforming angle, deforming plate, and expanding tube will also need to be mounted into position. What makes this concept different from others is that although some work will be done to mount the material within the crash cushion; no extra work will be required to prepare it to absorb energy.

Through time, crash cushions have used various methods to absorb the kinetic energy of a vehicle. Previous methods have utilized the energy absorbing characteristics of different materials. The designs that use steel as the energy absorbing material rely on the shearing and tearing of the metal to absorb the energy of the vehicle. One design uses the crushing of steel cylinders. The crash cushions that make use of steel to absorb energy require fabrication of the actual energy absorbing component which can be very costly and time consuming. Steel is a strong material that can withstand great loads before yielding. The challenge in crash cushion design is altering the geometry of the steel and positioning it in the crash cushion in a manner that allows it to deform, shear, or tear and efficiently absorb energy. In order to shape the steel to effectively absorb the energy, most crash cushions require that the steel is manufactured to desired dimensions. The manufacturer will either have to mold a specific part or purchase readily available material to alter by drilling, cutting, punching, welding or one of many other methods to develop it into the desired shape in addition to the modification required for mounting. This is where added cost comes into play. If you can use this readily available material in the form that it comes in when purchased you will have saved the added cost of modifying it to fit your needs. Using structural shapes such as pipe, angle, and channel, one can use the material in the same form that it was purchased to absorb energy. The use of readily available structural steel shapes is a new efficient method of absorbing energy for use by a crash cushion.

Literature Review

The Federal Highway Administration has made it a policy that all roadside devices meet the criteria given in the National Cooperative Highway Research Program (NCHRP) Report 350, Recommended Procedures for the Safety Performance Evaluation of Highway Features (Ross et al. 1993). This report presents the procedures required for conducting crash tests to evaluate the competency of a particular design. The procedures focus on testing a design by applying the most severe conditions that the design would face with the understanding that if a design could withstand the most difficult of impacts, it would also perform as expected in the event of a minor collision. Structural adequacy, occupant risk, and after-collision vehicle trajectory are the primary factors taken into consideration when conducting full scale crash tests (Ross et al. 1993).

Testing Requirements

Before implementation on the highway, crash cushions must be tested to see if they will function properly in the field. Crash cushion designs are involved in a number of different tests, testing various situations that the design may encounter. The testing procedures discussed here will be those that have a direct correlation and are directly affected by the energy absorbing component of the crash cushion.

Due to the fact that the testing is intended to simulate highway situations, testing must imitate these situations as closely as possible. Crash cushions placed in front of rigid structures that will not move when impacted. This must be carried over into the testing of the crash cushion. It is required that when a crash cushion is tested, a rigid, non-yielding backup structure that simulates a highway feature is to be used (Ross et al. 1993).

The vehicles used in the testing of crash cushions are small cars that weigh 820 kg and pickup trucks weighing 2000 kg. This is to take into account

the large variety of vehicles on the road today. It is expected that if a highway safety device can safely stop the lightest and the heaviest of vehicles, it will not have a problem safely stopping all others in between. For head on impacts, the vehicle is to be traveling at 100 km/hr (Ross et al. 1993). Although these vehicles are used for various impact scenarios, the mass is directly affected by the energy absorbing component of the crash cushion during head on impacts. Decelerating the car and truck at acceptable rates is the main function of the energy absorbing component.

Impact Conditions

The National Cooperative Highway Research Program has designated eight tests to evaluate non-gating, redirective crash cushions. The tests evaluate the crash cushions ability to not only absorb the vehicles energy in a head on impact but to test the cushions ability to redirect the vehicle on a side impact. The tests that directly test the energy absorbing component of the cushion are those that impact the cushion head on. It is these head on collisions that require energy absorption through the length of the installation.

The first of these tests is for both an 820 kg passenger car and a 2000 kg pickup truck traveling at 100 km/hr to impact the cushion at 0 degrees from the center line of the cushion. The second of these tests is for both the car and pickup traveling at 100 km/hr to impact the end of the crash cushion at an angle of 15 degrees from the center line. These tests evaluate the occupant risk and vehicle trajectory (Ross et al. 1993). The test that involves the vehicle impact to be lined up with the centerline of the cushion is a true head on impact and will require the cushion to absorb the most kinetic energy out of the two tests. When impacting at a 15 degree angle, there is a reduction in the kinetic energy traveling along the centerline of the cushion. This means that more energy must be absorbed when the head on impact is at 0 degrees from the centerline and this is what the energy absorbing component will be designed to accommodate.

Energy Absorbing Component Requirements

Structural adequacy is evaluated on the cushions ability to perform its intended function. This has to do with the ability of the cushion to redirect a vehicle in a side impact and to bring the vehicle to a stop in a controlled manner in the event of a head on collision.

Occupant risk is evaluated on the cushions ability to control an impacting vehicle without surpassing vehicular deceleration limits. Upon impact, the occupant in the front seat will have a motion relative to the occupant compartment that is affected by the deceleration of the vehicle itself. The occupant is assumed to move freely within the vehicle through a flail space of 0.6 m until striking a hypothetical instrument panel or windshield. The velocity that the occupant strikes the vehicles interior is the occupant impact velocity. The occupant is not to experience an occupant impact velocity greater than 12 m/s. After this contact has been made, the occupant remains in contact with the vehicles interior. Any decelerations experienced by the vehicle will also be experienced by the occupant. It is required that the occupant not experience average decelerations greater than 20 g's over a 10 millisecond time period. A running average of accelerations felt for every 10 millisecond time period from the point that the occupant impact velocity has been established to the point at which the vehicle stops. The highest 10 millisecond average during this time is considered the vehicles maximum ridedown deceleration (Ross et al. 1993). The deceleration unit of g's is the number of gravitational constants. Two g's is equivalent to two times the gravitational constant which is acceleration. When designing a crash cushion, it is a requirement that decelerations not surpass the above values. To achieve the shortest stopping distance possible, the energy absorbing component must decelerate vehicles as close to these values as possible.

The main purpose of a crash cushion is to protect the occupants of a vehicle from the effects of impacting a rigid highway structure. It must be noted that vehicles of various weights are expected to impact the cushion. Vehicles

with various masses traveling at various speeds will have different kinetic energies. Impact will not always be the same. Due to this fact, a crash cushion must be able to accommodate all the impact variations.

Stress and Strain

The underlying reason for deforming steel to be able to absorb the energy of a vehicle is strain. In order to create strain, forces must be applied to the material. In this case, the forces are coming from the vehicle. The kinetic energy of the vehicle will be transferred from the front sled component of the crash cushion down into its attached mandrel which deforms material where it is then absorbed through the deformation of steel. The steel deformation in the crash cushion will experience strain in both the elastic and plastic ranges. Engineering strain ε_E is defined as

$$\varepsilon_E = \frac{\Delta L}{L_I} \tag{1}$$

where ΔL is the change in length of the material and L_i is the initial length of the material. Engineering strain makes use of a material's final length and initial length. This is not the most accurate calculation of the strain in a material. A more accurate calculation does not just take pre and post test dimensions, it calculates the strain of the material in increments through its length. This is done because strain is not necessarily constant throughout the material. True strain ε_T is the sum of the instantaneous engineering strains throughout the length of the material.

$$d\varepsilon = \frac{dL}{L} \tag{2}$$

$$\varepsilon_T = \int d\varepsilon = \int_{L_I}^{L_F} \frac{dL}{L} = \ln \frac{L_F}{L_I} \tag{3}$$

This can be related to the engineering strain by

$$\varepsilon_T = \ln\frac{L_F}{L_I} = \ln\left(\frac{L_I + \Delta L}{L_I}\right) = \ln\left(1 + \varepsilon_E\right) \tag{4}$$

When plastic deformation occurs, the “stiffness” of the material can experience an increase as the rate that the strain is occurring increases. Strain is seen as the ratio of the change in length of a material and its initial length. This change in length can occur at various rates. This rate of strain is seen as

$$\dot{\varepsilon} = \frac{d\varepsilon}{dt} = \left(\frac{d}{dt}\left(\Delta L\right)\right)\left(\frac{1}{L}\right) \tag{5}$$

Due to the nature of crash cushions and the concepts below, strain rates are constantly changing throughout the impact process. This means that the strain-rate sensitivity will be changing throughout the course of the impact. This makes calculations very difficult. Computer simulations are a very powerful tool that will take the strain rate into consideration and include its influence in the dynamic simulations.

At any given point within a body, the stress can be defined with the stress tensor

$$T_\sigma = \begin{bmatrix} \sigma_{xx} & \sigma_{xy} & \sigma_{xz} \\ \sigma_{yx} & \sigma_{yy} & \sigma_{yz} \\ \sigma_{zx} & \sigma_{zy} & \sigma_{zz} \end{bmatrix} \tag{6}$$

From this matrix, the principal stress can be calculated. The three principal stresses can then be used to calculate the average stress. The mean pressure at a given point is seen as

$$\sigma = \frac{1}{3}\left(\sigma_1 + \sigma_2 + \sigma_3\right) \tag{7}$$

Due to the fact that each material will posses different mechanical properties, the stress tensor can be written in two parts seen as

$$T_\sigma = \sigma I + D_\sigma = \begin{bmatrix} \sigma & 0 & 0 \\ 0 & \sigma & 0 \\ 0 & 0 & \sigma \end{bmatrix} + \begin{bmatrix} \sigma_{xx} - \sigma & \sigma_{xy} & \sigma_{xz} \\ \sigma_{yx} & \sigma_{yy} - \sigma & \sigma_{yz} \\ \sigma_{zx} & \sigma_{zy} & \sigma_{zz} - \sigma \end{bmatrix} \tag{8}$$

where

$$D_\sigma = \begin{bmatrix} \sigma_{xx} - \sigma & \sigma_{xy} & \sigma_{xz} \\ \sigma_{yx} & \sigma_{yy} - \sigma & \sigma_{yz} \\ \sigma_{zx} & \sigma_{zy} & \sigma_{zz} - \sigma \end{bmatrix} \tag{9}$$

is the deviatoric stress. This deviatoric stress is the tangential stress and what actually causes distortion in the body. The hydrostatic components can be considered to be negligible in plastic deformation. The values of the stress deviatoric matrix are referred to as

$$s_{ij} = \sigma_{ij} - \sigma\delta_{ij} \tag{10}$$

The invariants of the stress deviatoric are

$$I_1(D_\sigma) = 0 \tag{11}$$

$$I_2(D_\sigma) = \frac{1}{6}\left[(\sigma_1 - \sigma_2)^2 + (\sigma_2 - \sigma_3)^2 + (\sigma_3 - \sigma_1)^2\right] \tag{12}$$

$$I_3(D_\sigma) = s_1 s_2 s_3 \tag{13}$$

The tangential stress intensity *T* can then be seen as

$$T = \frac{1}{\sqrt{6}}\sqrt{(\sigma_{xx} - \sigma_{yy})^2 + (\sigma_{yy} - \sigma_{zz})^2 + (\sigma_{zz} - \sigma_{xx})^2 + 6(\sigma^2{}_{xy} + \sigma^2{}_{yz} + \sigma^2{}_{xz})} \tag{14}$$

or

$$T = \sqrt{\frac{1}{2} s_{ij} s_{ij}} \tag{15}$$

Similar to the stress, the strain within a body is represented as

$$T_\varepsilon = \begin{bmatrix} \varepsilon_{xx} & \frac{1}{2}\varepsilon_{xy} & \frac{1}{2}\varepsilon_{xz} \\ \frac{1}{2}\varepsilon_{yx} & \varepsilon_{yy} & \frac{1}{2}\varepsilon_{yz} \\ \frac{1}{2}\varepsilon_{zx} & \frac{1}{2}\varepsilon_{zy} & \varepsilon_{zz} \end{bmatrix} \tag{16}$$

The strain within a body is seen as a function of displacement in the direction, u_i , and the components of Cartesian coordinates, x_i.

$$\varepsilon_{ij} = \frac{1}{2}\left(\frac{\partial u_i}{\partial x_j} + \frac{\partial u_j}{\partial x_i} \right) \tag{17}$$

Similar to the stress, principal strains also known as principal elongations can be solved for and a strain deviatoric matrix can be developed

$$T_\varepsilon = \begin{bmatrix} \varepsilon_{xx} - \frac{1}{3}\varepsilon & \frac{1}{2}\gamma_{xy} & \frac{1}{2}\gamma_{xz} \\ \frac{1}{2}\gamma_{yx} & \varepsilon_{yy} - \frac{1}{3}\varepsilon & \frac{1}{2}\gamma_{yz} \\ \frac{1}{2}\gamma_{zx} & \frac{1}{2}\gamma_{zy} & \varepsilon_{zz} - \frac{1}{3}\varepsilon \end{bmatrix} \tag{18}$$

The shear strain intensity which is a characteristic of the distortion of the materials shape is seen as

$$\Gamma = \sqrt{\frac{2}{3}}\sqrt{\left(\varepsilon_{xx} - \varepsilon_{yy}\right)^2 + \left(\varepsilon_{yy} - \varepsilon_{zz}\right)^2 + \left(\varepsilon_{zz} - \varepsilon_{xx}\right)^2 + \frac{3}{2}\left(\varepsilon^2{}_{xy} + \varepsilon^2{}_{yz} + \varepsilon^2{}_{xz}\right)} \tag{19}$$

or

$$\Gamma = \sqrt{2\varepsilon_{ij}\varepsilon_{ij}} \tag{20}$$

The total strain in the body is a combination of strain in both the plastic ε_{ij}^p and elastic ε_{ij}^e range.

$$\varepsilon_{ij} = \varepsilon_{ij}^e + \varepsilon_{ij}^p \tag{21}$$

where

$$\varepsilon_{ij}^e = \frac{1}{2G}\left(\sigma_{ij} - \frac{3\nu}{1+\nu}\sigma\delta_{ij} \right) \tag{22}$$

In plasticity, the deformation of the material can depend on the rate that strain occurs. The strain rate matrix can be seen as

$$T_\xi = \begin{bmatrix} \xi_{xx} & \frac{1}{2}\xi_{xy} & \frac{1}{2}\xi_{xz} \\ \frac{1}{2}\xi_{xy} & \xi_{yy} & \frac{1}{2}\xi_{yz} \\ \frac{1}{2}\xi_{xz} & \frac{1}{2}\xi_{yz} & \xi_{zz} \end{bmatrix} \tag{23}$$

where the diagonal represents the rates of relative elongations and the other components are the angular rates of change. The components of strain rate are seen as

$$\xi_{ij} = \frac{1}{2}\left(\frac{\partial v_i}{\partial x_j} + \frac{\partial v_j}{\partial x_i}\right) = \frac{1}{2}\left(\frac{\partial}{\partial x_j}\frac{\partial u_i}{\partial t} + \frac{\partial}{\partial x_i}\frac{\partial u_i}{\partial t}\right) \quad (24)$$

and the shear strain-rate intensity is

$$H = \sqrt{\frac{2}{3}}\sqrt{\left(\xi_{xx} - \xi_{yy}\right)^2 + \left(\xi_{yy} - \xi_{zz}\right)^2 + \left(\xi_{zz} - \xi_{xx}\right)^2 + \frac{3}{2}\left(\xi^2{}_{xy} + \xi^2{}_{yz} + \xi^2{}_{xz}\right)} \quad (25)$$

Before taking plastic strain into effect, yield criteria must be met. This condition is a function of the principal stresses

$$f\left(\sigma_1, \sigma_2, \sigma_3\right) = K \quad (26)$$

where *K* is a constant of the material connected with its yield limit (Kachanov 2004).

Plasticity

Plasticity describes the inelastic behavior of a material that is deformed and does not return to its original shape after the load has been removed. (Boresi and Schmidt 2003) A majority of the material deformation used by the three concepts (to be presented in the following chapters) to absorb the kinetic energy of the vehicle will be in the plastic range. The deformation will fall into the elastic range for a short time on its path to the plastic deformation. In many engineering structures, failure is considered the point where a material begins to yield. This is not the case for the crash cushion designs in question. Plastic deformation has more area beneath the stress strain curve than elastic deformation. Because of this, material yielding is desired.

Plasticity has three main components:

- Yield criterion that defines the point at which yield occurs

- Flow rule relating plastic strain increments to stress increments after yielding has begun
- Hardening rule that predicts changes in the yield surface

While elasticity only uses the first of these three components, the other two must be understood when dealing with a structure whose main function revolves around plastic deformation.

When a material is strain rate-sensitive it can be considered a viscoelastic material. The material can be represented as a system of a spring and damper connected in parallel. When deforming at very slow rates, the time dependence can be neglected therefore canceling out the damper. At this point, the spring is all that is being used to resist the strain. When the rate of strain varies and increases, the dampers resistance force comes into play. The quicker the deformation occurs, the faster the rate of strain, the more resistance due to damping occurs. Various spring and damper combinations can be used to represent the behavior of various materials that that can be linear or nonlinear.

Structural steel can be illustrated as two components connected in series. The first component is a spring representing the elastic range of the material. The second component is a spring, damper, and a yielding component connected in parallel. The yielding component represents the yield strength of the material. Until the yield strength of the material is met, the spring and damper remain undisturbed. It is not until the material's yield strength has been surpassed that the spring and damper are allowed to stretch. This represents the plastic range of material which is nonlinear. This model is a linear elastic, nonlinear viscoplastic model.

The stress in the component that has both the damper and spring can be seen as

$$E\varepsilon + \eta\dot{\varepsilon} = \sigma_{app} \tag{27}$$

where σ_{app} is the stress applied to the material. The viscous tensile parameter η and modulus of elasticity *E* of steel are both constants. This can be divided by η which reveals the strain retardation time

$$t_e = \frac{\eta}{E} \tag{28}$$

which yields

$$\dot{\varepsilon} + \frac{\varepsilon}{t_e} = \frac{1}{t_e}\left(\frac{\sigma_{app}}{E}\right) \tag{29}$$

This equation can then developed into a nonlinear equation resulting as

$$\dot{\varepsilon} + \frac{\varepsilon}{t_e} = \frac{1}{t_e}\left(\frac{\sigma_{app}}{\mu_p}\right)^n \tag{30}$$

The yielding component in the system is then to be taken into consideration. Due to the fact that strain rate has no effect when the material is in its elastic range, strain rate will be neglected until the stress in the body has surpassed its yield stress. Up to the point where this stress has been met,

$$\dot{\varepsilon} = 0 \tag{31}$$

and after the yield stress has been met,

$$\dot{\varepsilon} \geq 0 \tag{32}$$

This linear elastic, nonlinear viscoplastic model of the material has a total strain of

$$\varepsilon = \frac{\sigma_{app}}{E} + \varepsilon_p \tag{33}$$

where ε_p is plastic strain. The next step is to determine the plastic strain. As stated before, plastic strain does not take place until the yielding component releases allowing for plastic deformation. This means that there are two parts to the plastic strain, the first is the yielding component and the second is the spring and damper in parallel. Due to the fact that these are acting in parallel, the strain that occurs in each part is equal to the other. As long as the material is subjected to a stress beyond the yield strength, the yielding component will have

a stress equal to the yield stress. This is all that the yielding component is capable of withstanding. The excess stress beyond yield is called overstress and is transmitted to the spring and damper in parallel giving the following response

$$\dot{\varepsilon}_y + \frac{\varepsilon_y}{t_\varepsilon} = \frac{1}{t_\varepsilon}\left(\frac{\sigma_{app} - \sigma_y}{\mu_p}\right)^n \tag{34}$$

where ε_y is the strain in the yielding component and σ_y is the yield strength of the material. From this equation it is easy to see that when the stress induced on the body is equal to the yield stress, the right hand side of the equation will be zero. It is known that the plastic strain rate is equal the strain rate of the yield component. This means that both will go to zero when the applied stress equals the yield stress. The plastic strain is

$$\varepsilon_p = \varepsilon - \frac{\sigma_{app}}{E} \tag{35}$$

and the plastic strain rate in the material is

$$\dot{\varepsilon}_p = \frac{1}{t_\varepsilon}\left(\frac{\sigma_{app} - \sigma_y}{\mu_p}\right)^n - \frac{\varepsilon_p}{t_e} \tag{36}$$

and when the applied stress is less than the yield stress, plastic strain and plastic strain rate are zero. The strain rate of the system is seen as

$$\dot{\varepsilon} = \frac{\dot{\sigma}_{app}}{E} \tag{37}$$

before the material reaches its yield stress and

$$\dot{\varepsilon} = \frac{\dot{\sigma}_{app}}{E} + \frac{1}{t_\varepsilon}\left(\frac{\sigma_{app} - \sigma_y}{\mu_p}\right)^n - \frac{\left(\varepsilon - \sigma_{app}\right)}{t_e} \tag{38}$$

after it reaches its yield stress. These equations have been derived considering a tensile load. In the event of compressive loads, the plastic strain rate will change to the following

$$\dot{\varepsilon}_p = \frac{1}{t_\varepsilon}\left(\frac{\left|\sigma_{app}\right| - \sigma_y}{\mu_p}\right)^n \operatorname{sgn}\sigma_{app} - \frac{\varepsilon_p}{t_e} \tag{39}$$

when the absolute value of the applied stress is greater than the yield stress. In the even that the applied stress is less than the yield stress, the plastic strain rate will be zero just as before (Shames and Cozzarelli 1997).

When designing an energy absorbing device that makes use of the plastic deformation of steel, calculations based strictly on the material being in the elastic range will not be enough. It is clear that the strain in a material is dependent on the rate at which is loaded when in its plastic range. This rate dependency will "stiffen" the material as it is subjected to stresses greater than its yield stress.

Strain Energy

Strain energy is defined as the potential energy stored in a stressed material. It is equal to work done on the material by external forces. The energy that falls under the elastic range is recoverable after the load has been removed (Young and Budynas 2002). Once the material yields, plastic deformation begins to take place. This can be seen in Figure 3. The area under the elastic portion of the curve is work done that is recoverable. The area in the plastic region is work done that is not recoverable.

The strain that will take place in future concepts is in both the elastic and plastic ranges. Strain energy can measure the work done by the material while in its elastic range. The internal energy is the stored elastic strain energy and is measured per unit volume (Reddy 2002). It is work done by internal forces moving through displacements. The force within a body due to stress can be found from the stress σ and the area A that it acts upon.

$$F = A\sigma_{xx} \tag{40}$$

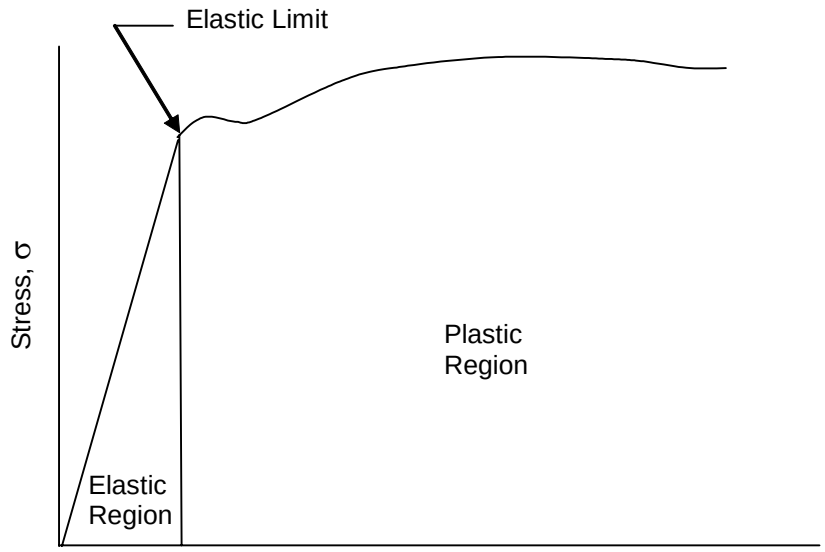

Figure 3. Stress Strain Diagram

The displacement *d* that this force moves through can be seen as

$$d = d\varepsilon dx \tag{41}$$

From these equations the work done by this stress can be seen as

$$dU_O = Adx\sigma_{xx}d\varepsilon \tag{42}$$

This is the elemental area beneath the stress strain curve. The strain energy density is then seen as

$$U_O = \int_0^{\varepsilon_{xx}} \sigma_{xx} d\varepsilon_{xx} \tag{43}$$

This is the area beneath the stress strain curve which is the internal work done by $A\sigma$ over the material section during its deformation. The total internal work done by the force over the length of the material (all sections) is then seen as

$$W = \int_0^L AU_o dx \tag{44}$$

Considering an Euler-Bernoulli beam seen in Figure 4, displacements u and w occur in the x and z directions.

Figure 4. Euler-Bernoulli Beam

Strain can occur not only from the axial displacement of the beam but from bending also. In this case the axial displacement of a point due to bending and axial deformation is

$$u = u_O(x) - z\frac{dw_O}{dx} \tag{45}$$

where u_0 and w_0 are displacements of a point in the x and z directions respectively. Under the assumption of small displacements, strain is then seen as

$$\varepsilon_{xx} = \frac{du_O}{dx} - z\frac{d^2 w_O}{dx^2} \tag{46}$$

The strain energy density then becomes

$$U_O = \int_0^{\varepsilon_{xx}} \sigma_{xx} d\varepsilon_{xx} = \int_0^{\varepsilon_{xx}} E\varepsilon_{xx} d\varepsilon_{xx} = \frac{E}{2}\varepsilon^2{}_{xx} = \frac{E}{2}\left(\frac{du_O}{dx} - z\frac{d^2 w_O}{dx^2}\right)^2 \tag{47}$$

where E is Young's modulus (Young and Budynas 2002). From this we can now solve for the strain energy by integrating U_0 over the volume of the body to get U

$$U = \int_V U_O dV = \int_0^L \int_A \frac{E}{2}\left(\frac{du_O}{dx} - z\frac{d^2 w_O}{dx^2}\right)^2 dA dx = \frac{1}{2}\int_0^L \left[EA\left(\frac{du_O}{dx}\right)^2 + EI\left(\frac{d^2 w_O}{dx^2}\right)^2\right] dx \quad (48)$$

Since the deforming material being used in the crash cushion will not have an axial load placed upon it, the material will be considered to be in bending. Because of this the strain energy due to bending is focused on and it is seen that

$$U = \frac{1}{2}\int_0^L EI\left(\frac{d^2 w_O}{dx^2}\right)^2 dx \quad (49)$$

the above equations are used to calculate the strain energy in the elastic range (Reddy 2002). The work done in the plastic range is not recoverable.

Motion Calculations

Theoretical ride down times, decelerations, and distances can be solved with the information given in the test requirements. In the requirements, the impact velocity V_o, flail space (*FS)* distance, and allowable occupant impact velocity (*OIV)* were given.

$$V_o = 100\frac{km}{hr} = 27.77\frac{m}{s} \quad (50)$$

$$OIV = 12\frac{m}{s} \quad (51)$$

$$FS = 0.6m \quad (52)$$

The flail space is the distance that an occupant is to travel before making contact with the vehicles interior. If the occupant is traveling more than 12 m/s upon impact, it is considered to be unsafe and therefore not acceptable. Since the crash cushion can only control the deceleration of the vehicle, the deceleration that is required to meet the occupant impact velocity can then be calculated. Knowing the maximum velocity of the occupant with respect to the interior of the vehicle *V* and the distance that the occupant will travel, *d*, the

acceleration required for the occupant to impact the interior at the maximum OIV value can be calculated. The initial velocity of the occupant with respect to the vehicles interior V_o is considered to be zero since at the instant before impact, the occupant is traveling at the same velocity as the vehicle itself and not independently of the vehicle.

$$a = \frac{(V^2 - V_o^2)}{2d} = \frac{\left(12\frac{m}{s}\right)^2}{2(0.6m)} = 120\frac{m}{s^2} = 12.24G's \tag{53}$$

In order for the occupant to be accelerating with respect to the vehicle's interior, the vehicle must be decelerating. The equation below shows that the occupant impact velocity will be reached when the vehicle reaches a deceleration of 12.24 g's. The theoretical time it takes to reach 12.24 g's is then calculated:

$$t = \frac{\sqrt{2ad + V_o^2} - V_o}{a} = \frac{\sqrt{(2)\left(120\frac{m}{s^2}\right)(0.6m) - \left(0\frac{m}{s}\right)^2} - 0\frac{m}{s}}{120\frac{m}{s^2}} = 0.1s \tag{54}$$

A time of 0.1 seconds elapses for the occupant to reach a deceleration of 12.24 g's. The distance that the vehicle has traveled and its velocity after reaching a deceleration of 12.24 g's are then calculated

$$V = V_o + at = 27.77\frac{m}{s} + \left(-120\frac{m}{s^2}\right)(0.1s) = 15.77\frac{m}{s} \tag{55}$$

$$d = \frac{\left(V^2 - V_o^2\right)}{2a} = \frac{\left(15.77\frac{m}{s}\right)^2 - \left(27.77\frac{m}{s}\right)^2}{2\left(-120\frac{m}{s^2}\right)} = 2.177m \tag{56}$$

After impact with the crash cushion the vehicle's speed reduces to 15.77 m/s and has traveled 2.177 meters at the point where the occupant impact velocity has been met. After the occupant has made impact with the vehicle's interior, the acceptable 10 millisecond maximum average deceleration is 20 g's. It is required that the occupant of a vehicle reach decelerations of no more than

20 g's (196 m/s^2) in a single 10 millisecond average segment of time to remain safe. The time and distance required to stop a vehicle now traveling 15.77 m/s with a deceleration of 20 g's is calculated

$$t = \frac{(V - V_o)}{a} = \frac{0 - 15.77\frac{m}{s}}{-196\frac{m}{s^2}} = 0.08s \tag{57}$$

$$d = \frac{(V^2 - V_o^2)}{2a} = \frac{\left((0)^2 - \left(15.77\frac{m}{s}\right)^2\right)}{2\left(-196\frac{m}{s^2}\right)} = 0.634m \tag{58}$$

It can be seen that a vehicle traveling 100 km/hr that is decelerated at 12.24 g's and then 20 g's will theoretically take 0.18 seconds and 2.811 meters to stop.

The above calculations are theoretical. In order to calculate what is happening in an actual test, an accelerometer is needed. When using accelerometer data to calculate the OIV, a different approach must be taken. The accelerometer measures changes in acceleration from changes in strain on a beam. The beam is located within the accelerometer itself. In order to deflect a beam, a force must be applied to it. This force can be created by accelerating the beam itself. When the beam is accelerated, its mass will cause it to deflect. The amount of deflection is measured by the strain gauge on the beam. This allows for accurate measurements of acceleration of the accelerometer itself. When rigidly mounted to a mass, the acceleration of the mass is equal to the acceleration of the accelerometer. An analog-to-digital card in the computer then converts the voltage output from the accelerometer to numeric engineering units based on calibration factors previously determined. A computer then reads the acceleration value at incremental points in time during the test. This is how deceleration data is collected from test vehicles and test masses.

After the acceleration data has been recorded by the computer, a plot of the data can be developed. The plot will illustrate the acceleration that had occurred at any given time during the test. The allowable velocity that the occupant may impact the vehicle interior is defined at 12 m/s. The occupant also has a flail space of 0.6 m. The occupant impact velocity can then be calculated with these given requirements and acceleration data. The average velocity V_i in a given increment of time can be determined from the acceleration a_i data at various points. It must be noted that prior to occupant impact with the vehicles interior, the body flails freely. This means that when the vehicle decelerates at 2 g's with respect to its surroundings, the occupant will be accelerating at 2 g's with respect to the interior of the vehicle. The acceleration of the vehicle will have negative values as it is slowed to a stop. This gives the occupant a positive velocity within the vehicle. Since the occupant is to travel with a positive velocity, the integration is multiplied by a negative to account for this. The velocity of the occupant with respect to the vehicles interior V is also calculated making use of this incremental velocity V_i.

$$V_i = \int_{t_i}^{t_{i+1}} -\left(\frac{a_i + a_{i+1}}{2}\right) dt \tag{59}$$

$$V = \sum_{i=1}^{n} V_i \tag{60}$$

$$V = \sum_{i=1}^{n} \int_{t_i}^{t_{i+1}} -\left(\frac{a_i + a_{i+1}}{2}\right) dt \tag{61}$$

The above equation makes use of the average acceleration within two points in time to solve for the occupants velocity in that increment of time. The distance traveled within this increment of time can then be calculated by integrating the velocity with respect to time. This distance is then tabulated over the duration of the test.

$$d_i = \int_{t_i}^{t_{i+1}} V_i dt \tag{62}$$

$$d = \sum_{i=1}^{n} d_i \tag{63}$$

$$d = \sum_{i=1}^{n} \int_{t_i}^{t_{i+1}} \int_{t_i}^{t_{i+1}} -\left(\frac{a_i + a_{i+1}}{2} \right) dt dt \tag{64}$$

When the distance traveled *d* is equal to 0.6 m the occupant has made contact with the interior of the vehicle. The velocity of the occupant *V* at this point is occupant impact velocity.

After the occupant makes contact with the vehicle they are considered to be in contact through the remainder of the crash. The vehicle and the occupant are considered to have the same decelerations after this contact has occurred. The acceleration recorded from this point on is considered to be ridedown acceleration. The data measured from the accelerometer is not only considered to be the deceleration data for the vehicle but for the occupant too. It is known that the occupant cannot safely be decelerated at rates greater than 20 g's. This means that the deceleration of the vehicle must not exceed 20 g's. The ridedown deceleration is then calculated as the highest average acceleration within a 10 millisecond time increment from the time that the OIV was met to the time the vehicle comes to a complete stop.

It is desired to have a crash cushion that will stop the vehicle in the shortest distance possible. A shorter stopping distance means the crash cushion itself can be shorter in length. With an increase in installation size, there will be an increase in material required, time to install, installation room on the highway, and cost. It would not be desirable to bring a vehicle to a complete stop at a rate of 20 g's to keep a short installation distance. If deceleration starts immediately at 20 g's it will not meet the 12 m/s occupant impact velocity requirements. Due to the fact that the vehicle has more than one deceleration requirement to meet, the crash cushion will have to have more than one deceleration stages in order to reach its optimal length. It is acceptable for the vehicle to be brought to a stop at 12.24 g's but the installation distance will be reduced if a second stage that decelerates the vehicle at 20 g's is implemented

after the occupant impact velocities have been met. These deceleration stages can be created with the use of various material sizes, thicknesses, and mandrel sizes causing less or more plastic deformation in the deforming steel. Changing of these variables will allow the above methods to control a vehicles deceleration.

Due to this fact that the crash cushion will be required to stop vehicles of various weights, the theoretical stopping distance of 2.811 m can never be met with one crash cushion for more than one vehicle mass. It must be noted that the above calculations are theoretical and that the vehicles mass will affect the stopping distance. A truck weighing 2000 kg will require a greater stopping distance than an 820 kg car. The crash cushion will be absorbing the kinetic energy of the vehicle. The kinetic energy *KE* of a vehicle is dependant on the velocity *V* and mass *m* of the vehicle:

$$KE = \frac{1}{2}mV^2 \tag{65}$$

The kinetic energies of the car KE_{car} and pickup truck KE_{truck} are calculated below. It can be seen that the cars energy is less than the trucks.

$$KE_{car} = \frac{1}{2}(820kg)\left(100\frac{km}{hr}\right)^2 = 316.358kJ \tag{66}$$

$$KE_{truck} = \frac{1}{2}(2000kg)\left(100\frac{km}{hr}\right)^2 = 771.604kJ \tag{67}$$

The remaining energy left in the truck after passing through the energy absorbing material required to bring a car to a stop can now be calculated.

$$771.604kJ - 316.358kJ = 455.246kJ \tag{68}$$

It can be seen that there is still a large amount of energy left to be absorbed. Although the cushion was able to absorb all the energy of the car, it was unable to consume half of the pickup truck's energy. The remaining velocity of the truck after passing through this stage can then be calculated.

$$KE_{truck} = \frac{1}{2}mV^2 \Rightarrow V = \sqrt{\frac{2(KE_{truck})}{m}} = \sqrt{\frac{2(455.246kJ)}{2000kg}} = 76.81\frac{km}{hr} \quad (69)$$

After traveling through the energy absorbing component that absorbed all the energy in the car, the truck has a velocity of 76.81 km/hr.

Each combination of mandrel displacement and material thickness will yield a constant deceleration that is different from other combinations. As long as the material being deformed stays at a constant thickness with a constant deformation, a constant acceleration will be applied.

Knowing that a mass of 2000 kg is being decelerated at a constant deceleration of 20 g's, the force required to displace this particular mandrel within its deforming material set up can be calculated

$$F = ma = (2000kg)(20g's)\left(9.81\frac{m}{s^2}\right) = 392{,}400N \quad (70)$$

The same can be done for an 820 kg mass

$$F = ma = (820kg)(20g's)\left(9.81\frac{m}{s^2}\right) = 160{,}884N \quad (71)$$

It is seen that the force to slow a 2000 kg mass at 20 g's is much larger than the force required to slow the 820 kg mass at 20 g's. Since the mandrel-material combination used in the 2000 kg scenario requires 392,400 N to move along, it can be said that regardless of the mass impacting it, a force of 392,400 N will be required to move it even a little bit.

In the event that the 820 kg mass impacts a cushion that requires 394,000 N to move along its length, its deceleration can then be calculated

$$F = ma \rightarrow a = \frac{F}{m} = \frac{392{,}400N}{820kg} = 478.5\frac{m}{s^2} = 48.8g's \quad (72)$$

This clearly illustrates that a crash cushion that is able to bring a 2000 kg mass to a stop with safe decelerations cannot be used for the smaller 820 kg mass. The stopping deceleration of 48.8 g's is much larger than the allowable 20 g's. In order for a crash cushion to accommodate both small and large vehicles, it

must have safely brought the smaller mass to a stop before changing into the stage that brings the larger mass to a stop.

Due to the fact that the two vehicles have different kinetic energies, a crash cushion must be developed to accommodate various vehicle weights. A heavier vehicle will require a “stiffer” installation to meet the deceleration requirements while a lighter vehicle will require a “softer” installation. If a crash cushion is designed for a heavier vehicle, the initial stage required to decelerate the vehicle at 12.24 g’s may actually decelerate a lighter vehicle 20 g’s or more. A combination of deceleration stages must be found to accommodate both heavier and lighter vehicles.

The staging decided on will have to be a combination that works both for light cars and heavier trucks. Absorbing the energy of the car will need to be tended to first. It is known that a heavier truck will have more energy than a lighter car. A device that only has enough energy absorbing capability to stop a light car will be insufficient when impacted with a heavier truck. The device will only absorb a portion of the trucks energy. This leftover energy will allow the truck to continue in motion. If staging is designed for the truck first, the system will be soft enough to bring the truck to a safe stop, but too stiff for a small vehicle and will bring it to a stop at unsafe decelerations.

The first stage will be focused on slowing the vehicles travel at a rate that does not violate the occupant impact velocity requirements. After an acceptable occupant impact velocity for a car has been met, the second stage can take effect. The second stage will be used to bring the car to a stop while staying below the maximum deceleration allowed. This ends the crash cushions focus on the lighter car. Understanding that both a car and a truck will be impacting the crash cushion, the above two stages will then need to be applied to the truck. This may be enough to bring the truck to an acceptable occupant impact velocity. If not, the third stage will be to decelerate the truck to conform to the occupant impact velocity requirements. After these requirements have been met

the truck may be brought to a complete stop at decelerations which do not violate the ridedown criteria.

The theoretical calculations above do not take into account several variables that also play a part in the absorption of the vehicles kinetic energy and reducing its velocity. Upon impact, the front of the vehicle begins to crush and the front of the crash cushion begins to displace. Several things are taking place all at once at this point. The vehicles crush acts as a spring that absorbs energy. Kinetic energy is also absorbed by the inertia of other cushion components when setting them into motion from their initial resting state. As the front component of the crash cushion moves along, it forces a mandrel along the length of material that is being deformed by the mandrel. This material deformation also absorbs the kinetic energy of the vehicle. Friction also plays a part in the energy absorption. There is friction between the mandrel surfaces and the material that it makes contact with while traveling the length of the installation. There is also friction between materials forming other cushion components that make contact with one another during impact. Wind resistance of the vehicle and crash cushion components also plays a very small roll in reducing the vehicles speed.

In the case of a crash cushion, it is difficult to calculate frictions contribution in the absorption of vehicular kinetic energy. The crash cushion will initially have static friction resisting the motion of the components. Once in motion, the movement of the components will be resisted by the kinetic friction. The force required to overcome friction is calculated with the normal force N between two surfaces in contact and the coefficient of kinetic friction f_k or the coefficient of static friction f_s (Avallone and Baumeister 1996).

$$F_s = f_s N \tag{73}$$

$$F_k = f_k N \tag{74}$$

Although the above friction equations are very simple, implementing them into a crash cushion will be very difficult. At any given point in time different

forces throughout the system will be directed in different directions yielding different values of normal forces. Although the coefficient of friction stays constant, the normal force magnitudes and where their locations are always changing. This is where computer simulation comes into play and is very helpful in accurately implementing the effect of friction in the velocity reduction of a vehicle. Due to the fact that every crash cushion design concept will have various configurations, the effect of friction on the absorption of kinetic energy will be difficult to gauge. The simulations conducted in this research did include coefficients of friction but kept the mandrel models as simple as possible. It is obvious that there will be normal forces in the areas where material is deforming and friction can play a role there but the addition of more material in anticipation of where other crash cushion components would lie were left out. This also aided in the focus of the research which is on the energy absorbing components themselves, not other cushion components.

The energy absorbing component in the crash cushion will not be the only thing “cushioning” the vehicles impact. When a vehicle collides with a structure, there is noticeable crush that has taken place in the front portion of the car. This crush comes from the deformation of the vehicle’s frame along with the deformation of and movement of the components under its hood. The crushing characteristic of the vehicle can be represented with a spring constant. This spring constant was calculated after observing results of full-scale automobile collisions. The average value or the spring rate per unit mass, k/m, is 41.01g/m (Emori 1968). Each vehicles spring constant is a function of its mass. After multiplying the vehicle mass by the constant, a force per unit length is left. If a crash cushion is designed to decelerate a 2000 kg mass at 20 g’s and a 2000 kg vehicle impacts it, the deceleration may be less than 20 G’s because of this spring constant that is also absorbing the vehicles kinetic energy. It may also be slightly higher than 20 g’s due to the mass of the crash cushion components being displaced by the vehicle. Seeing how there are an infinite number of

vehicle mass and cushion component configurations, the scope of this research is focused on the energy absorbing component of the crash cushion only.

The vehicular spring rate will vary between every vehicle. The mass of the vehicle will change from vehicle to vehicle as the passenger and cargo weights change. Every vehicles configuration will change with different parts located in different places. The material used to make these parts also plays a role because different materials will deform in different manners. The point of impact will also play a roll in the vehicles spring constant. Since a crash cushion is not wide enough to crush the entire front end of the vehicle, it will be applying a force in a concentrated area. This can reduce the vehicle spring rate to 29.53 g/m from 41.01g/m times the mass of the vehicle (Bullard 1995b). The location the front end of the vehicle impacts the crash cushion will also vary the vehicle spring constant. Having said this, it can be seen that a spring constant does exist which will aid in the absorption of kinetic energy. Unfortunately, accurately using it in calculations will be very difficult due to the fact that it can vary so much from vehicle to vehicle. It is for this reason that simulations conducted did not use the spring constant and focused mainly on the energy absorbing ability of the concepts.

Summary

In this chapter, an overview of highway safety and crash cushion technology has been discussed. The testing that crash cushions must undergo before being implemented on roadways along with calculations illustrating the requirements has been presented. The mathematics behind the conversion of vehicular kinetic energy to the strain of steel has also been discussed. Application of these requirements and calculations will be seen in following chapters.

CHAPTER II

DEVELOPMENT OF STEEL DEFORMATION TECHNOLOGY

Overview

In the previous chapter, a need for crash cushions was illustrated through a history of highway safety. As more improvements are made on the energy absorbing devices makes, highway safety increases. These designs are expected to perform to regulations implemented upon them. This chapter presents new energy absorbing technology that will improve current designs and meet all requirements expected of the technology.

Need Statement

When developing a new design, a purpose is expected to be served. The design is expected to do a job. From the early stages of design, the job that the design must do and the duties it must fulfill need to be clear. A well developed need statement should be made.

The need statement for the research at hand is to develop a new method to transform the kinetic energy of a vehicle traveling up to 100 km/hr into the elastic and plastic strain in the deformation of readily available structural steel to be implemented into a crash cushion.

Function Structure Evolution

This need statement can then be broken up into smaller tasks. Reducing the velocity of a vehicle at a rate safe enough for the occupants is broken into four separate stages. The four stages are identified by four different deceleration requirements that must be met by crash cushions. These are

referred to as functional requirements. These four requirements are then broken down to components. By identifying the controlling factor or root of the function, the design concept can be better quantified. Every component of a design has a certain task that it is intended to carry out. The job that this task does will create a result that is seen as performance. The performance of the component is governed by its individual parts. The component has a function asked of it. By altering specific parameters of the component, the performance is altered. This can be compared to a mathematical function,

$$f(x) = y \tag{75}$$

The performance *y* of the above function *f* is controlled by the parameter *x*. Similarly the performance of the energy absorbing component of a crash cushion is expected to meet certain deceleration criteria. The performance of the energy absorbing method is the function of the component itself. Altering parameters within the energy absorbing component will in turn have an affect on its performance.

In order to develop an optimal design, the “lowest lying” parameter of the function must be identified. The question of what parameter directly affects the above function must be asked. The question should then be asked as to what affects this parameter directly. This question should be asked over and over, until the parameter has been broken down into its most basic form. This is referred to as the design parameter which is the “root” of the functional requirement at hand. This design parameter is focused on to meet the functional requirement. When modifying the design parameter to meet the functional requirement, there will be some limitation as to how much alteration can occur. This limitation is the critical parameter. The above method as applied to this research is illustrated in Figure 5.

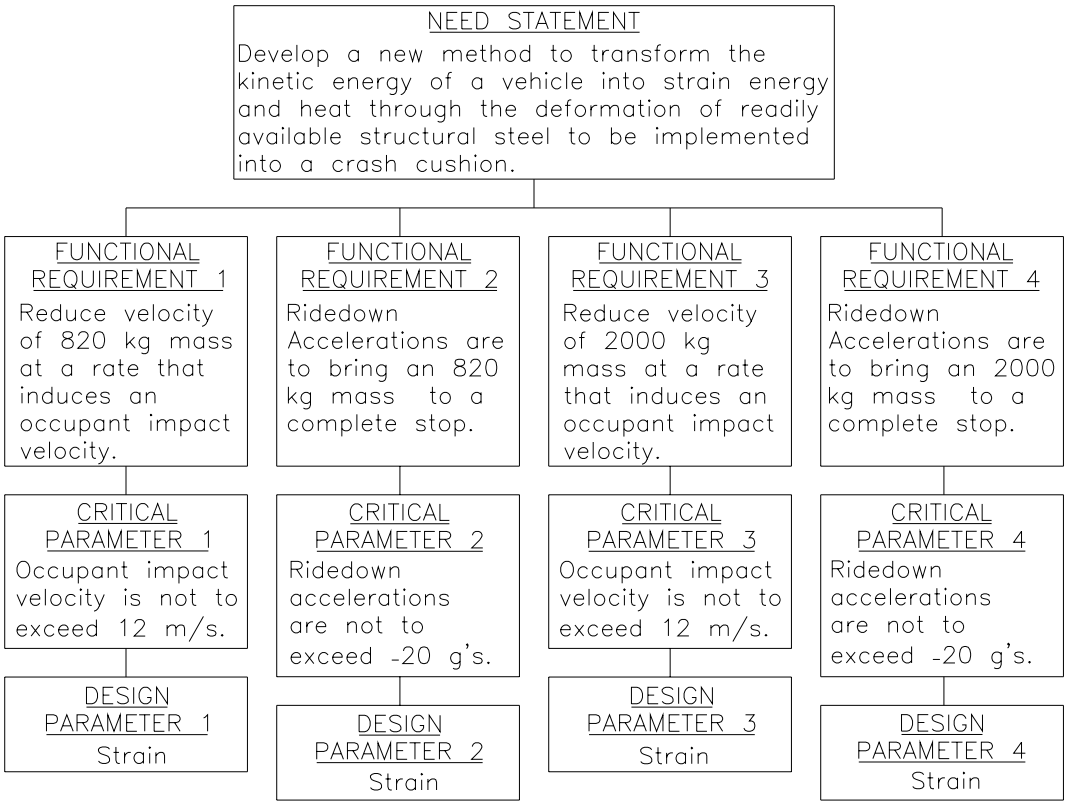

Figure 5. Function Structure

Functional Requirements and Design Parameters

Functional Requirement 1. The first of the four stages is to reduce the velocity of an 820 kg mass traveling at 100 km/hr at a controlled rate that induces an occupant impact velocity.

- Vehicle velocity must be reduced at a controlled rate which depends on deceleration control
- The deceleration is controlled by the cushions ability to transform the vehicles kinetic energy into work required to deform steel
- The amount of steel deformation is controlled by the steel geometry and deformation characteristics
- This deformation control is just a method to control the strain that occurs

Critical Parameter 1. The occupant impact velocity is not to exceed 12 m/s.

Design Parameter 1. Strain is the underlying parameter for this particular functional requirement. Controlling the strain that occurs will aid in achieving the functional requirement.

Functional Requirement 2. After an occupant impact velocity for the 820 kg mass has been met, bring the mass to a complete stop in a controlled manner.

- Vehicle velocity must be reduced at a controlled rate which depends on deceleration control
- The deceleration is controlled by the cushions ability to transform the vehicles kinetic energy into work required to deform steel
- The amount of steel deformation is controlled by the steel geometry and deformation characteristics
- This deformation control is just a method to control the strain that occurs

Critical Parameter 2. A 10 millisecond deceleration average of 20 g's is not to be exceeded.

Design Parameter 2. Strain is the underlying parameter for this particular functional requirement. Controlling the strain that occurs will aid in achieving the functional requirement.

Functional Requirement 3. The first of the four stages is to reduce the velocity of a 2000 kg mass traveling at 100 km/hr at a controlled rate that induces an occupant impact velocity.

- Vehicle velocity must be reduced at a controlled rate which depends on deceleration control
- The deceleration is controlled by the cushions ability to transform the vehicles kinetic energy into work required to deform steel
- The amount of steel deformation is controlled by the steel geometry and deformation characteristics

- This deformation control is just a method to control the strain that occurs

Critical Parameter 3. The occupant impact velocity is not to exceed 12 m/s.

Design Parameter 3. Strain is the underlying parameter for this particular functional requirement. Controlling the strain that occurs will aid in achieving the functional requirement.

Functional Requirement 4. After an occupant impact velocity for the 2000 kg mass has been met, bring the mass to a complete stop in a controlled manner.

- Vehicle velocity must be reduced at a controlled rate which depends on deceleration control
- The deceleration is controlled by the cushions ability to transform the vehicles kinetic energy into work required to deform steel
- The amount of steel deformation is controlled by the steel geometry and deformation characteristics
- This deformation control is just a method to control the strain that occurs

Critical Parameter 4. A 10 millisecond deceleration average of 20 g's is not to be exceeded.

Design Parameter 4. Strain is the underlying parameter for this particular functional requirement. Controlling the strain that occurs will aid in achieving the functional requirement.

It is concluded that the parameter that controls the energy absorbing components ability to reduce the vehicles velocity meeting the requirements of all four stages is the strain that occurs. The strain that occurs will be in both elastic and plastic deformation. By being able to control the strain within the material, the vehicle deceleration is controlled.

Quantitative Evaluation for Geometric Simplicity

All concepts will have the same number of major components. There is the mandrel and the material that is intended to deform. Due to the energy absorbing ability being different in each material, some concepts will vary in the number of mandrels and deforming materials required to accommodate the deceleration requirements. When implemented into a crash cushion it may also be desirable to vary the number of mandrels and deforming materials to add to the stability of the structure. A structure balancing on one very strong energy absorbing material may not be as stable as a structure held in place by two weaker absorbing materials whose combined energy absorbing ability is equal to that of the first single strong one. It is also desired for the concept to be simple. When more parts are added to a concept, the concept is only complicated. This makes for a more difficult installation and possible increase in cost.

Parameter Analysis

There are two stages of design to be considered when developing the conceptual designs. The first stage is one in which physical laws, principles, and ideas are taken into consideration. The second stage is the configuration stage where the concept is evaluated against the design requirements (Tiwari 2002). After being evaluated against the requirements, a decision can be made as to whether the concept needs to be modified in order to meet the requirements. The designer then loops back into the concept stage to alter the idea to meet a requirement that was not met before. The entire concept is evaluated with the requirements and looped back to the conceptual stage as many times as necessary until the concept finally meets the requirements.

Looping Concept

When developing solutions to decelerate a vehicle, various concepts *Ca* have been developed where *a* is the concept number. The concepts in the

group will be *C1*, *C2*, *C3*, *C4* etc. Each concept has several variables that are capable of changing the outcome of its performance by being altered slightly. It is because of these variables that looping is necessary. As the number of variables in a concept increase, so do the number of loops. A general three variable loop can be seen in Figure 6.

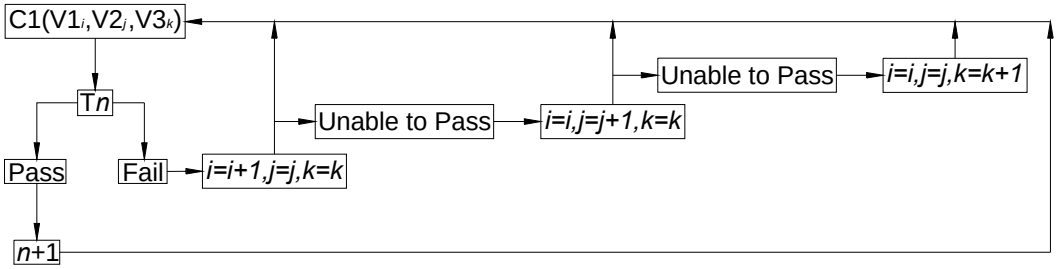

Figure 6. Design Loop for Numerous Variables

Each variable *V* can be altered several times. The concept *C1* will be a function of all three variables and their variations.

$$C1(V1_i, V2_j, V3_k) = V1_i + V2_j + V3_k \tag{76}$$

The concept is then subjected to *n* number of tests, *T.* Each concept *Ca* must pass all tests *Tn.* In the event that concept does not pass T1, then a variable must be altered while the others can stay the same.

$$i = i+1,\ j = j, k = k \tag{77}$$

The concept is then retested. In the event that test T1 is not passed, the second variable is altered until all possibilities have been exhausted.

$$i = i,\ j = j+1, k = k \tag{78}$$

The tests are continued until all variations of the second variable have been exhausted. In the event that the test still has not passed before the second variable has been altered in every possible way, another variable is changed.

$$i = i,\ j = j, k = k+1 \tag{79}$$

The looping process is then started over. The third variable is altered until all variations have been exhausted. After the first test T1 has been passed, the next test T2 is conducted and the looping process is continued.

No two concepts will ever be exactly the same. The above looping method can be altered to accommodate any number of variables in each concept. The variables can have several variations which are also accommodated in the above method. This method allows the designer to move in the correct direction when developing an optimal design.

Expanding Tube Looping Example

One of the conceptual designs described in future chapters deals with the deformation of steel pipe to convert the kinetic energy of the vehicle into the strain of deforming steel. Steel pipe that has not been welded shut down its length can have a mandrel with a larger outer diameter than the inner diameter of the pipe. By running this mandrel through the length of the pipe forces the pipe walls to deform outward. This deformation creates strain in the material from both elastic and plastic deformation.

In the case of deforming readily available structural steel to absorb energy the conceptual stage would be started with the selection of structural steel. Pipe with no welded seam is first chosen. It is known that pipe comes in various sizes. An appropriate size must be selected. Two questions come to mind when installing the pipe in a crash cushion. What is the cost and is it too bulky to implement it into a crash cushion. Typically, with structural steel, the smaller and thinner the pipe, the less it will cost. Since smaller and less expensive pipe is desired, smaller sizes will first be considered. An educated estimate of the size and thickness of the pipe used must be made. This can be done with basic calculations on deforming steel. The start of the loop will first choose a small diameter pipe with a thin wall. The next part of the loop will be to subject the pipe to the basic calculations. If it is discovered that the pipe is too weak, the loop continues and a larger or thicker pipe is chosen. This loop

continues until the smallest and thinnest pipe that will most likely be able to absorb a significant amount of energy for crash cushion implementation is chosen.

After the pipe has been selected, the appropriate mandrel must be selected. A mandrel must be used to deform the metal. It is known that a mandrel must fit within the pipe. The first entrance into the configuration stage will evaluate the mandrel with the pipe size. Is it too large to fit within the pipe? Is it too small and has a lot of room to move? If so, loop back to the conceptual stage and reduce the size. Continue this looping until a mandrel that fits properly within the pipe is chosen. The portion of the mandrel inserted in the pipe without flaring is expected to have a snug fit within the pipe. The more snug the fit, the more stable it will be when positioned inside the pipe. The portion of the mandrel inserted in the pipe is the portion that is not intended to expand the tube. If it is too large, it will not fit within the pipe and if it is too small, an unstable condition may be created allowing the front end of the mandrel to "dig" into the edge of the pipe creating a snag point. The portion of the mandrel inserted into the pipe without deforming it should be between 1/16" to 1/8" smaller than the inner diameter of the pipe it is traveling through. It is desired for one mandrel to be used in the entire installation. Various pipe thicknesses are going to be used in the installation. The mandrel must fit snug yet leave enough room when traveling from a thinner pipe to a thicker pipe to be able to fit. The thicker pipe that has about the same nominal diameter will have a smaller inner diameter. A cone shaped nose on the mandrel is desired to prevent from snagging as the pipe's inner diameter decreases.

Before going any further, the four deceleration stages must be acknowledged. The first stage is to meet the 820 kg mass OIV requirements. The second stage is for the 820 kg mass to meet the ridedown deceleration requirements. The third stage is for the 2000 kg mass to meet the OIV requirements. The fourth and last stage is for the 2000 kg mass to meet the ridedown requirements.

Before continuing it must be noted that more than one mandrel and pipe can be used in an installation. It is most likely that two or more mandrel pipe sets will need to be used. An educated estimate is two. If one pipe absorbs energy at a rate of 10 g's then if two of the same pipe and mandrel combinations are used, the deceleration would be doubled. In the following loops there will be a set of two mandrel and pipe combinations used. Or only one pipe and mandrel configuration will be use but instead of meeting a 20 g requirement, it will only need to meet a 10 g requirement. For simplification of computer simulations, it is desired that only one pipe mandrel configuration is used. In the event that the entire process is looped back to this point, three, four, or more mandrel pipe combinations could be used.

Once the proper mandrel has been chosen, it is known that the mandrel must flare out enough to deform the walls of the pipe. It is this deformation that absorbs energy. A simulation must be run to find out if the pipe absorbed energy at a rate that meet the fist of the deceleration requirements for an 820 kg mass traveling at 100 km/hr which is the occupant impact velocity requirements. Simulations are desirable because they are less costly than physically testing the material and give a good idea of how the material will behave in the physical testing. An educated estimate of the flare size of the mandrel is chosen. Displacement values were already taken into consideration when making basic calculations for initial pipe selection. The first run can now be made. Did the pipe decelerate the mass at a rate above or below 12.24 g's? Continue looping back and adjusting the pipe size and running simulations until the appropriate pipe size is found. When the appropriate size is found, the designer must acknowledge the length of this pipe used to meet the OIV requirements and implement this length into future simulations.

After meeting the occupant impact velocity, the ride down decelerations must then be met. It is desired that only one mandrel is used for the entire installation. This means that the deformation used to meet the occupant impact velocity requirement will be the same deformation for the ridedown stage. This

means that the only variable to change will be the thickness of the pipe wall. The next available pipe thickness for the same diameter pipe is chosen. A simulation is run to see if the next thickness is strong enough to decelerate the 820 kg mass at 20 g's. If not, loop back to the conceptual stage and choose the next thickest pipe, run a simulation. If this looping continues, one of three things will be discovered. The first is that there is a readily available thickness that will decelerate the 820 kg mass at 20 g's. The second is that for this particular diameter and mandrel deflection combination, there is no wall thickness to absorb energy at 20 g's. The third will be that with this mandrel deflection and pipe diameter combination, the mass is decelerating at rates above 20 g's. When the appropriate size is found, the designer must acknowledge the length of this pipe used to bring the 820 kg mass to a stop while obeying the ridedown requirements and implement this length into future simulations.

If it is found that the combination is decelerating the mass at rates above or below 20 g's then one must go back to the initial pipe and mandrel loops and find a new pipe then continue the loops that followed. These loops must continue until pipe that will work for the two deceleration requirements for an 820 kg mass have been met.

After the appropriate pipe and mandrel combination is found to satisfy the requirements for an 820 kg mass, one must move on to meeting the requirements of a 2000 kg mass. Since one mandrel is to be used through the entire installation and only one installation is desired to be used for both the 820 kg mass and 2000 kg mass, the mandrel pipe combination used in the 820 kg process must carry over into the 2000 kg process.

The 2000 kg mass must first travel through the tubing selected for the 820 kg mass. It is understood that this will absorb some of the energy in this mass. It will also reduce its velocity in the process. The tubing is constantly deforming the same amount as the mandrel travels through its length. This gives for a constant deceleration which yields a linear velocity reduction. Even though, the 2000 kg mass will be traveling at a velocity that is less than what it started with,

only deceleration requirements need to be taken into consideration. The 2000 kg mass must first be simulated with the pipe mandrel combination and first two stages decided upon for the 820 kg mass. If the 2000 kg truck goes over the occupant impact velocity requirements in the first two stages then the designer must start at the very beginning and find a combination of mandrel size, pipe size, pipe thickness, pipe length, and number of pipes and mandrels to be used that satisfy the 820 kg requirements and do not allow the 2000 kg mass to go over the occupant impact velocity requirement. One solution to be taken into consideration is varying the lengths of the firs two stages. Lengthening the first stage and reducing the second stage will help to reduce the occupant impact velocity decelerations in the 2000 kg mass. This must be found before continuing beyond this point.

After satisfying the 820 kg mass requirements one must look into a pipe that has the same diameter as the pipes in the above stages but with a thickness that reduces the speed of the 2000 kg mass at a rate of 12.24 g's. This is done by increasing the pipe thickness for the third stage. At this point, one of three things will occur. First, the deceleration is more that 12.24 g's which means the pipe wall is too thick. Since this is the next available pipe thickness for this particular pipe diameter there are no thicknesses in between this size and the previous size. This means that a reduction in material displacement must be used. One must then start the entire process over using a mandrel that causes less displacement. The second possibility is if the deceleration is under the 12.24 g's and there is no pipe thickness readily available for the pipe diameter at hand. This means that the mandrel must be modified to displace more material to absorb more energy. One must start from the beginning using either more mandrel pipe combinations or larger mandrels. The third possibility is that the 12.24 g requirement is met. In this case, one must record the length of pipe that was required to bring the 2000 kg mass to 12.24 g's and add this stage to the first two for future simulations.

After the occupant impact velocity requirements have been met for the 2000 kg mass the ridedown requirements must be met. Tubing with a readily available thickness larger than that of the previous stage must be chosen. If no thickness is available, the pipe used in stage three will be used in stage four. It will just be an elongation of the pipe used in the third stage. The length will be governed by the length required to bring the 2000 kg mass to a stop. If pipe is available, the same three possibilities as those for stage three from above also apply here.

These loops are continued until the appropriate pipe numbers, pipe geometries, and mandrel geometries meeting the given requirements are identified. The entire looping process is seen in Figure 7. At this point, the expanding tube has taken form. The cost of the material used in this concept can now be calculated. This cost will be used in the selection of the final design.

Conceptual Designs

Expanding Tube

The expanding tube will use a mandrel that has a larger outer diameter than the inner diameter of steel pipe that does not have a welded seam through its length. This is seen in Figure 8 when the mandrel is forced through the length of the pipe, the walls will deform outward absorbing energy in the process. Deformations will be in the elastic and plastic ranges. Deformation of the pipe wall will not be the only source of energy absorption in the design. The friction between the mandrel and the inner wall of the pipe will also have a hand in the energy absorption.

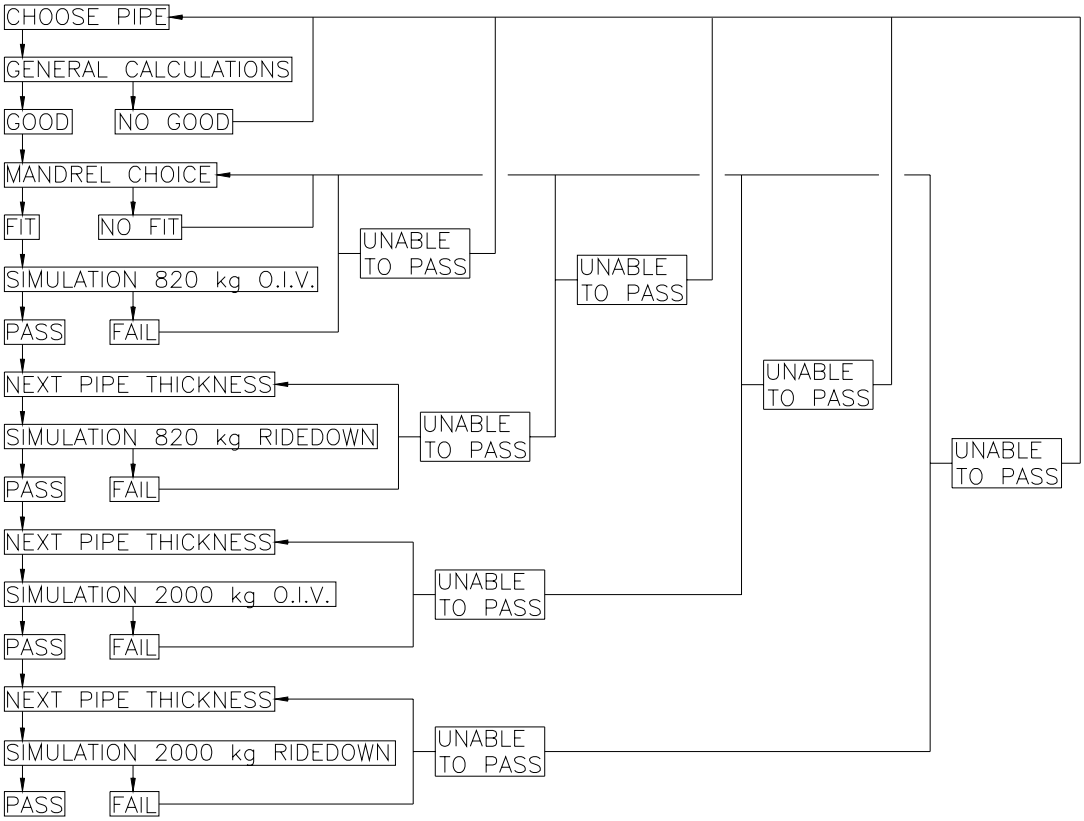

Figure 7. Looping Example for Expanding Tube Concept

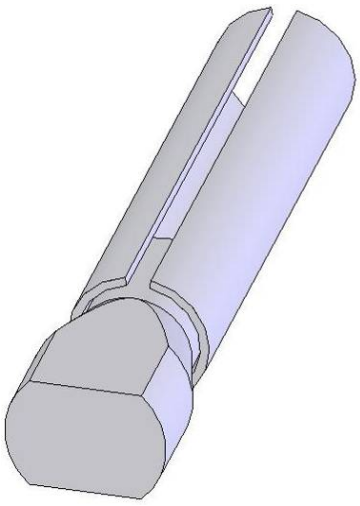

Figure 8. Illustration of Expanding Tube Concept

This concept can regulate energy absorption in several ways. The wall thickness of the pipe will increase or decrease the force required to advance the mandrel through it. The thicker the wall, the greater the force required to deform the material, which means a higher deceleration will result. Varying the amount of deformation in the material will also have an effect on the energy being absorbed. The size of the mandrel has a direct effect on the displacement of the material. An increase in the mandrel size relative to the inner diameter of the pipe will increase the force required to advance the mandrel through the pipe by increasing the deformation that takes place. This will in turn have an increasing affect on the deceleration.

Deforming Angle

The deforming angle will absorb energy through the deformation of the free leg of the structural angle. By mounting the structural angle and allowing a wedge to travel beneath it, the wedge will force the free leg of the angle upward thereby deforming it. The concept illustrated in Figure 9 and Figure 10 depicts a section of a structural angle mounted with bolts to a larger piece of structural angle. It should be noted that larger piece of angle is not required as the smaller angle could be mounted to any rigid structure. Beneath the free leg of the mounted angle is the mandrel with a wedge that will deform the leg.

The deforming angle's ability to absorb energy can be varied by altering several components of the design. The thicker the structural angle, the more force it will require to be deformed. The displacement of the free leg which is directly affected by the geometry of the mandrel will also affect the energy absorbed. The greater the displacement, the more energy absorbed, the greater the deceleration.

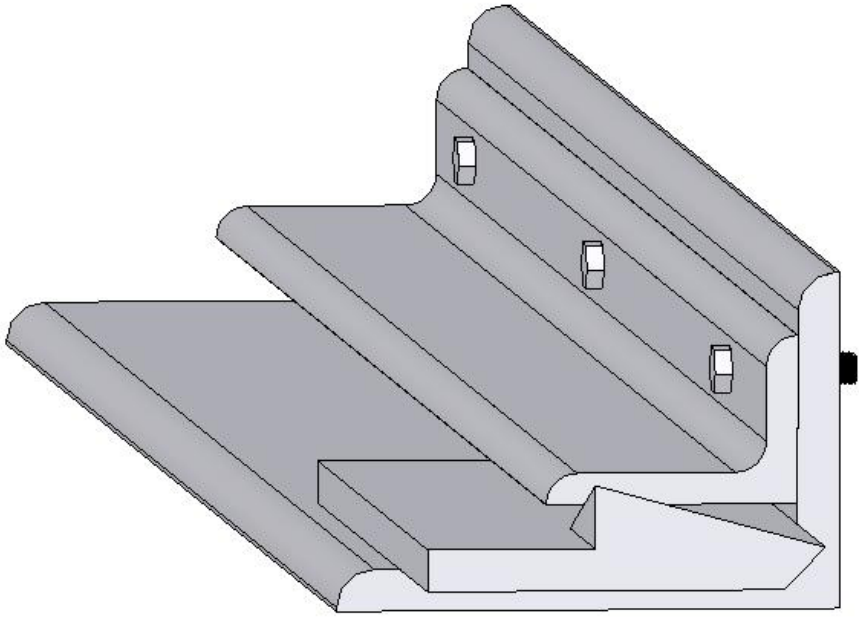

Figure 9. Illustration of Deforming Angle Concept

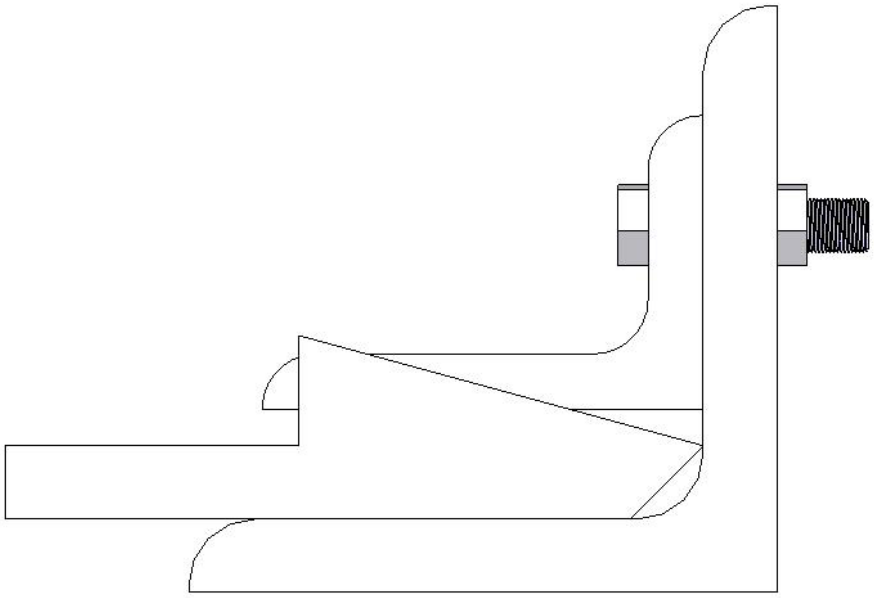

Figure 10. Rear View of Deforming Angle

Another effect on the energy absorbed will be the length of the moment arm created. In the figure above it can be seen that the highest point of the wedge is located close to the end of the free leg of the mounted angle. If the geometry of the wedge is modified so that its highest point is closer to the mounted end of the angle the moment arm will shorten. Shortening the moment arm will require more force to displace the material. This will increase the energy absorbing ability of the concept. It must be noted that friction will also have a role in the energy being absorbed.

Deforming Plate

Similar to the deforming angle concept, steel plate of various widths and thickness can be deformed to absorb energy. The concept uses mandrel similar to that of the deforming angle made of wedges intended deform material above it as it travels the length of the track. Figure 11 illustrates steel plate rigidly constrained by bolts along its length. Steel plate is inexpensive and can be purchased in various lengths, widths, and thicknesses. Two tracks on either side of the mandrel will serve as a guide as it travels the length of the plate. Installation of the plate is simple; all that is required is a wrench to tighten the bolts in place. This makes for an inexpensive replacement after the material has been deformed.

Just as the deforming angle can regulate the deceleration of a vehicle by varying its thickness, the plate can also vary its thickness. Due to the thin strap placed on top of the deforming plate, the plate acts similar to a cantilever beam being deformed upward at its end. The thin strap placed beneath the deforming plate serves two functions. The first is to help guide the mandrel through the length of the crash cushion and the second is to act as a spacer allowing the mandrel to fit beneath the base plate and deforming plate. Mounting the material in place is not complex, concrete anchor bolts are all that is needed. A support can be mounted on top of the two mandrels with ease. This makes for a simple design with minimal parts to replace after use. Using steel plate as an

energy absorbing material makes for a design that is not only efficient in its ability to absorb energy but inexpensive and easy to replace.

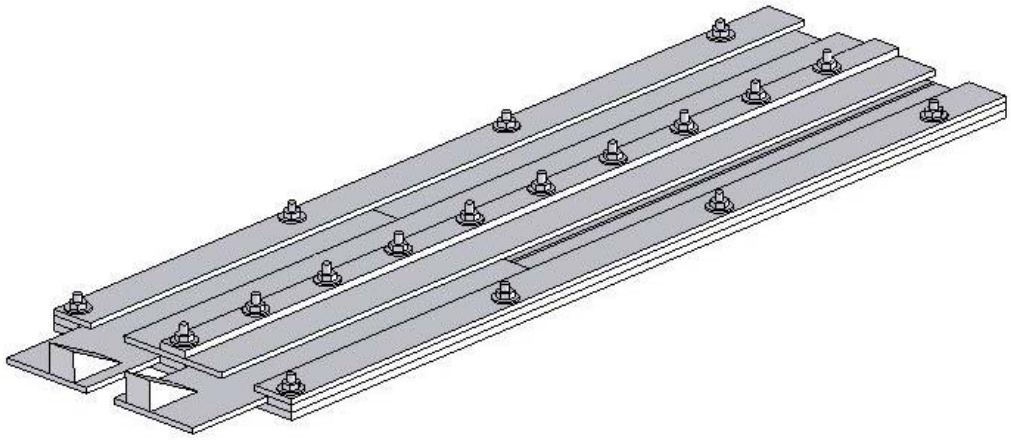

Figure 11. Deforming Plate Concept

Projected Cost

A very important factor in crash cushion design is cost. Part of a design's overall cost comes from the price of material to build the design. It will also cost extra for manufacturing the material into usable parts of the installation. A design that requires minimal manufacturing will greatly reduce the cost of the design. Installation of the design will also add to the overall cost. Different construction crews will charge different prices to install a design in the field. The time that it takes to install also adds to the price. A simple design with minimal parts and minimal field construction will be assembled faster, thus saving money. Due to the large number of crash cushions being used on the highway, small savings per installation will prove to be very large when many designs are installed.

Due to the fact that mounting the energy absorbing material into the crash cushion will be different for each concept, the mounting cost will differ for each. The cost comparisons will be done completely on the purchase cost of the

energy absorbing component and mounting will be neglected. Each concept has different possibilities of mandrel and deforming steel combinations. The expanding tube may use two pipe and two mandrels to stop a vehicle while the deforming plate will only use one plate and two mandrels to stop the same vehicle. In this case, when the comparison of the two is made, the cost of two steel pipes will be compared to the cost of one steel strap.

Structural steel prices found from manufacturers gave a good comparison of the prices of the three concepts. Price research conducted found that the deforming plate concept was the least expensive of the concepts and the expanding tube concept was the most expensive. The cost of deforming angle is roughly 33% higher than the plate and the cost of the steel pipe is roughly 80% higher than the deforming plate (Alamo Iron Works 2005). Due to the geometry of the pipe, welding will be required to mount it in a crash cushion which adds to the cost. The deforming plate and deforming angle concepts can have holes punched in the material to create holes for bolts which is much less costly than welding. It is clear that when it comes to price, the deforming plate is the best choice out of the other two concepts.

Selection of Final Design

After numerous design concepts have been developed, the most desired must be decided upon. To prevent bias in the conceptual decision, a quantitative approach must be taken in the selection process. Categories that the concepts will be judged on are developed. The concepts are then scored according to their performance in each category. The final scores are tabulated and the best concept is selected.

Evaluation Categories

There are several factors that come into play when selecting the final design. All three concepts must be compared with each other for judging. The

concepts will be judged on the material cost, vehicle decelerations, length required for installation, ease of implementation, cost of implementation, ease of replacement, and cost of replacement.

The cost of the material is self explanatory. It is the cost of the material used to allow the concept to decelerate a vehicle. The cost of the material used in all four stages combined. Different mandrels will be used for the three different concepts. Their cost is also a contributing factor in the overall material cost for the concept.

The main purpose of the energy absorbing component is to decelerate an impacting vehicle. If this component is very easy to install but is ineffective in safely stopping an impacting vehicle, then it is not a feasible concept. The concepts will be judged on their ability to convert the kinetic energy of a vehicle into elastic and plastic strain of steel.

Positioning the energy absorbing material within a crash cushion will also effect the decision. The concept that requires the simplest method to mount it within a crash cushion is more desirable. A concept can be very effective in stopping a vehicle but virtually impossible to implement into the crash cushion. If a crash cushion concept cannot be implemented, it does not matter how effective it is at stopping the vehicle, it is useless. The cost to implement the concept into the crash cushion is also important. Will it require additional material to hold it in place? Will it require welding or additional hardware? These are all factors that increase the cost to install it.

It is desired to remove the energy absorbing component with ease after a vehicle has impacted the cushion. The more reusable parts a crash cushion has, the lower its repair cost would be. It is expected to be able to replace the energy absorbing component of the crash cushion while reusing other parts. After being mounted in the cushion and after an impact has occurred, how much labor will be required to remove and replace the energy absorbing component? How much will this cost? Will it require additional hardware to remove it? These questions must all be taken into consideration.

Evaluation Matrix

Table 1 is used to evaluate the importance of the above criteria that each concept will be evaluated against. Each category is compared with all other categories. When compared, a decision must be made as to which of the two categories being compared is more important. The category that is most important receives a 1 while the other receives a 0. These comparisons are then tabulated to see how the categories rank in importance with respect to one another.

It can be seen that vehicle deceleration, cushion length, material cost, and cost of installation are the most important factors for concept evaluation. The concept that scores highest in these categories is ranked the highest amongst the others. These values are then used in Table 22 for concept evaluation. The three concepts are each graded on a scale from 0 to 100 for each category. Concepts that are unable to perform well in a given category will score poorly as opposed to those that score well that will receive a higher score. It is clear from Table 2 that the deforming plate concept will be more desired than the other two designs. This will be further supported through the simulations conducted in this research.

Summary

A number of conceptual designs have been developed. When selecting the best concept out of a group, a methodology must be used that eliminates as much bias from the decision as possible. By being able to quantify different areas of the designs themselves, a grading system was used to select the best design. The deforming plate concept is chosen as the better of the three concepts proposed. In future chapters, data will be developed that reinforce the accuracy of the concept selection.

Table 1. Percentage Weight Calculation for Design Evaluation Criteria

Criteria	1. Material Cost	2. Vehicle Deceleration	3. Cushion Length	4. Ease of Installation	5. Cost of Installation	6. Ease of Replacement	7. Cost of Replacement	Total	Net Weights %
1. Material Cost		0	0	1	1	1	1	4	19.05
2. Vehicle Deceleration	1		1	1	1	1	1	6	28.57
3. Cushion Length	1	0		1	1	1	1	5	23.81
4. Ease of Installation	0	0	0		0	1	0	1	4.76
5. Cost of Installation	0	0	0	1		1	1	3	14.29
6. Ease of Replacement	0	0	0	0	0		1	1	4.76
7. Cost of Replacement	0	0	0	1	0	0		1	4.76
Total								21	100.00

Table 2. Evaluation Matrix for the Three Design Concepts

Criteria	% Weight (W)	Expanding Tube Score (S1)	WxS1 / 100	Deforming Angle Score (S2)	WxS2 / 100	Deforming Plate Score (S3)	WxS3 / 100
Material Cost	19.05%	90	17.15	90	17.15	90	17.15
Vehicle Deceleration	28.57%	80	22.86	85	24.28	90	25.71
Cushion Length	23.81%	75	17.86	80	19.05	88	20.95
Ease of Installation	4.76%	80	3.808	87	4.141	95	4.522
Cost of Installation	14.29%	80	11.43	85	12.15	90	12.86
Ease of Replacement	4.76%	70	3.332	88	4.189	95	4.522
Cost of Replacement	4.76%	80	3.808	85	4.046	95	4.522
Total	100%		80.24		85		90.24

CHAPTER III

PENDULUM TESTING

Overview

Before extensive research is conducted with computer modeling, it is good to have a feel for the types of data that should be expected. Running several preliminary physical tests before the simulations are conducted allow for the researcher to match the physical tests with the simulation. By doing this, it ensures that the models have been properly developed and give an accurate depiction of what will occur in physical tests. The physical testing not only provides numerical data seen on plots but also gives good visual data on what happens when the concept is performing its intended function. This and more will be discussed in the following chapters.

Test Facility

The pendulum testing facility at Texas Transportation Institute located at the Texas A&M University Riverside Campus. A mass is suspended with cables that are 38 ft – 10 in long and attached directly above the mass to the main frame seen in Figure 12. The pendulum mass is allowed to swing freely between the supports of the frame. The device that is being tested is installed in the path that is traveled by the pendulum mass and at the lowest point of the swing. The pendulum mass' velocity and kinetic energy can be controlled by controlling the height that it is raised to before being released to swing freely. This is not a concern seeing how the actual mass velocity is measured by instruments at impact.

Figure 12. Pendulum Frame

A motor is used to pull the mass into position at a specified height. The height governs the velocity that the mass will be traveling at the lowest point of the swing and therefore controlling the energy put into the test device. Once at its desired height, the mass is released using a latch and allowed to swing freely into the test structure. The pendulum mass used for expanding tube testing was 870 kg and can be seen in Figure 13. Four tabs are attached to the mass seen below to allow for the attachment of cables used to suspend it.

The front end of the mass has a bumper on it for tests that require the mass to impact the test design. A pin is seen on the other end of the mass. This pin allows for the attachment of cable giving the mass the capability to pull at a test design rather than impact it. The pendulum test allows for testing of a design making use of a reusable mass. This saves time and the cost of a full scale crash test with an actual vehicle.

Figure 13. Pendulum Mass

Figure 14 illustrates the setup used for testing of the expanding tube concept. The pendulum mass suspended by four cables is seen in the upper right hand side of the figure. Attached to the mass is a cable which connects the mass and mandrel which is fastened on to the opposite end of the cable. This allows the energy of the pendulum to be transferred directly to the mandrel. The mandrel is seen at the back end of the pipe seen in the bottom left hand corner of the figure. The pipe is mounted to a stand which is anchored to a concrete footing below preventing movement of the pipe during the test. This allows for the mandrel to be pulled directly through the center of the pipe.

Figure 14. Expanding Tube Pendulum Setup

Instrumentation

An ENDEVCO 22626A-100 accelerometer was used to measure acceleration. A speed trap which uses a pressure sensitive switch is used to measure the velocity at impact. Two wooden dowels are used mounted at the lowest point of the pendulums swing. The distance between the two dowels is measured. When the sensor makes contact with the first dowel, the switch is engaged and measures the time it takes to make contact with the second dowel. Knowing the time the pendulum took to travel the known distance gives the pendulum velocity just before the cable engages with the mandrel. High speed cameras were also used for testing. This made viewing the mandrels travel through the pipe possible. The high speed cameras gave insightful information on the behavior of the mandrel during the test.

Pipe Samples

Figure 15 shows a pipe that has not been welded shut. This is the material intended for use in the expanding tube concept. The pipe is manufactured without being welded shut and then is sold to the consumer.

Three of the test samples can be seen in Figure 16. The pipe samples are welded on to flat plates with holes drilled in the sides. These plates are responsible for holding the pipe in place during testing.

Figure 15. Pipe That Has Not Been Welded Shut

Figure 16. End View of Expanding Tube Test Sample

Mandrel

Figure 17 and Figure 18 show the mandrel used for pendulum testing. The hole bored in the rear of the mandrel is to allow for a threaded swage attached to a cable to be inserted through. The swage will then have a nut fastened on to its end. The pipe welded on to the front adds more stability and gives extra protection against pull out from the expanding tube. This pipe will extend into the unopened portion of the pipe which in turn aids in containment of the mandrel during the test.

The front and rear views of the mandrel are seen in Figure 19 and Figure 20. The front view illustrates the two different size holes inside the design. It can be seen that the pipe welded on to the front of the mandrel has a larger outer diameter than the hole bored into the end for the cable swage.

Figure 17. Expanding Tube Mandrel Rear View

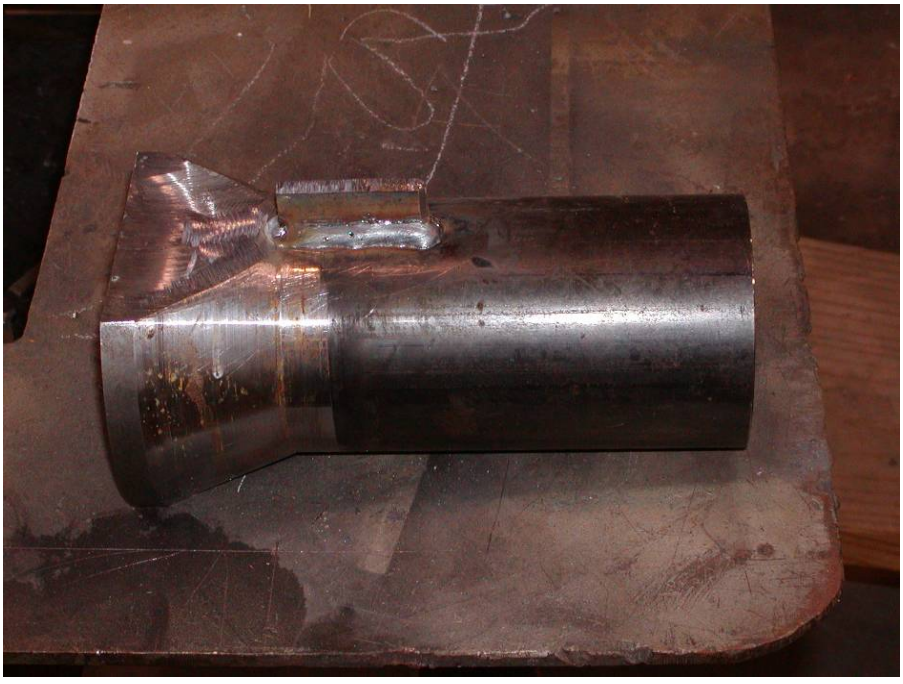

Figure 18. Side View of Expanding Tube Mandrel

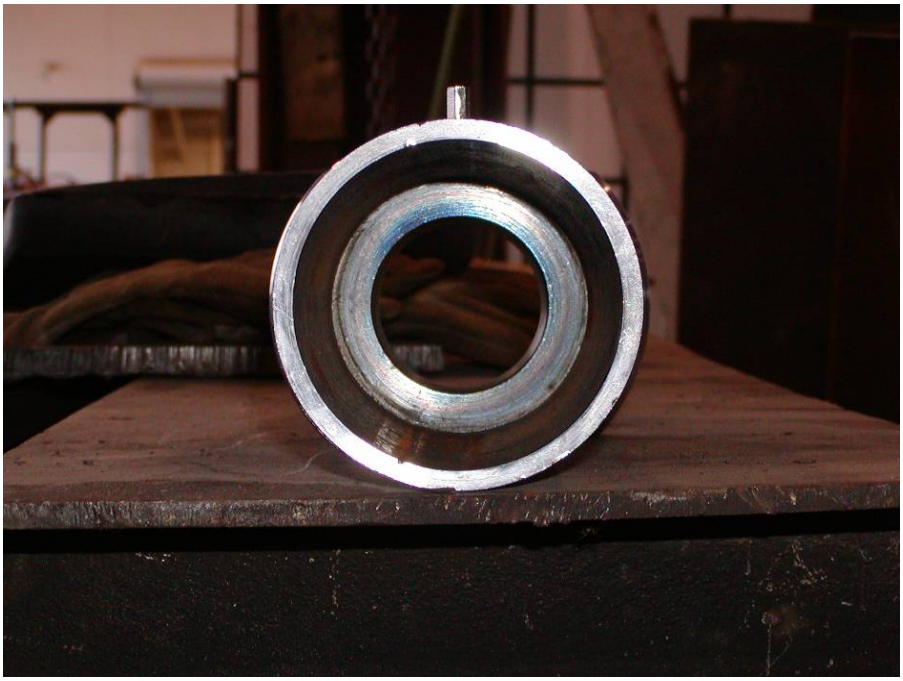

Figure 19. Front View of Expanding Tube Mandrel Illustrating Opening for Cable Swage

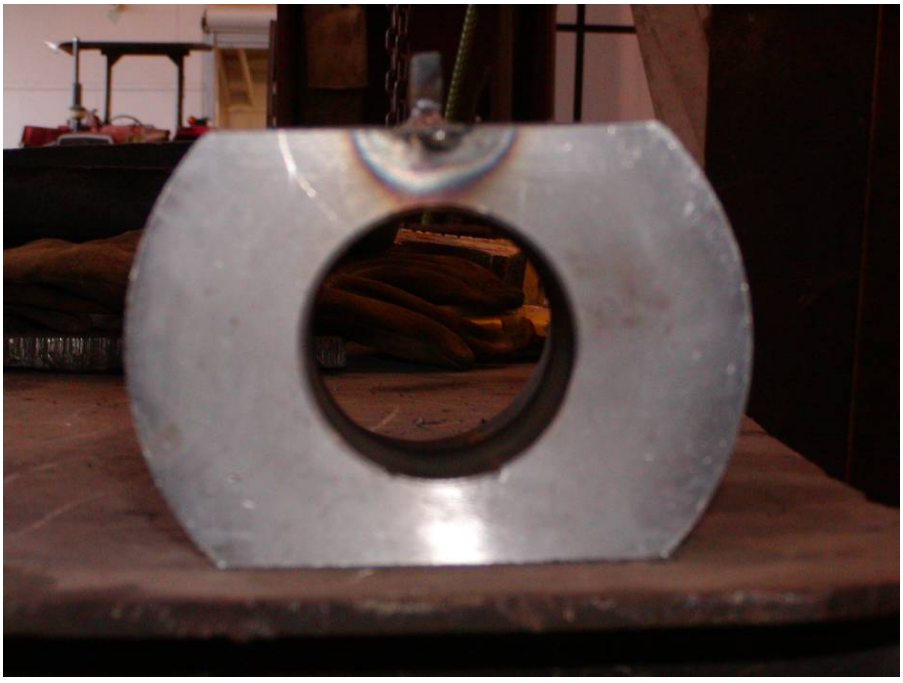

Figure 20. Rear View of Expanding Tube Mandrel Illustrating Weld Penetration

The rear view illustrates the weld penetration from the top “fin” welded in place. The only loads applied to the fin will be from the mandrel trying to rotate during the test. These loads are insignificant and do not pose a threat to the welds used.

Figure 21 and Figure 22 show the mandrels in position inside of the test pipe. The pipe section of the mandrel forms a snug fit in the larger pipe to be expanded. The mandrel will displace and deform the pipe walls a combined 25.4 mm from their initial position.

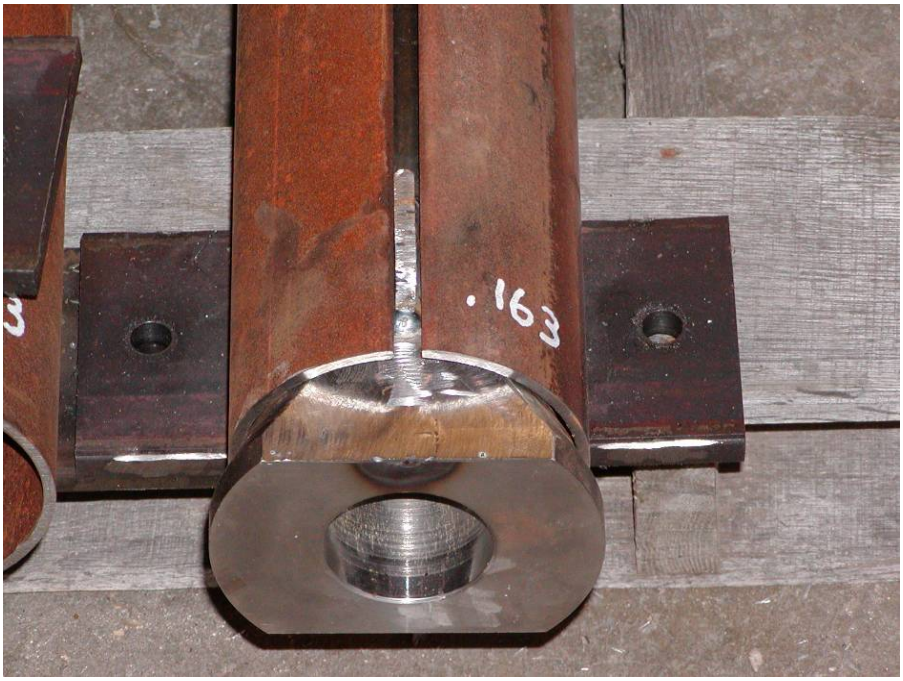

Figure 21. Expanding Tube Mandrel Placed Inside 4-inch Pipe

Figure 22. Expanding Tube Mandrel Placed Inside 3-inch Pipe

Data Recorded

Although various types of data can be taken from a pendulum test, the data that directly pertains to the expanding tube is the deceleration of the mass and its initial velocity. The energy absorbed by the tubing and the velocity reduction through the length of the pipe are then calculated.

Setup

Figure 23 illustrates the mandrel placed inside of the pipe. The cable is then run through the pipe where the threaded swage is then inserted into the mandrel. A nut seen in Figure 24 is then fastened to the swage ensuring that the load from the pendulum mass will be transmitted through the cable and into the mandrel.

Figure 23. Expanding Tube Setup

Figure 24. Nut Fastened to Threaded Swage

Pendulum Test Results

Pendulum testing gave insightful information on the energy absorbing ability of the pipe along with material behavior. Difficulties were encountered when making use of the cable to pull the mandrel through the pipe that affected the data taken. More than just numerical data was taken from these tests. A good deal of valuable information was also gathered from observation of how the material behaved that could not be captured with numeric data. Figure 25 illustrates the testing setup moments before the pendulum mass is raised.

In Figure 25, the test sample with the mandrel inserted inside of it can be seen. The cable fastened on to the mandrel is also attached to the pendulum mass. The mass will then be raised and dropped pulling the mandrel through the length of the pipe. Figure 26 shows the mandrel still lodged inside of the pipe with a 7.62 mm wall thickness after the test had been conducted. This means that the pipe absorbed all the energy supplied by the pendulum mass.

Figure 27 shows the mandrels orientation in the pipe after a test has taken place. If the mandrel had been much wider, there would be a strong possibility of the pipe expanding so much that the opening at the top of the pipe is too wide to contain the mandrel. The rotation of the mandrel would not occur in a physical application in a crash cushion. The mandrel would not travel freely through the pipe; it would be attached in some manner to a sled or frame above it. Rigidly attaching it to a structure will constrain the mandrel and prevent it from rotating.

The thinner walled pipes were unable to absorb all the energy supplied by the mass. Figure 28 shows a thinner walled pipe that has been tested. The resistance to deformation supplied by the pipe's wall was not enough to prevent the mandrel from traveling through its entire length.

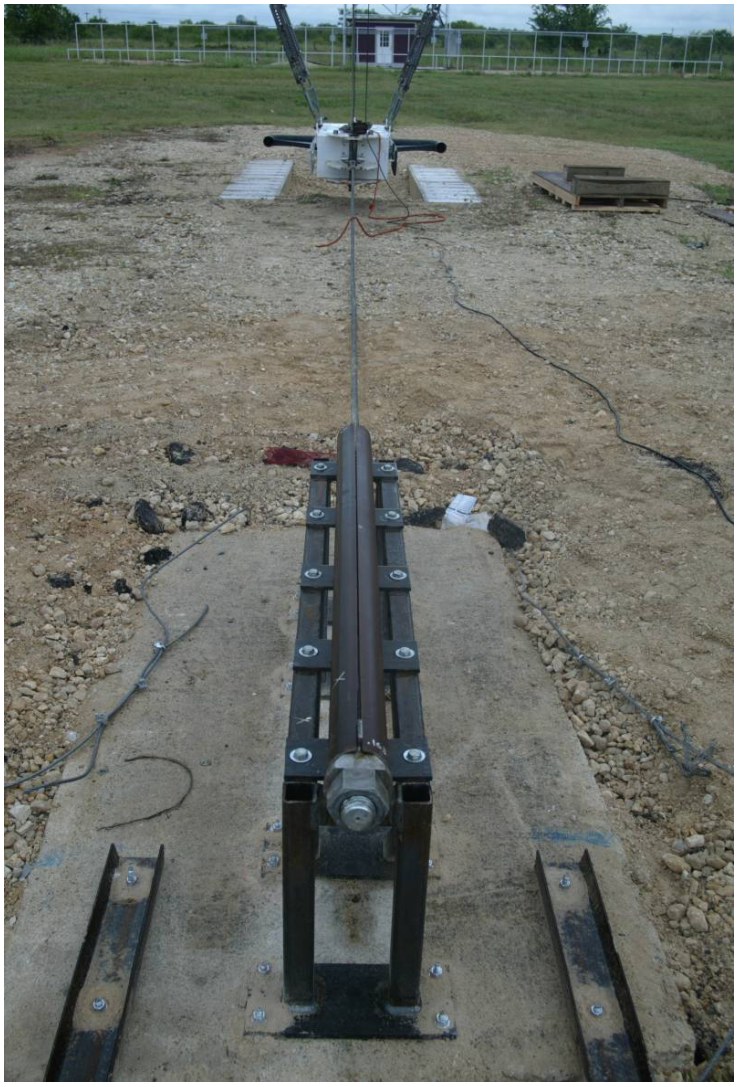

Figure 25. Pre-Test Setup

Figure 26. Mandrel Lodged in Pipe

The mandrel was designed to push the outer walls outward. The pipe is welded at its base and the opening is directly above it. When deformation occurs, the walls will be deformed outward. A round mandrel with a round end cross section versus more of an oval cross section would not have wanted to apply force to 360 degrees around it, not just to the sides like an oval would. Since the pipe is rigidly mounted at its base due to the weld, it cannot deform in that direction. If it cannot deform in a direction that the mandrel is pushing on it, the mandrel will in turn move in the opposite direction. This would have caused the mandrel to displace upward and not have its centroidal axis aligned with the centroidal axis of the pipe. The maximum outer diameter of the mandrel that was pulled through the 76.2 mm pipes was 101.6 mm. The outer diameter of the mandrel pulled through the 101.6 mm pipes was 127 mm. The displacement in the pipe material was 1 inch.

Figure 27. Mandrel Position in Pipe

Figure 28. Pipe after Mandrel Has Traveled Through

Figure 29 shows a thinner walled pipe after the test. It is clear that the only significant plastic deformation that took place during the test is along the welded line at its base. The two sides seemed to “V” outward, pivoting about the welded end. This figure illustrates that the pipe walls still have a great deal of curvature. This indicates that little deformation actually occurs in the pipes walls. The pipes ability to absorb energy relied on the bending along the welded line and friction between the mandrel and the pipe. Seeing how the pipe behaves when the mandrel has been run through it, it is clear that a rounded mandrel is not necessary. Since the wall of the pipe is acting in a manner similar to two cantilever beams fastened to the welded section, it is clear that a flat plate with a greater width dimension than the inner diameter of the pipe could be used to push the walls in opposite directions. This will save on the cost of the mandrels being machined and welded. All that would be needed is a flat plate cut to fit inside the pipe and the addition of a flared back end to deform the wall of the pipe. This mandrel will take on the shape of a trapezoid.

Figure 29. Deformed Pipe after Test

Testing Table

There were 11 test runs on 1473 mm sections of pipe. Two different diameter pipes with varying wall thicknesses were tested. The 76.2 mm diameter pipe had wall thicknesses ranging from 4.14 mm to 7.62 mm. The 101.6 mm diameter pipe had wall thicknesses ranging from 5.23 mm to 6.30 mm. The impact velocities ranged from 26.96 km/hr to 39.27 km/hr. Two of the test samples were neglected for specific reasons. Tests 1 through 7 were on

pipe with wall thicknesses under 5.33 mm. It was noticed as the results were recorded that pipes with this thickness were not absorbing enough energy to have a strong effect if implemented into a crash cushion. The test sample for Test 8 had been measured and logged in to be conducted next. It was decided that testing this sample would not benefit the research because it would not have enough energy absorbing properties to be implemented into a crash cushion. Test 8 was removed from the line up and the testing continued to Test 9. The other test sample left out of the data was Test 10. When running Test 10, the cable used to pull the mandrel through the pipe snagged on the frame holding the pipe in place. The force of the pendulum mass broke the cable. There were no results recorded from this test. Table 3 describes the tests in the order in which they were conducted.

Table 3. General Physical Testing Information

Test No.	Tubing Size	Wall Thickness	Velocity at Impact
1	76.2 mm	4.14 mm	39.27 km/hr
2	76.2 mm	4.27 mm	32.5 km/hr
3	76.2 mm	4.27 mm	26.96 km/hr
4	76.2 mm	4.83 mm	27.57 km/hr
5	101.6 mm	6.29 mm	29.82 km/hr
6	101.6 mm	6.29 mm	26.97 km/hr
7	101.6 mm	5.26 mm	27.52 km/hr
9	76.2 mm	7.62 mm	36.69 km/hr
11	76.2 mm	7.62 mm	36.37 km/hr

Pendulum Test Data

After the tests had been conducted, the accelerometer data was collected and plots were formed.

Figure 30 illustrates the occupant impact velocities induced by the pipe being tested. It is seen that only two pipes were “stiff” enough to decelerate the pendulum mass enough to record an occupant impact velocity. Both occupant

impact velocities recorded were relatively low and fell beneath the maximum allowable occupant impact velocity.

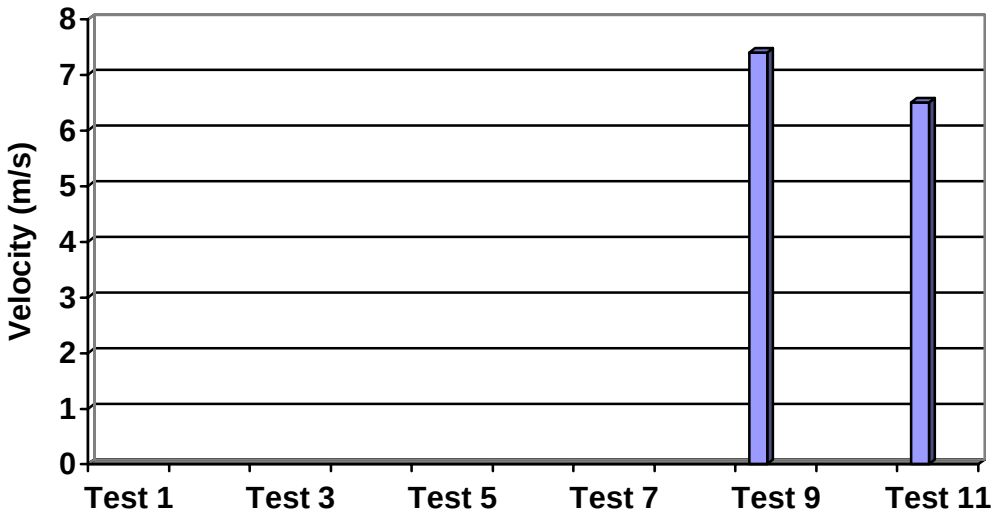

Figure 30. Pendulum Test Occupant Impact Velocities

Figure 31 shows the ridedown accelerations from the pendulum tests. It has been mentioned before that a ridedown acceleration does not occur until an occupant impact velocity has occurred. Only two testing samples produced occupant impact velocities so only two would be eligible to have a ridedown acceleration.

Figure 32 illustrates the 50 milliseconds average acceleration from the tests. Unlike the ridedown accelerations, the 50 millisecond average acceleration does not have to have an occupant impact velocity occur in order to be recorded. It is clear from the figure that Test 9 and Test 11 had the highest decelerations of the pendulum mass. This can be explained by their walls being thicker than the rest making them “stiffer” samples. The ridedown decelerations have about a 4 g difference. This does not seem correct since both tests were run at the same velocity on the same pipe and the same displacement. This discrepancy can be described by the whipping of the cable adding random

acceleration spikes in the data. The ridedown deceleration is a 10 milliseconds average of the accelerations and will not capture a good average of accelerations. The 50 milliseconds average accelerations of these two tests are much closer varying by close to 0.5 g's. This is because the 50 milliseconds average of accelerations will capture more high and low spots than the 10 milliseconds average. In the event there is a grouping of deceleration spikes, these were averaged in with the low spots. The 50 milliseconds average gave a better idea of the deceleration that the pipe can create.

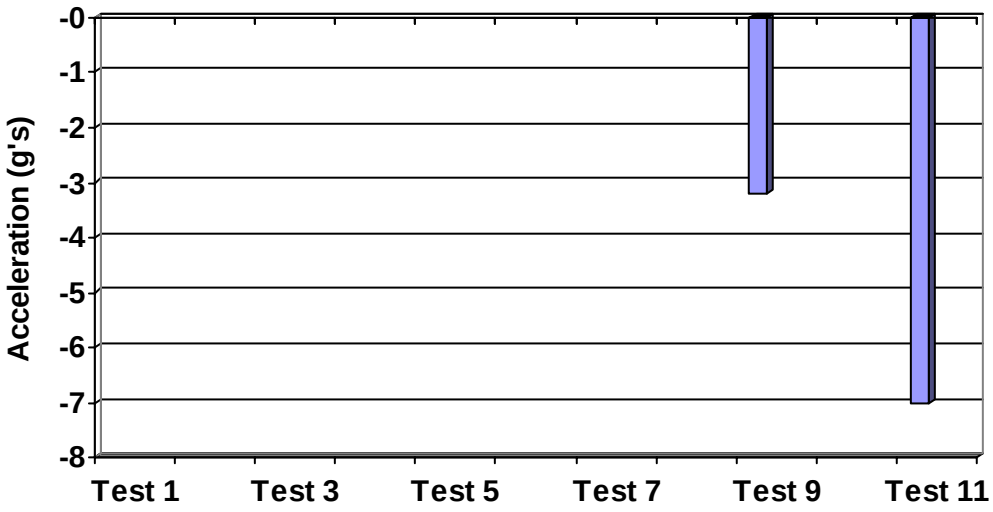

Figure 31. Pendulum Test Ridedown Accelerations

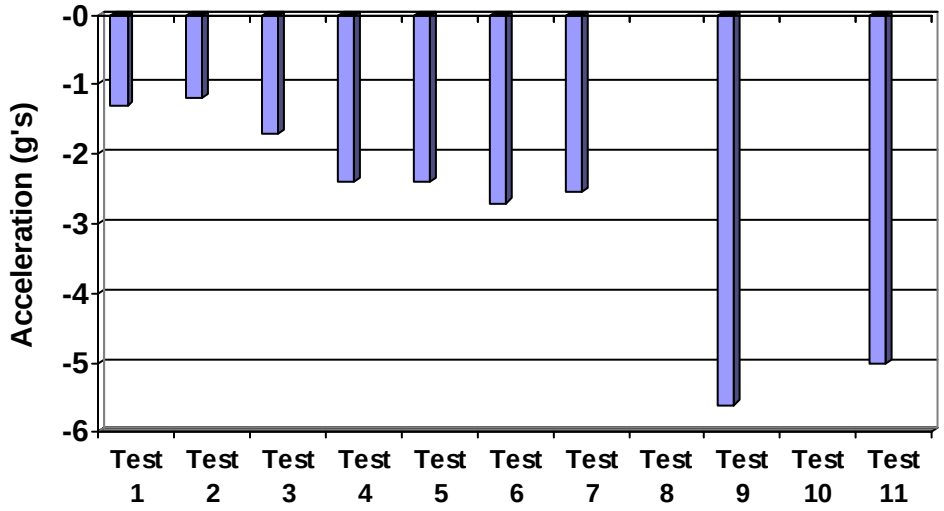

Figure 32. Pendulum Test 50 Milliseconds Average Accelerations

The first three tests were 76.2 mm diameter pipes with thicknesses that were very similar. The wall thickness varied by only 0.127 mm in one of the tubes. This was evident in the results as all three pipes had decelerations that were very close. The fourth test used a pipe that was slightly thicker than the first three. The result was no surprise; it had a deceleration that was greater than the first three.

The focus of the testing was then placed on the 101.6 mm diameter pipe. This pipe had thicker walls than the previous four tests. Although the pipe had thicker walls, the deceleration values were not much higher. This can be explained by the behavior of the pipe wall during deformation. The pipe walls can be considered to be similar to two cantilever beams attached at the point of weld. When bending a cantilever beam, the further away from the constrained edge that the load is applied, the greater the moment arm created. With the moment arm increasing, the force required to bend the beam decreases. This concept applies to the deformation of the pipes. The mandrel applied a force very close to the center of the pipe wall (half the distance from the welded base to the opening on the top). When the pipe diameter is increased, the mandrel actually applies a load at a point higher than that of the smaller diameter pipe.

This causes a larger moment arm. This can be seen in Figure 33 where the moment arm of the smaller pipe A is smaller than the moment arm in the larger pipe B. Choosing larger pipe with thicker walls is not necessarily the most efficient way to absorb more energy. The cost of the pipe will increase only to have its added size work against itself in performance.

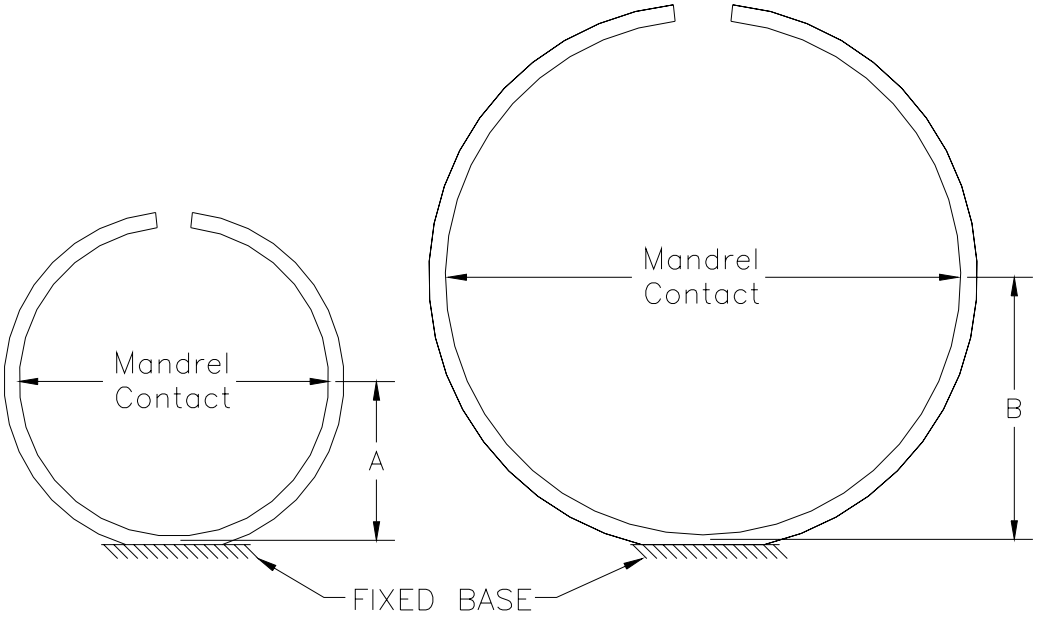

Figure 33. Moment Arm in Pipe

Although the pipe wall is thicker, the force required to deform it reduces due to the increased moment arm. The larger pipe also experienced the same one inch deformation. If you compare two cantilever beams, one with a short length and the other with a longer length. Displace the very end of both beams the same amount. It will be found that there will be less plastic deformation in the longer beam and less force will be needed for this displacement in the longer of the two. This explains why the larger pipe did not decelerate the pendulum mass much more than the smaller diameter pipe.

The acceleration plots seen in Figure 34, Figure 35, and Figure 36 show various spikes that are not consistent with the rest of the data recorded for that

particular test. A review was done of the high speed camera footage used during the test and the reason for the spikes was discovered. When the pendulum mass was dropped, the cable that attached the mass to the mandrel also fell causing slack in the cable. The weight of the mass then pulled the cable tight. Due to the size of the cable, its mass had considerable momentum while whipping. This momentum carried over and the cable stayed in motion sideways pulling the mandrel further through the pipe. After traveling sideways, the cable came to a stop with slack in it. The mass continued to pull the slack out of the cable causing it to “whip” back in its initial direction. In the time that the cable traveled from its slacked position to its taut position, the mandrel came to a complete stop. It was only when the cable traveled from its taut position to the slacked position that the mandrel was pulled further through the pipe.

The cable “whipping” during the test created a characteristic trait in the deceleration plots of the test. Figure 34 shows the decoration of the pendulum mass versus time as the mandrel traveled through the length of the pipe. These spikes are also seen in Figure 35 and Figure 36. As the cable whipped from side to side, the mandrel would come to a complete stop in the pipe.

The force of the pendulum mass would be transmitted into the mandrel only at certain times through the duration of the test. The load was not constant applied to the mandrel through the duration of the test. In response to this, the mandrel actually came to stops in the pipe several times. Each time the mandrel was forced to a stop, the pendulum mass experienced a deceleration. This explains the peaks from the spikes on the deceleration plots.

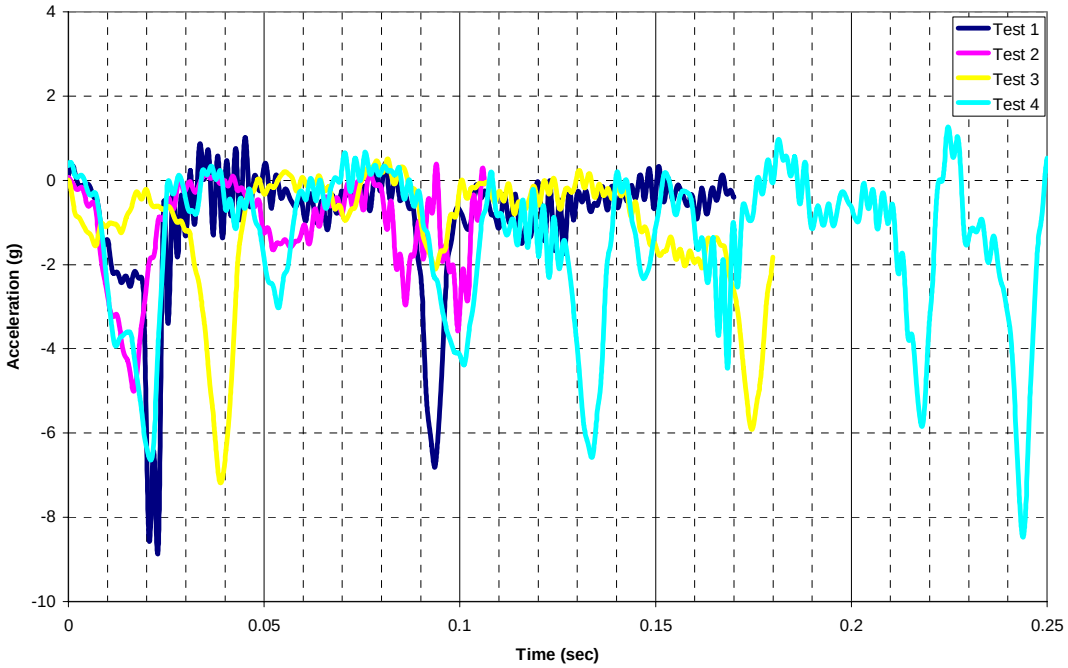

Figure 34. Acceleration Plots from Test 1 through Test 4

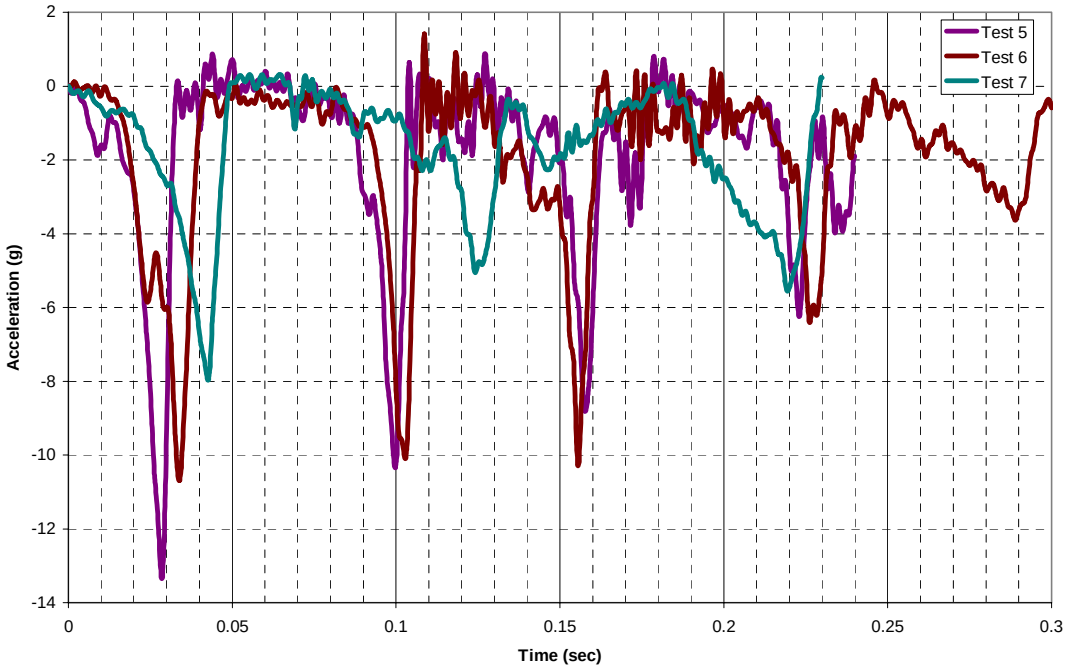

Figure 35. Acceleration Plots from Test 5 through Test 7

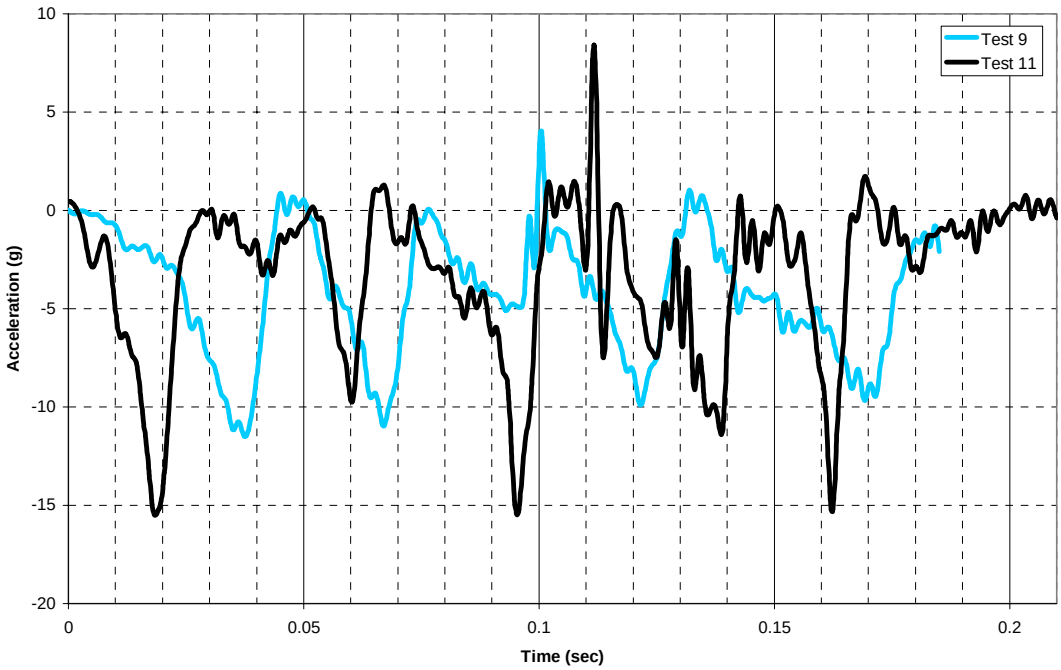

Figure 36. Acceleration Plots from Test 9 and Test 11

It must be noted that the occupant impact velocity, ridedown acceleration, and the 50 milliseconds average acceleration were all calculated from the acceleration data provided by these plots. With random acceleration spikes that could occur anywhere on the plot it is clear that the smaller the window of time within which an average is taken, the less accurate it may be. If these acceleration spikes occur evenly distributed throughout the test then the 10 and 50 milliseconds average accelerations will average out a section of time that may have one high spot and the rest low spots. When the maximum average acceleration from all the time intervals taken is given, it will be very low compared to a plot that had all the acceleration spikes grouped together in one section of time. On the data received from the pendulum tests, the spikes are relatively evenly distributed throughout the length of the time duration.

Pendulum Velocity

The velocity of the pendulum mass can be calculated from the acceleration and time data recorded by the instrumentation. Acceleration data is measured every 0.000099 seconds. By taking the value of acceleration a_i at a given point in time t_i and the value of acceleration a_{i-1} at the time t_{i-1}, the overall change in velocity of the pendulum can be calculated.

$$\Delta V_i = \Delta V_{i-1} + \left[\left(\frac{a_i - a_{i-1}}{2} \right) \left(t_i - t_{i-1} \right) \right] \qquad (80)$$

This will yield ΔV which is the overall change in velocity of the mass from one point in time to another. The speed of the pendulum at that instant can then be calculated. The pendulum mass' velocity at any point in time during the test can be calculated by subtracting the change in velocity ΔV_i from the initial velocity.

Knowing this, the velocity of the pendulum as the mandrel travels through the pipe can be calculated.

Energy Absorbed

The above velocity calculations will now be used to help calculate the energy that is absorbed by the expanding tube. The swinging mass has kinetic energy that is absorbed by the pipe wall deformation. This deformation is caused by the mandrel that is attached to the mass being pulled through the pipe's length. The kinetic energy is being transformed into strain of the deforming steel. Work done by the mandrel on the tubing as it passes through is seen as the resisting force that the pipe walls apply to the mandrel in the direction of its travel over the distance the mandrel travels. It should be noted that the mandrel and the swinging mass both travel the same distance because they are attached to one another.

$$Work\_Done = \left(\mathrm{Re}\, sisting\_Force\_of\_Pipe \right) \left(Dis\tan ce\_Mandrel\_Travels \right) \qquad (81)$$

In the case of the pendulum mass swinging, the force F applied to the mandrel is measured when the deceleration $a_{Pendulum\_i}$ and mass $m_{Pendulum}$ values are known.

$$F_i = \left(m_{Pendulum}\right)\left(a_{Pendulum\_i}\right) \tag{82}$$

When this force is applied over a distance $d_{Mandrel}$ the work done can be calculated. The distance must first be calculated.

$$d_{Mandrel\_i} = d_{Mandrel\_i-1} + \left[\left(\frac{V_i + V_{i-1}}{2}\right)\left(t_i - t_{i-1}\right)\right] \tag{83}$$

The calculated work done by the mandrel deforming the pipe wall is

$$Work\_Done = \sum_{i=1}^{n}\left(d_{Mandrel\_i}\right)\left(F_i\right) \tag{84}$$

This is a measure of the energy that is absorbed by the tubing. The plot of energy absorbed is seen in Figure 37. It is clear that the pipe samples with the largest wall thickness were able to absorb the most energy. It was seen that as the vehicular deceleration increased, the amount of energy being absorbed increased.

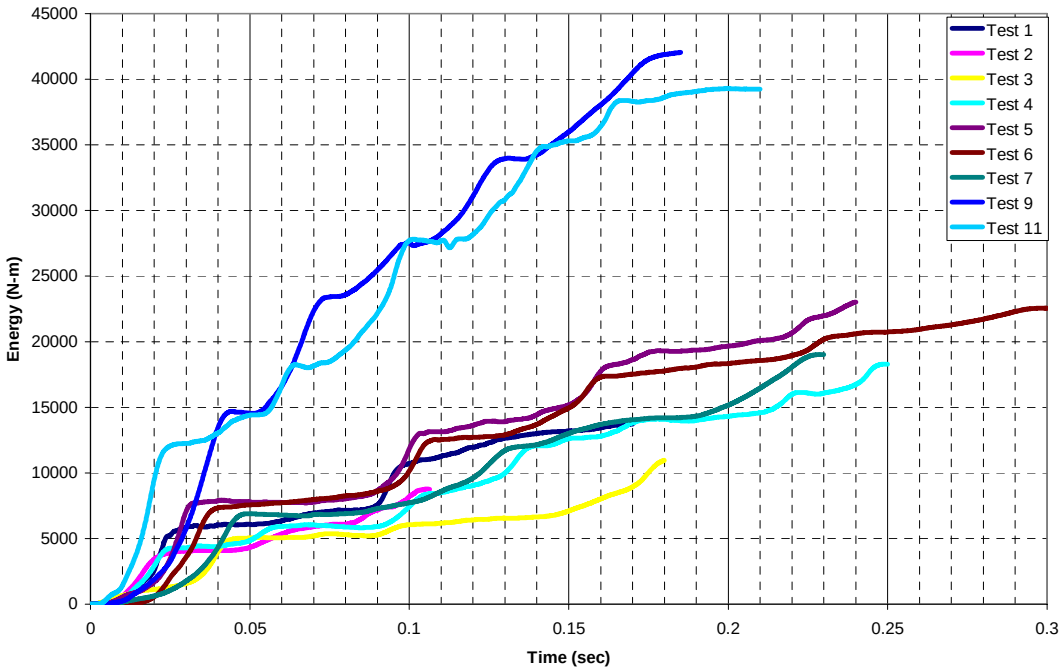

Figure 37. Plots of Energy Absorbed by Test Samples

Observations During Test

Tests 6, 9, and 11 were able to stop the mandrel before it exited the pipe. The mandrel was pulled completely through all other test samples. The 101.6 mm pipe stopped the mandrel after it traveled 1474 mm through the pipe. The 76.2 mm pipe used in Test 9 and 11 were samples that had the same length, were made of the same material, and had the same pipe thickness. The impact velocity's of the two tests differed by only 0.089 m/s. This means that the pipes both absorbed virtually the same amount of energy. The two samples were able to stop the mass after traveling 1083 mm and 1253 mm through the pipe sample. The discrepancy could be explained by the uniformity of the wall thickness throughout the pipe. Measurements of pipe wall thickness cannot reasonably be taken at every single point through the pipes length. It is possible for a wall to measure 7.62 mm at two points on its length and fall beneath this thickness at other points. The different stopping distances could possibly be described by the wall being thinner at some locations.

Summary

The data gathered from physical testing was captured not just in plots and data points but in photographs and high speed film. All of these used together provide valuable information that is useful in judging and improving the concept in question. Future sections will explore the computer modeling and simulation of the concepts being researched. The pendulum testing on the expanding tube will be used to verify the accuracy of the simulations.

CHAPTER IV

SIMULATIONS

Overview

In previous chapters, energy absorbing conceptual designs have been developed. Crash cushion requirements that these concepts must meet have also been discussed. The concepts developed must be tested to ensure their viability. Although a full scale physical test is preferred, the significant cost of physical testing makes tests for every concept economically infeasible. A way to test the viability of the concepts is to make use of finite element analysis (FEA). This allows the same tests required to verify a concept's worthiness to be conducted without the high cost of physical testing. Numerical experiment of the concepts using FEA is a good way to identify the best concept and optimize it before the high cost physical tests are conducted. The following section is a discussion of the FEA procedures conducted on the three concepts discussed earlier.

Software

Finite element simulation is used to gain valuable information on the materials behavior under the loads applied to them. Hypermesh which is a product of Altair, Inc., is used to create a model's geometry, boundary conditions, and element mesh. This model is then used by LS-DYNA which is capable of analyzing dynamic events. The results of this are then processed using Hyperview which is a program used to present the data from the LS-DYNA run. Another program called TRAP is then used to aid in the calculation of occupant impact velocity, ridedown decelerations, and 50 milliseconds average decelerations. The software used in this research are helpful tools to judge how

a concept would perform. Over all, 128 simulations were conducted on the concepts. Simulations are an effective way to gather data while saving time and cost that would be spent on numerous physical tests.

Element and Material Properties

Each of the models developed for this research are very similar. They each consist of three main components which were a large mass which simulated the vehicle, the deforming steel component, and a mandrel used to deform the steel component. The simulations used to verify the pendulum data also made use of a cable. The mass simulating the mass of a vehicle was made of solid elements which were given rigid material properties. The deforming steel components made use of shell elements that were given piecewise linear plasticity material properties. The mandrels also made use of shell elements but were given rigid material properties since they are not expected to deform in physical tests. The cable made use of beam elements and were given cable discrete beam material properties.

Shell elements were used because they were able to accurately simulate the geometry of the structural steel. They are good for materials that are much thinner in one direction than the other two. Shell elements are located in the space in the middle of the plane of the solid that they are representing. They are then given a specified thickness equal to that of the deforming steel in question. They are capable of resisting axial loads and moments just as structural steel can. The solid element was used because it is a good way to represent a bulky component such as the vehicle mass. They were not used to represent other components of the model because it would require an unreasonable amount of these elements. The increase in elements will increase the simulation's run time. The beam elements represent the a structure that is much longer in one direction than the other two. This is a good representation of the cable in use.

For the deforming components of the concepts, piecewise linear plasticity material was the best choice. This means that up to the point at which the material yields, it is considered to be linearly elastic. Once yielding occurs, it can deform plastically and strain hardening can occur. As a piecewise linear plastic material, the material is subject to strain-rate effects. In order to accurately evaluate the nonlinear behavior of the material, a series of stress and strain points that come from physical tensile tests were loaded into the model. The material properties used in the model are seen in Table 4. It should be noted that the yield stress used for the models was the same yield stress of the steel used in the pendulum testing on the expanding tube. This is seen in the mill test certificate for the expanding tube in Appendix A. The certificate indicates that one of the yield stresses recorded from the material was 48738 psi which is equivalent to 336.04 MPa. This is the value that was used in the simulations. The steel can be considered mild steel because it has less than 0.25% of Carbon. The material simulated had 0.07% of Carbon. The stress and strain points for steel used are seen in Table 5.

Table 4. Material Properties Used for Steel

Mass Density (kg/m^3) ρ	7.86E+03
Young's Modulus (MPa) E	200,000
Poisson's Ratio Nu	0.29
Yield Stress (MPa) σ_y	336

Table 5. Stress-Strain Curve for Yielded Steel

Effective Plastic Strain	True Stress (MPa)
0	336
0.024	336.7
0.042	401.2
0.05	434.3
0.141	537.2
0.213	589.6
0.25	675
0.259	667

The model meshes developed were done with the monetary cost of the simulation in mind. The longer a run takes to complete, the more it will cost to use the facilities. With limited funds, this must be taken into consideration. One of the largest factors in simulation run time is element size and shape. The elements used were kept at a square shape where possible. The elements of material that were not expected to deform or undergo any significant loads were kept to approximately 25.4 mm squares. The elements which were deforming and providing the needed data were kept to approximately 12.7 mm square. These values did vary slightly to appropriately accommodate the concept being modeled. An example of a LS-DYNA key file is seen in Appendix B.

Applicable LS-DYNA Theory

Since LS-DYNA is being used as a tool for the research at hand, it is imperative to have an understanding of how it works in order to effectively use it. When LS-DYNA is running, it travels through an integration loop. This loop is the process of what the program is doing and in what step order.

1. Apply force boundary conditions
2. Process brick, beam, and shell elements
3. Process discrete elements
4. Process penalty based contact interfaces
5. Update accelerations and apply kinematic B.C.’s
6. Kinematic based contact and all rigid walls
7. Write databases
8. Update velocities
9. Update displacements and new geometry
10. Update current time and check for termination
11. Return to Step 1 and repeat

This loop is repeated until the run is terminated. Once terminated, the user can then use the data calculated to make educated decisions about the configuration being tested.

Although this software is very powerful and useful, there are fees for usage. It is because of this that the run times are desired to be as short as possible. One factor that influences the length of the run is the time step calculation. The simulation is programmed to run for a specific time. It can take days to run a simulation that simulates a 0.3 second simulation. As the number of elements in a model increases, so does the time it takes to run through the loop above. When running at a very small time step, this loop takes place many more times than if the time step were large. The time step size for shell elements is calculated by

$$\Delta t = \frac{L_e}{c} \tag{85}$$

where L_e and c are the characteristic length and longitudinal stress wave respectively.

$$c = \sqrt{\frac{E}{\rho\left(1-v^2\right)}} \tag{86}$$

Where the value of c is dependent on the materials modulus of elasticity E, poisons ratio v, and density ρ. The characteristic length is seen as

$$L_e = \frac{\left(1+\beta\right)A_e}{\max\left(L_1, L_2, L_3, \left(1-\beta\right)L_4\right)} \tag{87}$$

In the event that a quadrilateral element is used, β=0 and if a triangular element is used, β=1. A_e is the elements area and L_1, L_2, L_3, and L_4 are the lengths of the shell elements sides. From the above equations it can be seen that the elements geometry effects the time step. A larger element with a larger area will yield a larger time step. The large time step will make for a shorter simulation run time. This does not mean that a user should use as big of elements as possible. A finer mesh will give more realistic data as to how the material will perform.

The elements that will be providing the needed information are the shell elements. They are used to make up the deforming components of the model which provide the needed data used to evaluate a design. For a shell element, this information is derived from the mean pressure *p*, deviatoric stress s_{ij}, deviatoric strain $\varepsilon_{ij}^{'}$, and volumetric strain ε_v.

$$p = -\frac{1}{3}\sigma_{ij}\delta_{ij} \tag{88}$$

$$s_{ij} = \sigma_{ij} + p\delta_{ij} \tag{89}$$

$$\varepsilon_{ij}^{'} = \varepsilon_{ij} - \frac{1}{3}\varepsilon_v \tag{90}$$

$$\varepsilon_v = \varepsilon_{ij}\delta_{ij} \tag{91}$$

The deviatoric strain rate $\dot{\varepsilon}_{ij}^{'}$, deviatoric stress rate $\dot{s}_{ij}$, and volumetric strain rate $\dot{\varepsilon}_v$ are then seen as the following.

$$\dot{\varepsilon}_{ij}^{'} = \dot{\varepsilon}_{ij} - \frac{1}{3}\dot{\varepsilon}_v \tag{92}$$

$$\dot{s}_{ij} = 2G\dot{\varepsilon}_{ij}^{'} \tag{93}$$

$$\dot{\varepsilon}_v = \dot{\varepsilon}_{ij}\delta_{ij} \tag{94}$$

The Jaumann rate of deviatoric stress is

$$s_{ij}^{\nabla} = \dot{s}_{ij} - s_{ip}\Omega_{pj} - s_{jp}\Omega_{pi} \tag{95}$$

The deviatoric stress s_{ij}^{n} is updated to s_{ij}^{n+1} elastically

$${}^{*}s_{ij}^{n+1} = s_{ij}^{n} + s_{ip}\Omega_{pj} + s_{jp}\Omega_{pi} + 2G\dot{\varepsilon}_{ij}^{'}dt = s_{ij}^{n} + R_{ij} + 2G\dot{\varepsilon}_{ij}^{'}dt = s_{ij}^{R^n} + 2G\Delta\varepsilon_{ij}^{'} \tag{96}$$

The left superscript * indicates a trial stress value. The effective trial stress is

$$s^{*} = \left(\frac{3}{2}\,{}^{*}s_{ij}^{n+1}\,{}^{*}s_{ij}^{n+1}\right)^{1/2} \tag{97}$$

If s^{*} exceeds the yield stress σ_y of the material

$$\phi = \frac{1}{2}s_{ij}s_{ij} - \frac{\sigma_y^2}{3} \le 0 \tag{98}$$

does not hold true and the trial stress is scaled back to the yield surface

$$s_{ij}^{n+1} = \frac{\sigma_y}{s^*} {}^* s_{ij}^{n+1} = m^* s_{ij}^{n+1} \tag{99}$$

The plastic strain increment is then found by subtracting the deviatoric part of the strain increment that is elastic

$$\frac{1}{2G}\left(s_{ij}^{n+1} - s_{ij}^{R^n}\right) \tag{100}$$

where *G* is the shear modulus. From the total deviatoric increment $\Delta\varepsilon_{ij}^{'}$

$$\Delta\varepsilon_{ij}^{p} = \Delta\varepsilon_{ij}^{'} - \frac{1}{2G}\left(s_{ij}^{n+1} - s_{ij}^{R^n}\right) \tag{101}$$

where

$$\Delta\varepsilon_{ij}^{'} = \frac{{}^* s_{ij}^{n+1} - s_{ij}^{R^n}}{2G} \tag{102}$$

which gives

$$\Delta\varepsilon_{ij}^{p} = \frac{{}^* s_{ij}^{n+1} - s_{ij}^{n+1}}{2G} = \frac{1-m}{2Gm} s_{ij}^{n+1} \tag{103}$$

The definition of the increment in effective plastic strain is

$$\Delta\varepsilon^{p} = \left(\frac{2}{3}\Delta\varepsilon_{ij}^{p}\Delta\varepsilon_{ij}^{p}\right)^{1/2} \tag{104}$$

and from the above equations, the following can be developed

$$\Delta\varepsilon_{ij}^{p}\Delta\varepsilon_{ij}^{p} = \left(\frac{1-m}{2G}\right)^2 {}^* s_{ij}^{n+1\,*} s_{ij}^{n+1} \tag{105}$$

and then

$$\frac{3}{2}\Delta\varepsilon^{p^2} = \left(\frac{1-m}{2G}\right)^2 \frac{2}{3} s^{*2} \tag{106}$$

which means that

$$\Delta\varepsilon^{p} = \frac{1-m}{3G} s^* = \frac{s^* - \sigma_y}{3G} \tag{107}$$

where

$$m = \frac{\sigma_y}{s^*} \tag{108}$$

When considering isotropic hardening

$$\sigma_y^{n+1} = \sigma_y^n + E^p \Delta\varepsilon^p \tag{109}$$

and from earlier equations

$$\Delta\varepsilon^p = \frac{\left(s^* - \sigma_y^{n+1}\right)}{3G} = \frac{\left(s^* - \sigma_y^n - E^p \Delta\varepsilon^p\right)}{3G} \tag{110}$$

therefore

$$\left(3G + E^p\right)\Delta\varepsilon^p = \left(s^* - \sigma_y^n\right) \tag{111}$$

making the incremental plastic strain into

$$\Delta\varepsilon^p = \frac{\left(s^* - \sigma_y^n\right)}{\left(3G + E^p\right)} \tag{112}$$

When a simulation is taking place, the following steps are taken for plastic loading if the effective trial stress is greater than the yield stress.

1. Solve for the plastic strain increment

$$\Delta\varepsilon^p = \frac{\left(s^* - \sigma_y^n\right)}{\left(3G + E^p\right)} \tag{113}$$

2. Update the plastic strain

$$\varepsilon^{p^{n+1}} = \varepsilon^{p^n} + \Delta\varepsilon^p \tag{114}$$

3. Update the yield stress

$$\sigma_y^{n+1} = \sigma_y^n + E^p \Delta\varepsilon^p \tag{115}$$

4. Compute the scale factor using the yield strength at time n+1

$$m = \frac{\sigma_y^{n+1}}{s^*} \tag{116}$$

5. Return the deviatoric stresses to the yield surface

$$s_{ij}^{n+1} = m^* s_{ij}^{n+1} \tag{117}$$

One powerful aspect of the simulation software is its ability to take a materials increase in stiffness due to strain rate into consideration. The material used in the models are piecewise linear isotropic plasticity material. This material's behavior to stress application is influenced by strain rate $\dot{\varepsilon}$. Deformations are considered to be in the elastic range until the following inequality with yield function, ϕ, is satisfied,

$$\phi = \frac{1}{2} s_{ij} s_{ij} - \frac{\sigma_y^2}{3} \leq 0 \tag{118}$$

The new yield stress σ_y is also defined as a function of σ_o which is the current yield strength and β which is a factor that scales the yield stress and accounts for strain rate effects.

$$\sigma_y = \beta\left[\sigma_o + f_h\left(\varepsilon_{eff}^p\right)\right] \tag{119}$$

$$\beta = 1 + \left(\frac{\dot{\varepsilon}}{C}\right)^{1/p} \tag{120}$$

$$\dot{\varepsilon} = \sqrt{\dot{\varepsilon}_{ij}\dot{\varepsilon}_{ij}} \tag{121}$$

In the above equation, C is a Cowper-Symonds strain rate parameter and $f_h\left(\varepsilon_{eff}^p\right)$ is the hardening function. It is also seen that for linear hardening

$$f_h\left(\varepsilon_{eff}^p\right) = E_p\left(\varepsilon_{eff}^p\right) \tag{122}$$

where E_p is the is the plastic hardening modulus defined as

$$E_p = \frac{E_t E}{E - E_t} \tag{123}$$

where E_t is the slope of the plastic strain of the stress-strain curve and the effective plastic strain rate is seen as

$$\varepsilon_{eff}^p = \int_0^t \left(\frac{2}{3}\dot{\varepsilon}_{ij}^p \dot{\varepsilon}_{ij}^p\right)^{1/2} dt \tag{124}$$

and

$$\dot{\varepsilon}_{ij}^p = \dot{\varepsilon}_{ij} - \dot{\varepsilon}_{ij}^e \tag{125}$$

which is the difference between the total strain rate, $\dot{\varepsilon}_{ij}$, and elastic strain rate, $\dot{\varepsilon}_{ij}^{e}$.

The deviatoric stresses are updated elastically

$$s_{ij}^{\nabla^{n+1/2}} = 2G\dot{\varepsilon}'^{n+1/2}_{ij} \tag{126}$$

and the yield function is checked. If it is not satisfied, an increment in plastic strain is computed

$$\Delta\varepsilon_{eff}^{p} = \frac{\left(\frac{3}{2}s_{ij}^{*}s_{ij}^{*}\right)^{1/2} - \sigma_{y}}{3G + E_{p}} \tag{127}$$

When this is done, the trial deviatoric stress state s_{ij}^{*} is scaled back

$$s_{ij}^{n+1} = \frac{\sigma_{y}}{\left(\frac{3}{2}s_{ij}^{*}s_{ij}^{*}\right)^{1/2}} s_{ij}^{*} \tag{128}$$

and

$$s_{ij}^{*} = \sigma_{ij}^{*} - \frac{1}{3}\sigma_{kk}^{*} \tag{129}$$

at n+1. The superscript * indicates a trial stress value (LS-DYNA 1998). It must be noted that the Cowper-Symonds model was not needed for this research because a plastic curve was input for the material being deformed.

Concept Models

All three of the concepts were modeled and tested in a similar fashion. They all had two different masses constrained to the mandrels. When the mass is in motion, it pulls the mandrel through the length of the energy absorbing concept. Figure 38 illustrates the mass used for all the models. The density of this element could be varied to increase or decrease its mass. This increase and decrease in mass allowed this particular element to accurately represent

smaller vehicles along with larger vehicles. The required masses of 820 kg and 2000 kg were used for the two different vehicle sizes. This figure shows the mass close to a concept. It can be noticed that it is not attached to anything. The program allows for the mass to be constrained to the mandrel without having anything in between them. This means that the axial displacement of the mandrel and the mass will always be the same. Due to the fact that only the mandrel is being tested, the block cannot push it through the concept due to the small geometry of the energy absorbing component and the larger geometry of the mass element. Since the block is unable to push the mandrel through the concept, it pulls it through instead. Figure 38 illustrates the mass at the exit end of the energy absorbing concept. Not seen in the figure is the mandrel which is located at the front of the concept. The mass will be moving away from the concept and pulling the mandrel along.

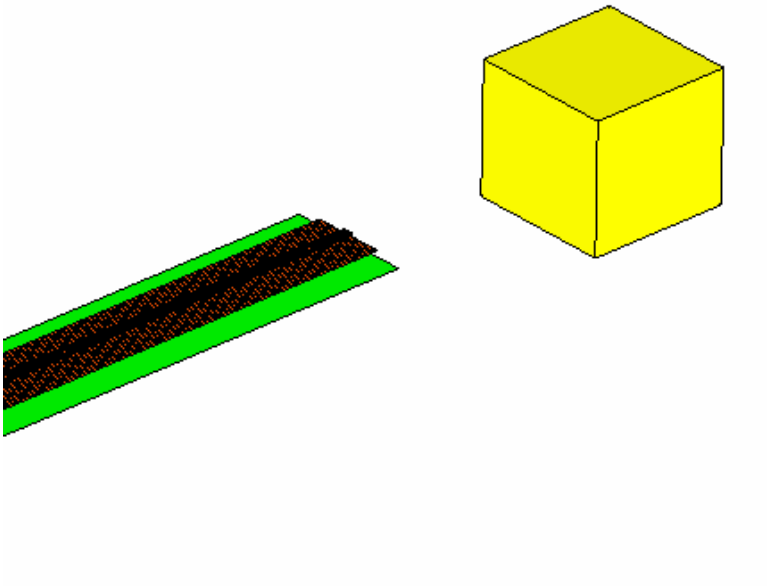

Figure 38. Mass Used in Models

It must be noted that each of the concepts has similar variables. There is the thickness of the material being deformed, the orientation of the mandrel with the deforming material, and the displacement of the deforming material caused by the mandrel. There are an infinite number of deforming material thickness,

mandrel orientation, and displacement combinations. It would be impossible and unrealistic to test every possible combination. The variations tested in the simulations were the most realistic. The data plots created from the results of the simulations leave room for interpolation to get an idea of how other combinations would perform. Although the plots only show a limited number of points compared to the number of combination possibilities, the plots can still be useful in the development of crash cushions. These data points found through the research allow one to make educated decisions as to what material and deformations to use in the analysis looping described above. Without the data, one would be blindly testing random variations. These data plots will reduce the number of future simulations required to explore the energy absorbing capability of various geometries.

In order to reduce the simulation times, the runs were stopped after an occupant impact velocity, ridedown acceleration, and 50 milliseconds average acceleration were found. These are the data values that are desired from the simulations. The crash cushion is desired to be physically as short as possible. This makes stopping distances an important focus. The stopping distance is controlled by the acceleration of the vehicle. As the vehicle's acceleration approaches the maximum allowable acceleration, the stopping distance will approach its optimal length. Since acceleration is the controlling factor in stopping distance, the focus was placed upon it and stopping distances were not recorded from the simulations that were able to stop the mass.

Each of the three concepts used a single mandrel. No two mandrels for the three concepts were alike. The conceptual mandrel traveled through 4.572 meters of deforming material. If decelerations within this length are not high enough to yield an occupant impact velocity or ridedown deceleration then the material is not desired. If a certain configuration is able to yield values for this criterion in an acceptable distance then it should not be considered an appealing configuration and should not be used.

Expanding Tube Model

Expanding Tube Simulation Model with Oval Mandrels. The mandrels modeled for simulation are composed of two main parts. The first is tubing which is used to guide the mandrel in a straight direction through the pipe by not allowing it to rotate inside of the pipe which is expanding. Attached to the tubing are flared ends that have a span larger than that of the inner diameter of the pipe which will be doing the actual deforming of the pipe walls. This can be seen in Figure 39. The mandrels will be doing the deforming of the pipe and are not expected to deform and are modeled as rigid components for the simulations.

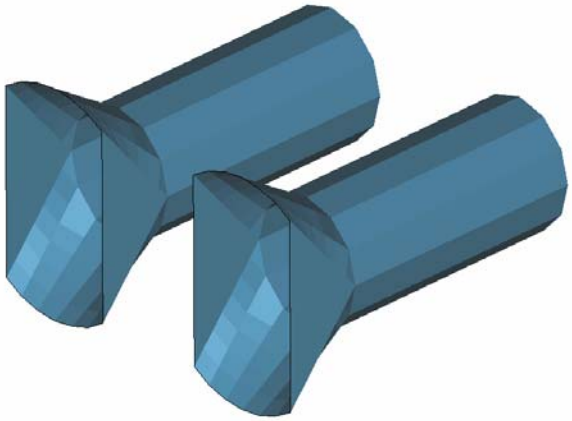

Figure 39. Expanding Tube Mandrels

The mandrels are then inserted into two separate pipes that have been modeled with an opening throughout their length caused by the absence of a welded seam seen in Figure 40. In order to keep the mandrels straight, several constraints are applied to ensure they behave in a manner similar to that of an actual physical test. Since it is most likely for a crash cushion to contain two or more expanding tubes, the model in Figure 40 is used to illustrate one possible orientation of numerous pipes and mandrels. Figure 41 illustrates how this configuration would look when mounted to the ground. The pipes are then attached to plates placed intermittently through the pipe's length. These plates have holes in them for anchor bolts to fasten them to the ground.

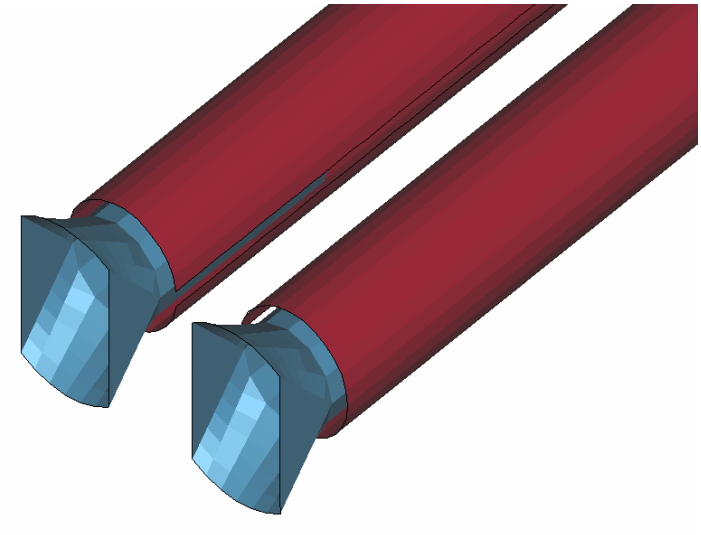

Figure 40. Mandrel Placement in Expanding Tube

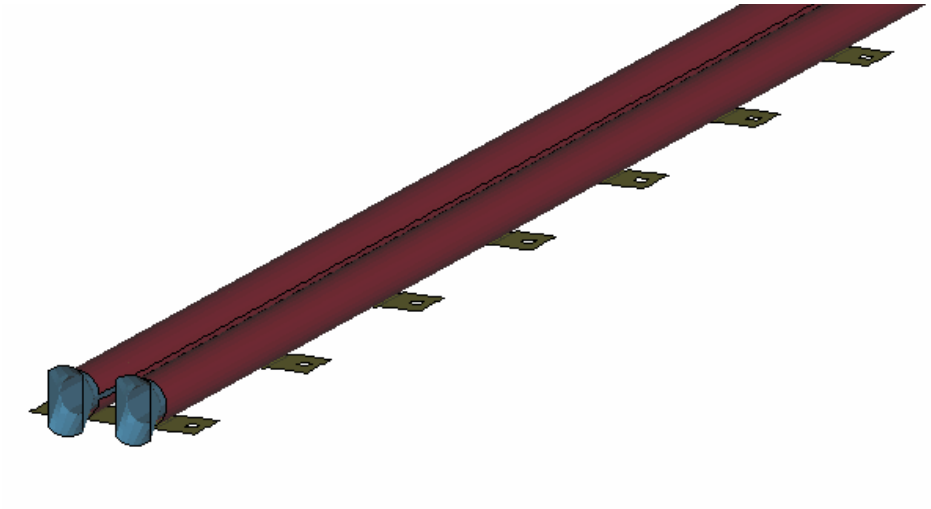

Figure 41. Expanding Tube Model

Figure 42 illustrates an example of an expanding tube concept that can be used for simulations. The pipe is constrained along its bottom side simulating the welds that would hold it in place. The plates with holes for anchors have been removed to reduce the number of elements used. This reduced the time that the run took. The mandrel is placed in position in one end of the pipe. A block is then used to simulate the mass of a vehicle. The blocks density is varied to meet the 2000 kg and 820 kg requirements. The block is then given an initial velocity of 100 km/hr along the axis of the pipe. The mandrel is rigidly constrained to the block. This means that the block will be pulling the mandrel through the length of the pipe. The velocity of the mass will also be that of the mandrel. The distance between the two never changes throughout the simulation. The pipe cannot reduce the velocity of the mandrel without reducing the velocity of the mass. They are rigidly constrained and considered to be one part. This allows for the pipe to experience forces from decelerating the larger mass and not just the mandrel mass.

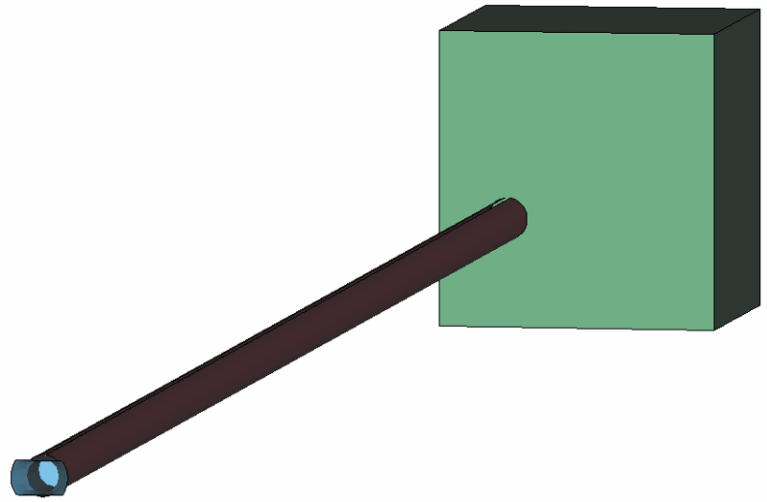

Figure 42. Variation of Expanding Tube Model

Modified Expanding Tube Model. It was recognized during the pendulum testing on the expanding tube concept that the mandrel cost could be greatly reduced by using steel plates. The plate concept for the mandrel is a better design than the rounded and will be much lower in cost. This is the mandrel that will be used in the event that further design work is done on the concept. It is for this reason that this trapezoidal shaped plate is what was used in the expanding tube simulations. All other aspects of the simulation were the same as what was described above and what is seen in Figure 42.

Deforming Angle Model. The mandrels used in the deforming angle tests are made from two main parts seen in Figure 43. The first of which is a base plate that slides in between a rigid base and a free leg of a rigidly mounted structural angle. The second part is the wedge which is used to force the steel that it travels beneath to deform upwards.

The wedge's geometry can be modified to increase or decrease the deformation in the steel above it. Figure 44 shows the mandrels orientation beneath the angle intended to deform. The mandrels are constrained in a manner that simulates its actual movement in a physical test. Two mandrels are used in the testing of this concept. Unlike the expanding tube concept which is able to "grip" the mandrel traveling its length, the deforming angle concept is unable to contain the mandrel during the run. The deforming motion of the angle leg will tend to push the mandrel out from beneath it. Adding a second mandrel and angle component opposite the initial angle will prevent this from happening. Although, the computer model allows for the possibility of constraining the motion of the mandrel allowing it to travel the length of the angle without moving out from under the angle leg, it was desired to construct the models in a fashion that closely resemble the actual configuration of the concept. The more realistic the model, the more useful the data will be for developing crash cushions using this concept.

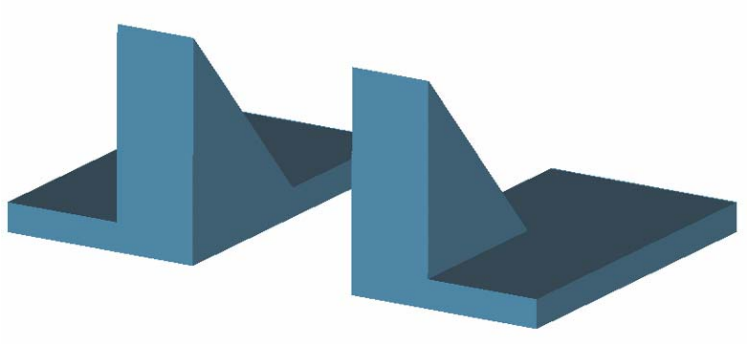

Figure 43. Deforming Angle Mandrels

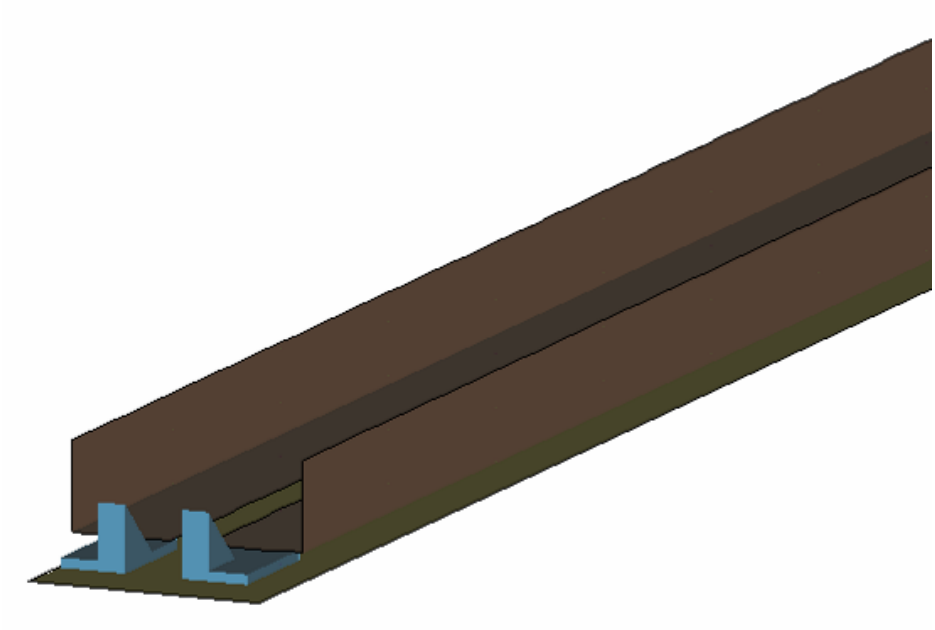

Figure 44. Mandrel Placement beneath Structural Angle

The structural angle being deformed is constrained to the material mounting it in place at various points through its length where it would be bolted in a physical test. To simulate the bolts, the nodes on the deforming angle are tied to the nodes of the structural steel mounting the angle in place. In order for the tied nodes on the deforming angle to displace, all other nodes of the mounting structure that are tied to it must displace. This is a realistic representation of what would happen in a physical test. These nodes are not

constrained through the length of the run, only at the points where bolts would be located.

Deforming Plate Model

The deforming plate concept has been modeled in a similar fashion to the two previous concepts. The deforming plate has a thin plate positioned directly above its center. The plate located on top of the deforming plate serves as a restraint, preventing unwanted warping between the points where the bolts are applied. This plate also helps to make the deforming plate take on behavior similar to that of a cantilever beam. The mandrel used is similar to the one used in the deforming angle model. The position of the wedge can be modified to alter the moment arm created. The height of the wedge can also be modified to induce greater material displacement. The deforming plate is constrained a designated distance above the base plate allowing a space for the mandrel to travel.

Just as before, the mandrel and the mass are constrained to one another. All other parts are rigidly constrained by the appropriate nodes to simulate as close as possible an actual installation. This allows these components to stay in place as the mandrel is pulled through the length of the concept. This concept's model is seen in Figure 45 and Figure 46.

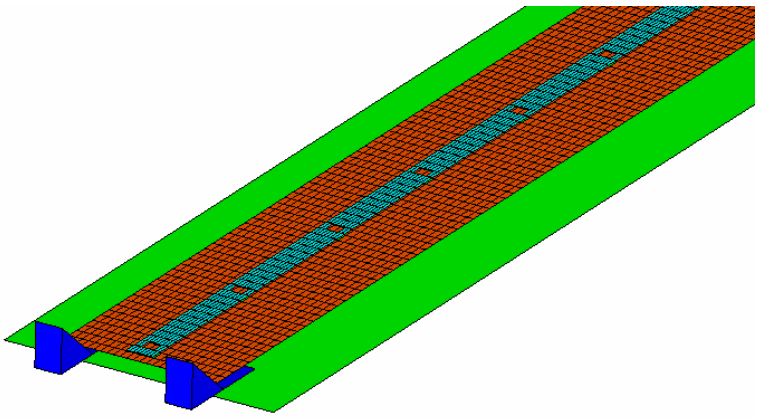

Figure 45. Mandrel Placement beneath Deforming Plate

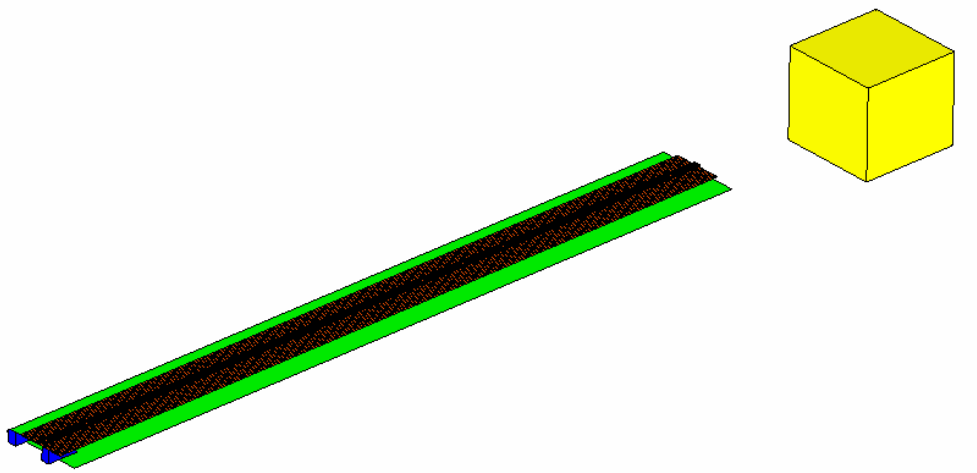

Figure 46. Deforming Plate Model

Simulation Verification

In order to verify the accuracy of the computer simulations, an attempt to recreate the physical pendulum tests was made. The physical testing which uses a swinging mass attached to the mandrel with a cable is modeled to get a more realistic effect. The orientation can be seen in Figure 47. The block simulates the pendulum mass and will be set into motion. The cable is attached to the mass and the mandrel. As the mass advances, it will pull the mandrel through the pipe using this cable. Simulating the events that occurred during physical testing was found to be a challenge. Every test is going to have different amounts of slack in the cable which varies with the way that the cable falls in each test. The results will vary due to this slack in the cable and will not match the data from the FEA models. It must be noted that simulating the exact motion of the cable is not possible. Only an approximation of the cables behavior can be captured using a finite element model.

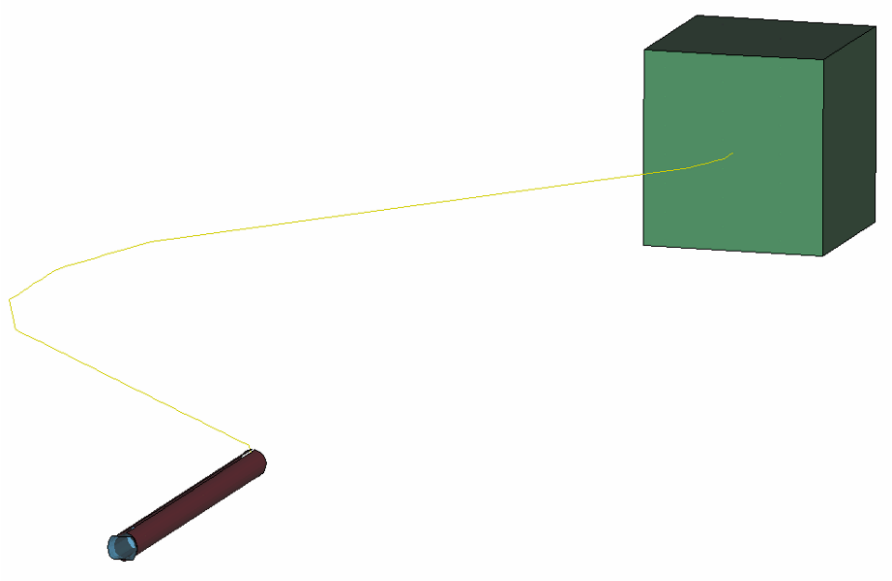

Figure 47. Model of Actual Pendulum Test

Pendulum Test Results

The pendulum test conducted on the 76.2 mm pipe with a 7.62 wall thickness brought the pendulum mass to a complete stop. The mandrel had a maximum outer diameter of 101.6 mm. The stopping distance was measured to be 1083 mm and the ridedown decelerations and 50 milliseconds average decelerations were 7 and 5 g's respectively. The OIV measured from the pendulum test was 6.5 m/s. The acceleration plot of the pendulum test is seen in Figure 48. Data collection began when the mandrel began to move. The tubing brought the mass to a stop in 0.213 seconds. The peaks seen in the plot are due to the cable whipping. After being brought to a stop, the motion of the pendulum mass did not terminate. It was noticed that the motion of the mass did not come to a complete halt after being stopped by the mandrel deforming the pipe. After being released, the mass swung down pulling on the cable attached to the mandrel which brought the mass to an initial stop. Immediately after this, the mass "bounced" back in the opposite direction. This occurs at around 0.28 seconds and can be seen on the plot. The last negative acceleration spike at this time occurs because the pendulum comes to a rest and then accelerates

slightly in the reverse direction. This positive acceleration in the negative direction is measured as a deceleration.

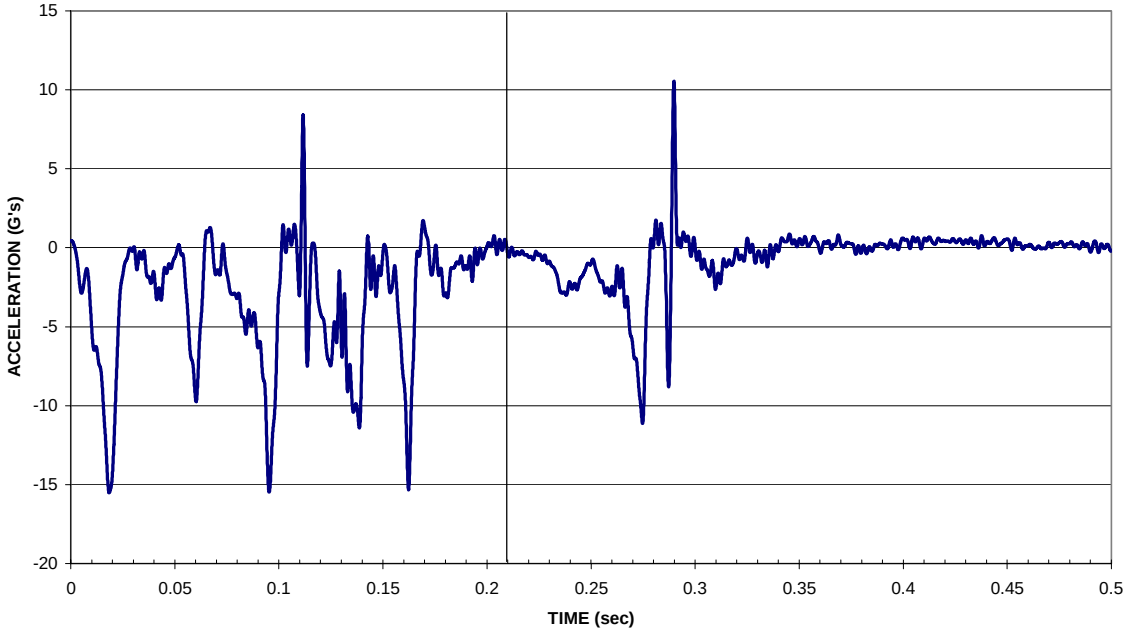

Figure 48. Acceleration Plot from Pendulum Test 11 with SAE 180 Filter

The plot itself is rather choppy. This is due to the slack in the cable being pulled taut just to slacken up and be pulled taut again several times. The choppy data will vary from test to test because the cable will never fall in the same motion every time.

Pendulum Test Simulation Results

The simulation of the pendulum test proved to have results very similar to the actual pendulum test. Figure 49 shows the acceleration data from the simulation. The mass begins to move at 0 seconds. The cable tension did not begin to move the mandrel until later. The mandrel began pulling through the tubing at 0.095 seconds and came to a complete stop at 0.29 seconds. The large initial deceleration spike at 0.195 seconds is from the mandrel initially engaging with the pipe and opening it up after sitting at rest. This initial spike is

also witnessed in the physical test data. The modeled pipe took 0.195 seconds and 1012 mm to bring the mass to a complete stop. The simulation had ridedown accelerations and 50 milliseconds average accelerations of -4.8 G's and -4.9 G's, respectively. The simulation also produced an OIV of 6.5 m/s. Figure 50 uses a different filter that makes the acceleration spikes more prominent.

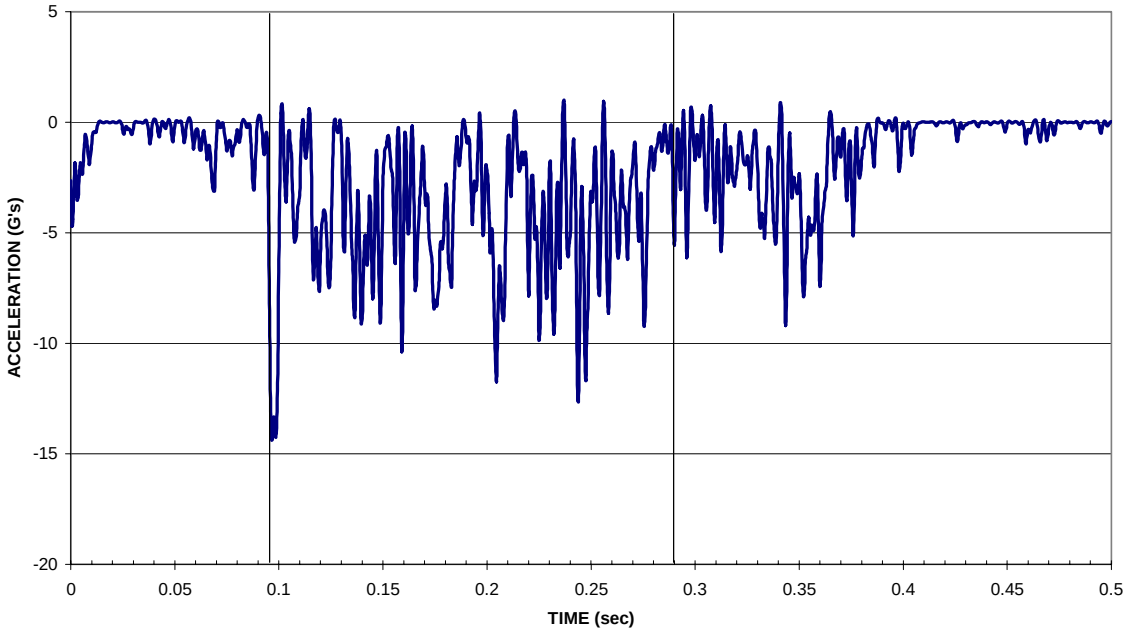

Figure 49. Pendulum Simulation Acceleration Data with SAE 180 Filter

Comparison of Physical Testing and Simulation

Comparison of the simulation and physical test show that the results were close enough to conclude that the simulations are accurate. The OIV of the simulation was 5.8% higher than the OIV of the physical test. The 50 milliseconds average acceleration was 2% less than that of the physical test.

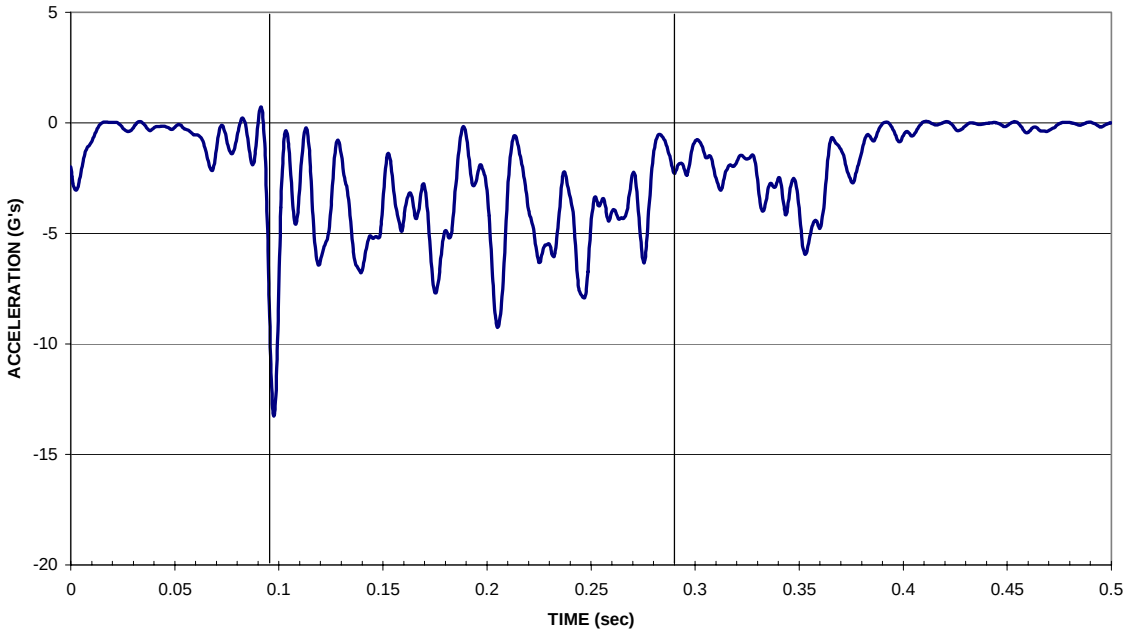

Figure 50. Pendulum Simulation Acceleration Data with SAE 60 Filter

The ridedown acceleration of the simulation was 31.4% lower than that of the physical test. Although this is a large discrepancy, it does not deface the accuracy of the simulation. It must be noted that the ridedown acceleration is a running 10 millisecond average of accelerations throughout the run. The whipping of the cable will vary in every test and is virtually impossible to match through simulation. The cable whipping created varying acceleration spikes in both the physical test and simulation through the length of the run. These spikes will occur at random times. Some acceleration peaks will be grouped close together while others will be spread further apart. At the point where the peaks are grouped closer together, a larger ridedown acceleration will be recorded if they fall within a 10 milliseconds range. Due to the spikes being so condensed in one area, more of them will be averaged in for a 10 millisecond period of time. When the peaks occur more spread out, fewer occur within that 10 millisecond range so there will be less spikes to average. Because of this, smaller ridedown accelerations will be recorded. The 50 milliseconds average will take into account a larger group of acceleration peaks.

The stopping distance of the simulation was 6.6% less than that of the pendulum test. It must be noted that the wall thickness in the simulation is constant throughout the length of the pipe. The wall thickness in the physical test cannot be guaranteed to be a constant thickness throughout its length. This could mean that at a point in the pipe where the thickness is slightly lower than the intended thickness, a lower acceleration will be developed. The time that the simulation took to stop the mass was also slightly smaller at 9% less. Figure 51 and Figure 52 illustrated the mandrels position in the pipe after the pendulum mass had been brought to a stop.

Figure 51. Physical Pendulum Test

Figure 52. Simulated Pendulum Test

The mass used in pendulum testing and the mass used in the simulation had the same values. Due to the initial mass velocities being the same for both the simulation and the physical test, the kinetic energy of the mass was the same in both. This means that the tubes in both the simulation and physical test absorbed the same amount of kinetic energy when bringing the mass to a stop. Figure 51 and Figure 52 illustrate the final resting point of the mandrel after the mass had been stopped in both the simulation and physical test.

A second verification simulation was conducted to ensure the accuracy of the simulations. The first pendulum test was conducted on pipe with a 76.2 mm nominal diameter. The pipe wall was 4.14 mm in thickness. The mandrel pulled through it had a maximum outer diameter of 101.6 mm. The physical test pulled the mandrel completely through the pipe without stopping the pendulum. A model was constructed that matched the dimensions and material properties of the physical test.

The pendulum test on the pipe in question did not have an occupant impact velocity or a ridedown acceleration reading because it was unable to create decelerations great enough for these to be measured. The physical test did have a -1.4 g, 50 milliseconds acceleration average. The mandrel also took 0.11 seconds to completely travel through the pipe. The simulation also took 0.11 seconds for the mandrel to travel the length of the pipe before exiting. The simulation yielded a 50 milliseconds acceleration average of -1.5 g’s. No occupant impact velocity was induced and no ridedown acceleration was recorded. The simulation was within 6.7% of the physical test. This is an acceptable variance.

The validity of the computer simulations was verified twice. This means that the material properties used in the computer models are a close approximation of what was happening in physical test. This proves that the computer simulations are a good indicator in prediction of what will actually occur in a physical test.

Simulation Run Data

Simulation data has been recorded and will be used for two purposes. The first purpose is to illustrate the concepts ability to convert the kinetic energy of a vehicle into strain of steel in both elastic and plastic deformations. The second purpose will to aid a designer who is designing a crash cushion using these concepts. The information provided by the simulations will show what mandrel-material combinations should be used to meet the requirements.

It must be noted that the computer simulations are simplified versions of the energy absorbing component of a crash cushion. All data gathered illustrates the energy absorbing ability of the concept by itself and not with the influence of other components involved in the crash cushion. Crash cushions contain many parts such as intermediate supports, side paneling, and others to stabilize the design in the event of an impact. All of these components add mass and extra friction to the design which could vary the results of the simulations. Due to the infinite number of crash cushion variances, these added influences cannot be taken into account in simulations testing only the energy absorbing component. The data taken from the simulations conducted simply prove that one concept is more desirable than the other two. Once implemented into a crash cushion, the added masses and friction may vary the results and slight adjustments may need to be made to the energy absorbing component to accommodate the change.

The data collected from the simulations run give an accurate idea as to how the material will perform in a physical test. It must be noted that the useful data in the form of occupant impact velocity, ridedown acceleration, and 50 millisecond average accelerations are all determined with averages of acceleration given from the simulation. The simulation data returned from a test is not “smooth and clean”, there are acceleration spikes that occur at various times. This is also what occurs in the data taken from physical tests. The spikes may occur for various reasons, one being the contact made between the

mandrel and the deforming material. Every displacement variation creates a different contact conditions. The mandrel may be applying force to the point where two elements meet or to the very center of an element at any given time. It is these variations that prevent the random acceleration spikes from being exactly the same from one simulation to the next. When these acceleration spikes occur randomly, it is possible for more to fall within one 10 millisecond timeframe and less to fall in another. This will yield slightly higher or lower recorded occupant impact velocities, ridedown decelerations, and 50 millisecond average accelerations.

This does not mean that the simulation data is inaccurate if it yields a value slightly different from what is expected. There is a concern as to the accuracy of a simulation that yields data that falls far from expected values and does not follow its expected trend. In the data collected from the simulations for the three conceptual designs, there is an occasional data point that is slightly different from what is expected. Although the point may be off by 5% or so, it still falls in the trend of other similar data collected. The data is still a reliable source to be used in the design of an energy absorbing component to be implemented into a crash cushion.

Expanding Tube Simulation Data

After seeing the results from the physical pendulum tests, it was observed that the mandrel which had a round outer diameter actually only made contact at a point along the inner surface of the pipe. After the test was conducted, there was little deformation in the pipe itself. Most deformation occurred near the point at which the pipe was welded to the base plates. This is discussed in further detail in later sections. After observing that the pipes curvature experienced minimal deformation it was decided that for future design, a plate would be used instead of the oval shaped mandrel. A flat plate cut in the shape which imitates a trapezoid was used. The front of the trapezoid had a width small enough to fit inside the pipe. The rear of the trapezoid had a width equal

to the outermost points of the oval shape. It is clear that if the only significant contact made with the pipe by the oval shape was its outermost points. The smaller end of the trapezoidal plate would be inserted into the pipe first and the flare of the trapezoid would extend out past the diameter of the pipe displacing the material just as the oval shaped mandrel had done. With this design change, the cost of a mandrel would be greatly reduced and thus making the design more desirable. This trapezoidal plate was used for the simulations on the expanding tube concept instead of the mandrel with a radius used in the verification simulations.

The data collected from the expanding tube simulations illustrates the concept's ability to convert vehicular kinetic energy into elastic and plastic strain of the deforming steel. This data can be found in Appendix C and Appendix D. The possibility of using one section of a pipe in a crash cushion exists. This is why it was tested alone and not in groups of two or more. Data gathered for individual sections of the pipe can be used in determining how the material will perform in groups of two or more. Occupant impact velocity, ridedown acceleration, and 50 milliseconds average accelerations were recorded. The expanding tube had several varying properties. The nominal diameter's of the pipe tested were 76.2 mm, 88.9 mm, 101.6 mm and 127 mm. The wall thickness varies due to type of pipe used. Standard and extra heavy pipe were used for the four diameters mentioned. The metric designation for standard pipe is DN. Pipe with a nominal diameter of 76.2 mm is denoted as DN80 for standard pipe and DNX80 extra heavy pipe. The above standard pipe diameters tested are referred to as DN80, DN90, DN100, and DN125. The extra heavy pipe diameters tested are referred to as DNX80, DNX90, DNX100, and DNX125. The mandrel which was pulled through the length of the pipe had varying dimensions controlling the displacement of the pipe walls. The controlled displacements were 25.4 mm, 38.1 mm, and 50.8 mm. This displacement is a measurement of how much larger the outer diameter of the mandrel is than the inner diameter of the pipe. A 50.8 mm displacement means the mandrel pulled

through the pipe had a width that extends 25.4 mm past the width of the pipe on one side and another 25.4 mm on the other side.

There are plots that do not have any OIV or ridedown data recorded. Ridedown accelerations do not occur until the occupant has made contact with the interior of the vehicle at which point the OIV is recorded. The absence of an OIV value can occur when the vehicle does not experience decelerations large enough to cause the occupant to impact the interior of the vehicle. Another cause for the OIV absence is if decelerations are high enough to bring the vehicle to a stop before the occupant ever contacts the interior. If the OIV does not occur, then ridedown does not occur. This explains the absence of the OIV and ridedown data in the plots.

Just because an OIV and ridedown value is not measured on the tested section of the pipe does not mean that it cannot be achieved. If the pipe segment is increased in length, there would be more length for the mandrel to travel giving more time for the occupant to impact the interior of the vehicle. It is desired to keep the overall length of a crash cushion to a minimum. If it is necessary that a section of pipe is increased to unreasonable lengths just to achieve acceptable accelerations then the pipe in question is not a desirable pipe. This is why the pipe length was held at 4572 mm for all simulations. There is the possibility of using varying numbers of pipe to work together in a crash cushion. Running simulations on varying numbers of pipes in use are outside the scope of this research on the energy absorbing capabilities of single sections of pipe. Although, with acceleration data collected through the research of individual segments of pipe can be used to calculate OIV and ridedown values. Each pipe will yield a constant deceleration. This can then be multiplied by the mass of the impacting vehicle. This will give the force that is required to advance a mandrel through the pipe. When a second pipe is added, the force is doubled. This doubles the deceleration created.

The occupant impact velocities had increasing values as the material thickness increased and the material displacement increased. The increase in

pipe wall thickness and displacement increases the stiffness of the concept allowing for more control over decelerations. As this stiffness increases, the rate at which the vehicle decelerates also increases. Due to the 2000 kg mass having more kinetic energy than the 820 kg mass, there were less segments of pipe that were able to decelerate the mass at a rate that would induce an OIV.

The data gathered from the expanding tube simulations were consistent in showing that increasing the thickness and displacement of a material will increase the vehicles deceleration. Unfortunately the increase in deceleration with the increase in displacement was small. In order to get more deceleration from the pipes, greater deformations would be required. The only problem with this is that the greater you deform the pipe walls, the wider you spread the opening of the pipe. When this occurs, there is a chance of decreased stability because the pipe is no longer “gripping” the mandrel, thus making this particular concept less desirable.

Although, increases in material displacement did not yield large increases in deceleration, increases in the nominal diameter of the pipe along with increases in wall thickness did yield larger increases in deceleration. When the pipe being tested is increased from a standard (DN) pipe with a nominal diameter of 101.6 mm to an extra heavy (DNX) pipe with a nominal diameter of 127 mm, there was an increase of close to 10 g’s. This information is useful for crash cushion design using the expanding tube concept. Modifications of the mandrel being used to achieve greater decelerations is not the answer for decelerating the 820 kg mass, merely increasing the pipe thickness and nominal diameter will do the job and the pipe will not need to be opened to a point that it looses its “grip” on the mandrel.

Due to very few of the 2000 kg runs obtaining an occupant impact velocity, there is only a small amount of ridedown data. It can be seen in the plots that the occupant impact velocities and ridedown accelerations are zero because of this.

Expanding Tube Staging

From the data provided in the figures previously discussed, decisions can be made on pipe required to meet all four stage requirements. The first stage is the 820 kg OIV requirement where the occupant cannot impact the interior of the vehicle at a velocity greater than 12 m/s. All pipe size and mandrel combinations met the given requirements. It is ideal for the OIV to be met in as short a distance as possible. It is obvious from the above data that this can be accomplished with greater decelerations. Greater decelerations come from more deformation of larger pipe so the extra heavy (DNX) 127 mm nominal diameter pipe with a 50.8 mm mandrel displacement is chosen for the 820 kg mass OIV.

The second stage is the 820 kg ridedown accelerations. The 127 mm nominal diameter pipe with a 7.62 mm wall thickness and a 50.8 mm mandrel displacement worked fine and passed this test with accelerations above the -20 g criteria.

The third stage is meeting the 2000 kg OIV requirement. The 127 mm nominal diameter pipe with a 7.62 mm wall thickness and a 50.8 mm mandrel displacement worked fine and passed this test with a velocity below the 12 m/s criteria.

The fourth stage is the 2000 ridedown accelerations. The 127 mm nominal diameter pipe with a 7.62 mm wall thickness and a 50.8 mm mandrel displacement worked fine and passed this test with accelerations above the -20 g criteria.

This means that it would be possible to have just one segment of extra heavy (DNX) 127 mm nominal diameter pipe with a mandrel displacement of 50.8 mm throughout the length of the crash cushion. The only problem with this is that the decelerations recorded for both the 820 kg and 2000 kg tests were not very close to the -20 g requirement. Due to this fact, the crash cushion would be much longer than it needs to be. More than one pipe can be used in an installation.

Another setback with this concept is that you are forced to use one nominal diameter pipe through the installation. If you have a mandrel that fits in a 101.6 mm diameter pipe and displaces it 50.8 mm at the beginning of the installation, you can never reduce the size of pipe needed for the next stage. The mandrel won't fit inside a smaller diameter pipe. In the event that a mandrel is designed with a head small enough to fit inside all diameters, the 50.8 displacement on a 101.6 mm pipe would come close to a 76.2 mm displacement in a 76.2 mm pipe. The pipe sizes may change from stage to stage but the mandrel must remain the same.

Two standard (DN) 101.6 mm nominal diameter pipes with mandrels that cause 25.4 mm displacements can be used. This should double the 6 m/s value giving 12 m/s meeting the 820 kg occupant impact velocity requirements. The same mandrel size can be used with two extra heavy (DNX) 101.6 mm nominal diameter pipes for a ridedown acceleration of close to -16 g's which falls below the -20 g requirement. The mandrel displacement must remain constant through the length of the cushion. This means that a 25.4 mm displacement in a 101.6 mm pipe will be much smaller in a 127 mm pipe. The pipe size for the next two stages is limited to a 101.6 mm nominal diameter pipe. Even the strongest extra heavy (DNX) pipe in this size was not able to yield OIV or ridedown values that would stop the 2000 kg mass in a reasonable length.

Another possibility would be to use three pipes and mandrels to capture the values needed to bring a vehicle to a stop in a reasonable distance. It must be kept in mind that the more pipes required to stop the vehicle means a more complex mounting in the cushion. This makes for more material, higher material cost, more difficult replacement, and a more expensive replacement. This illustrates a shortcoming in the expanding tube concept. Yes, the concept is capable of bringing a vehicle to a safe stop, it cannot be done in a reasonable distance without complicating the pipe mounts and increasing cost and decreasing ease of installation.

Deforming Angle Simulation Data

The deforming angle concept had several variables that must be taken into account for simulations. The simulation is run using a mass of 2000 kg and 820 kg to represent a large truck and a small car. The mass' initial velocity is held constant for all tests at 100 km/hr. The thickness of the structural angle is a factor that affects deceleration and is taken into consideration. Various arm lengths were used along with different wedge edge distances to vary the moment arm. There were also varying bend displacements which were the displacement in the free leg of the angle determined by the height of the wedge height.

The deforming angle simulation data can be seen in Appendix E. Due to the nature of the concept, it is desired that only one pair of deforming angles were used. Adding more will complicate the design adding to cost and installation difficulty similar to what was seen in the expanding tube concept. With the data acquired through computer simulations seen in the data figures, the concept of using a wedge to deform the free leg of rigidly mounted structural angle is an effective way to absorb energy. Various tests had shown a wide variety of energy absorbing capabilities. Structural angle can be weak enough to only provide 2.6 g ridedown decelerations yet strong enough to provide 36.7 g ridedown of decelerations. This means that various angle thicknesses and mounting configurations will allow the angle to accommodate both the occupant impact velocity and ride down acceleration requirements for both a small and large vehicles.

It must be noted with the deforming angle concept, the material hanging over the mandrel cannot be considered to be a cantilever beam. The end of the horizontal leg that overhangs the mandrel is not rigidly attached at its base. The point of attachment is further up the vertical leg of the structural angle. Although deformation does occur where the horizontal leg meets the vertical leg, there is also deformation at the point of attachment on the horizontal leg. The horizontal

leg seems to pull away from the mount with slight deformations at the location where the bolt would be.

Deforming Angle Staging

For the staging of the deforming angle, it was found that using a mandrel that causes 41.275 mm of deformation on angle with a 6.35 mm thickness and a 31.75 mm edge distance did accommodate the OIV requirements for the 820 kg mass. If all dimensions are kept the same and the thickness of the deforming angle is increased to 9.525 mm the 820 kg mass will be decelerated at a rate slightly greater than what is allowed by the ridedown criteria. Although this is not desired, this data does not take into account the energy absorbed through the crush of the vehicle. This crush varies with each individual vehicle and was not taken into account. The simulations were designed to test just the abilities of the material itself without other variables being included.

For the 2000 kg mass, holding the same mandrel geometries and positions will provide an acceptable OIV when the angle thickness is increased to 9.525 mm. The section of 9.525 mm thick structural angle has demonstrated its ability to accommodate the ridedown conditions for the 820 kg mass and the OIV conditions for the 2000 kg mass. Once the OIV for the 2000 kg mass has been met, the angle thickness can be increased to 12.7 mm to bring the mass to a stop with acceptable decelerations. Although a 41.275 mm displacement was not simulated on 12.7 mm thick structural angle, a mandrel that created a 44.45 mm displacement was. This mandrel had acceptable ridedown decelerations. Decreasing the material displacement slightly did not increase the deceleration that occurred.

One setback to the deforming angle concept is mounting the deforming material into place. Working around the vertical and horizontal components can be relatively difficult. The vertical component of the deforming angle will be transmitting large loads into the vertical face of the mount that holds it in place. If the mount experiences deformation because of these forces, it will not only

reduce the energy absorbed by the intended deforming angle but will also add to another component that will need to be replaced increasing the cost of replacement. Deformation of the mount is also an undesired event because it reduces the stability of the structure. Because of this, it is desired to have a mount that is as rigid as possible. This leads to the use of very thick steel as a mount which leads to large cost increases. This research is being done to eliminate the large cost of the energy absorbing components of a crash cushion.

Deforming Plate Simulation Data

Unlike the expanding tube concept where increasing material size and thickness will help performance and also hinder performance at the same time, increasing plate thickness and dimensions for the deforming plate concept only helps performance. Just as the previous two concepts were tested with 820 kg and 2000 kg masses traveling at 100 km/hr the deforming plate concept was also subjected to these conditions. The mass was constrained to the mandrels and pulled them the length of the plate.

The deforming plate concept was intended to perform similar to a pair of cantilever beams deforming to absorb the kinetic energy. The concept is not like the expanding tube concept where single lengths of deforming arms were used in various configurations. Since it is expected to perform as a pair of beams, the simulations were modeled in this fashion. The data recorded from the simulations can be found in Appendix F and Appendix G. It is clear that the deforming plate concept is “stiff” enough to decelerate a 2000 kg mass with a ridedown deceleration of 38.3 g’s and “soft” enough to decelerate an 820 kg mass with a ridedown decelerations less than 3.2 g’s. This is preferred because it illustrates the concept’s capability to decelerate masses, large and small at rates well above and well below what is acceptable. By being able to cover this wide range of decelerations the concept can accommodate the requirements for each mass which fall in between these two extremes.

It should also be noted that when the occupant impact velocity is not met, there will be no ridedown data recorded. This occurs because ridedown data is not recorded until the occupant impact velocity is met. This explains the blanks left in the data tables and the absence of these points on the plots.

It can be seen from the data plots that the deforming plate concept is capable of inducing acceptable occupant impact velocities on the 820 kg mass. It is expected that increasing the deforming plate's thickness along with the increase of its deformation and the reduction of the moment arm will induce more strain that must occurs for the mandrel to advance through the concept. This increase in strain requires an increase in work to have the mandrel travel the length of the plate. Due to the fact that more work is required to advance the mandrel through the length of the concept, more energy is being absorbed from the vehicle. By absorbing the vehicles energy at higher rates, the decelerations of the vehicle will increase. This yields higher occupant impact velocities and higher ridedown decelerations.

For the 2000 kg mass, the occupant impact velocities were smaller than that of the 820 kg mass occupant impact velocities. The increased larger mass requires more effort on the cushions behalf to yield the same decelerations as for a smaller vehicle. The 6.35 mm thick plate did not do a very good job at decelerating the 2000 kg mass at a rate that would induce an occupant impact velocity.

Similar to the occupant impact velocities which increase with thicker deforming material and increasing amounts of steel deformation, the decelerations also increase. The ridedown acceleration plots and 50 milliseconds average acceleration plots depict an increase in decelerations as the material thickens and the mandrel displacement increases. This trend was expected and is accurate. Both masses react similarly to the varying configurations in a sense that the deceleration values increase as the installation becomes "stiffer". The data from the 50 milliseconds average acceleration plots are good at giving an idea of the energy absorbing ability of the material when it

is not “stiff” enough to induce an occupant impact velocity or ridedown deceleration.

Deforming Plate Staging

Staging for the deforming plate concept will be effective due to the variety of readily available plate thicknesses. The same material displacement was used through the length of the design and satisfied the different staging requirements. For the 820 kg occupant impact velocity a 6.35 mm thick deforming plate with a 76.2 moment arm and a 76.2 mm displacement yielded an 11.9 m/s occupant impact velocity. This is an allowable rate. The next stage is to bring the mass to a stop with a ridedown under 20 g’s. Keeping the same plate will bring the mass to a stop at -13.4 g’s which is also acceptable. The plate thickness will then be increased to 9.53 mm thickness which will give the 2000 kg vehicle an occupant impact velocity of 10.6 m/s. This same thickness will also bring the vehicle to a stop at -14 g’s.

It is clear that the closer to the allowable deceleration you are, the shorter the stopping distance for the vehicle will be. The stopping decelerations are 6.4 and 6 g’s away from the acceptable limit. This is where the data trends will come in. Using the data provided by the simulations, one can decide that by reducing the displacement by 12.7 mm or increasing the moment arm by 12.7 mm, results would come closer to the limit. Having said this, it must be noted that coming as close to the limit as possible is not always the most desirable. It is a good safety measure to stay slightly beneath the acceptable decelerations.

One thing that was not taken into consideration in the simulations was the other components of the crash cushion. When a vehicle impact head on with the crash cushion, it will not only have to push the mandrels through the deforming material, it will also have to push the steel that constitutes the crash cushion. As the vehicle advances through the cushion, the amount of steel being displaced increases. The mass of all this steel being pushed by the vehicle will also work against the vehicle in increasing its decelerations.

Summary

The above section discussed the process taken to develop the finite element models used to test the viability of the concepts. The simulation data gathered were presented and each concept's ability to convert the kinetic energy of a vehicle into the deformation of steel was illustrated.

CHAPTER V

SUMMARY AND CONCLUSIONS

Overview

One of the greatest conveniences that man has available is the ability to travel great distances in short amounts of time using automobiles. Due to the great numbers of people using this convenience, there is plenty of room for accidents to occur. Roadway accidents claim the lives of many people every year. Engineers have developed many safe energy absorbing devices in the hopes of making our roadways a safer place. The ideas initially developed have been improved or replaced. There are current designs that perform just as well as previous designs but are lower in cost and easier to install. There are several areas in crash cushion design that can be improved upon.

The aim of this research is to explore alternative methods of converting the kinetic energy of a vehicle into strain from the deformation of readily available structural steel. The focus of the research was not on the crash cushion itself but on the energy absorbing component. By making use of readily available structural steel, the cost of the crash cushion can be reduced along with the cost of replacement parts after a collision has occurred. After developing a new method to absorb the vehicles energy, the concept can then be implemented into the design of a crash cushion.

Conclusions

In this research, various methods that convert the kinetic energy of a vehicle into strain from material deformation were explored. Three concepts were examined to serve this function but one stood out from the rest as the most

desirable of the three concepts. Making use of deforming steel plate is a very simple yet effective concept.

It is in its simple design that makes the concept so appealing. Simplicity allows for an inexpensive concept. The simplicity also makes designing a crash cushion around it very easy. Replacement of the deformed components is also simple and very inexpensive requiring only a wrench. No welding will be required for manufacturing, installation, or replacement. Along with simplicity, the deforming plate concept will be very low to the ground. The maximum height of the energy absorbing concept is expected to fall under 101.6 mm. This will not be done by any of the other concepts. A low energy absorbing component is desired due to the fact that the vehicle is expected to travel directly above it. Some cars are designed to ride very low to the ground. If the energy absorbing component is too high, it creates a snagging point which could catch on the vehicle which and make for a fatal design. The snagging could bring the vehicle to a very abrupt stop with decelerations much greater than what is allowed.

Although the simulations gave ridedown decelerations that were slightly less than desirable, it must be noted that the simulations were run in an ideal condition without many of the variable that would affect the deceleration. Added mass of the installation components being displaced as the vehicle travels the length of the installation will increase the vehicles deceleration. The plate thickness-mandrel displacement variations were held to a limited number. Many more variations are available which will aid in developing a cushion with an optimal length. This will lead to the vehicle coming to a stop at a rate much closer to the acceptable values. For crash cushions, it is better to be stopped at a rate under the requirements and keep the passenger's safe than to be stopped at a rate over the requirements which puts the occupant in danger. The data provided by this research is very valuable for the advancement of the deforming plate energy absorbing concept.

The readily available sizes and shapes of steel plates make for easily obtainable components. The only manufacturing required to prepare the

material for installation is to punch holes along its length to allow for bolts to fasten it in place. This is much faster and far less expensive than drilling and welding which would be required by the other two concepts. Due to the fact that plate comes in various readily available thicknesses, various amounts of elastic and plastic strain from material deformation can be obtained. This makes the concept very effective in accommodating the requirements of the four stages in stopping a vehicle. It is these reasons that the deforming plate concept has been chosen as an effective method of absorbing the kinetic energy of a vehicle impacting a crash cushion.

This research was a success. A new, innovative method for bringing a vehicle moving at very high speeds to a stop with acceptable decelerations was developed. Three concepts were developed. Data taken from physical testing and simulations were used to evaluate each design against the others for meeting design requirements. After this evaluation, an optimal design was identified. This concept was such a success that research is currently being continued to move the concept into a crash cushion design to improve highway safety.

Future Research

The next step for the deforming plate concept is to implement it into a crash cushion design. One of the first steps in designing a crash cushion is developing a structure to transfer the impacting vehicles kinetic energy into the energy absorbing component. In this case a sled will be used to transfer this energy into the deforming plate with the wedges as seen in Figure 53 and Figure 54. After this configuration is proven to work well, the remainder of the crash cushion components can be designed to form a complete crash cushion.

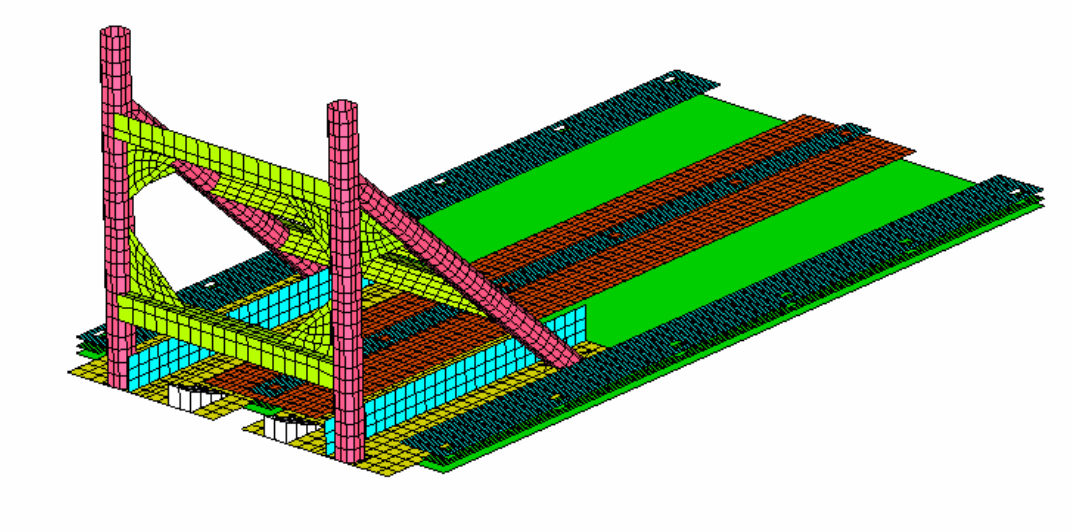

Figure 53. Deforming Plate Concept Implemented into Early Crash Cushion Design Stages

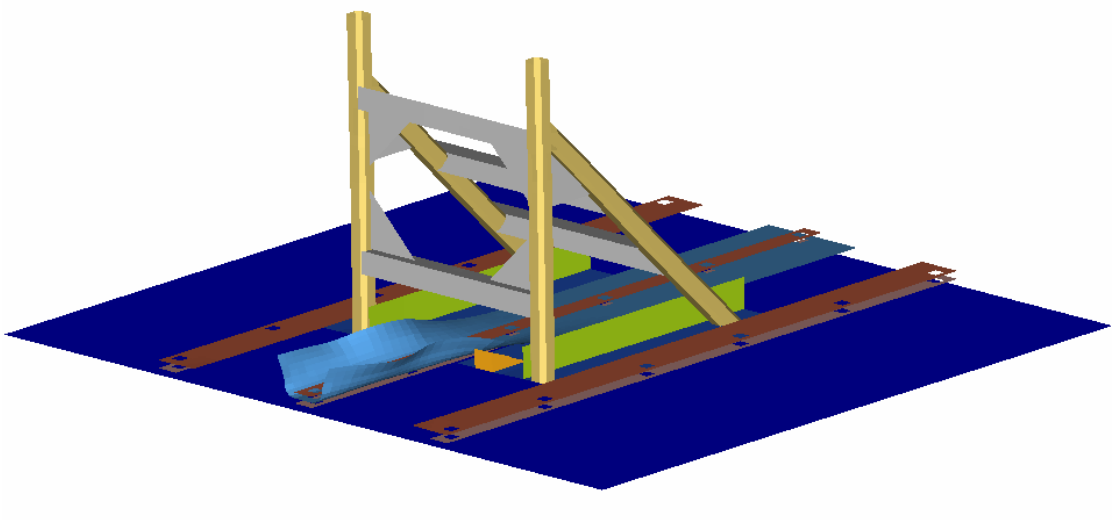

Figure 54. Image from Deforming Plate Sled Concept Simulation

REFERENCES

Alamo Iron Works. (2005). *Online Catalog*. Retrieved 4/3/2005, from http://www.aiwnet.com/aiwnet/servlet/CyberVendor/category/C9944943/catalog//.

Alberson, D.C. (1994). "Crash testing a reusable polyethylene narrow impact attenuation system" *Unpublished Report,* Texas Transportation Institute, Texas A&M University, College Station, TX.

Avallone, E., and Baumeister, T. (1996). *Marks' standard handbook for mechanical engineers* (10th Ed.). New York: McGraw-Hill.

Boresi, A., and Schmidt, R. (2003). *Advanced mechanics of materials*. (6th Ed.). Hoboken, NJ: John Wiley & Sons, Inc.

Bullard, L.D. (1995a). "Crash testing and evaluation of the Roadway Safety Service, Inc. Fitch Inertial System Crash Cushion." *Unpublished Report,* Texas Transportation Institute, Texas A&M University, College Station, TX.

Bullard, L.D. (1995b). "Development of a crash energy absorber." Unpublished master's thesis, Texas A&M University, College Station, TX.

Buth, E.C., and Menges, W.L. (1998). "Test 3-37 of the narrow Connecticut impact attenuation system (NCIAS)" (NHCRP Report 350). *Unpublished Report,* Texas Transportation Institute, Texas A&M University, College Station, TX.

Emori, RI., (1968). "Analytical approach to automobile collisions," SAE Paper #680016. Society of Automobile Engineers, Warrendale, PA.

Kachanov, L.M., (2004). *Fundamentals of the theory of plasticity.* New York: Dover Publications, Inc.

LS-DYNA theoretical manual. (1998). Livermore Software Technology Corporation, Livermore, CA.

Menges, W.L., and Alberson, D.C. (2002). "Testing and evaluation of the widetracc," (NCHRP Report 350). *Unpublished Report,* TX Transportation Institute, Texas A&M University, College Station, TX.

National Center for Statistics & Analysis. (2004, September 17). *Traffic Safety Facts 2003.* Retrieved December 26, 2004, from http://nhtsa-nrdweb.nhtsa.dot.gov/pdf/nrd-30/NCSA/TSF2003/809767.pdf, 1-2.

Reddy, J.N. (2002) *Energy principles and variational methods in applied mechanics* (2nd ed.). Hoboken, NJ: John Wiley & Sons, Inc.

Ross, H.E. (1995). "Evolution of roadside safety." *Transportation Research Circular,* Transportation Research Board, Washington, DC, 435(2), 5-16.

Ross, H.E., Sicking, D.L., Zimmer, R.A., and Michie, J.D. (1993). "Recommended procedures for the safety performance evaluation of highway features." *National Cooperative Highway Research Program Report 350*, Transportation Research Board, Washington, DC.

Shames, I.H., and Cozzarelli, F.A. (1997). *Elastic and inelastic stress analysis*, Washington, DC: Taylor & Francis.

Tiwari, S. (2002). "A quantitative approach for the objective evaluation and selection of optimal design in conceptual design stage." Unpublished master's thesis, Texas A&M University, College Station, TX.

Young, W., and Budynas, R. (2002). *Roark's formulas for stress and strain,* (7th ed.). New York: McGraw-Hill.

APPENDIX A

EXPANDING TUBE MILL TEST CERTIFICATE

M I L L T E S T C E R T I F I C A T E

Certificate No 54788 Page 1/ 2
Type of Document EN 10204 /3.1 B Date 24/03/2004
Contract No/Lot No 2694 / 32
Standard ASTM A 53
Material ASTM A 53 GR A Inspector's Stamp
Product E.R.W STEEL PIPE -----
Customer SUNBELT GROUP, INC. ! K !
Order No./LC No. 14902 ! 2 !
Shipment No 406 -----
Remarks

Item	Dimension OD X WT X L (INCH)	M.Type	Pieces	Total Length (Ft)	Total Weight (Tons)	Type
1	2 7/8 "X .276X21.00	NWB	1130	23730.00	82.418	VPE
2	3 1/2 "X .300X21.00	NWB	367	7707.00	35.828	VPE

Item	Heat No.	Chemical Composition(%) C x100	Si	Mn	P	S	Al	Mo x1000	Cr	Ni	Cu	V	N	Nb	Ti	Ceq
1	318076	7	25	62	1	6	54	1	16	7	15	1	1	3	2	.173
1	327807	8	21	59	9	11	49	1	19	29	20	2	9	1	1	.184
1	420732	6	23	59	9	7	43								2	.156
1	430637	16	1	93	10	11	64	0	20	32	17	2	4	1	1	.325
2	420726	7	22	60	10	17	55	1	29	30	29	2	13	2	1	.174
2	420738	6	23	58	12	8	45									.160
2	450960	7	22	60	9	17	54	1	28	31	29	2	12	2	1	.173

Item	Heat No.	Tensile Test ***	YS 234 psi	TS psi	E %	Impact Test ***	Ave 345	Tem	HT psi/Se	Threads EL	NP	B	V	F	D	D	N	
1	318076	KLB	48738	62977	31				2494/ 5			30	G	G	G	G	G	
1	327807	KLB	49303	59399	31				2494/ 5			30	G	G	G	G	G	
1	420732	KLB	39088	56855	32				2494/ 5			30	G	G	G	G	G	
1	430637	KLB	54598	75119	30				2494/ 5			30	G	G	G	G	G	

MANAGER OF QUALITY CONTROL DEPARTMENT
Koray YAÞAR

e-mail : kyasar@borusan.com

M I L L T E S T C E R T I F I C A T E

Certificate No 54788 Page 2/ 2

Item	Heat No.	Tensile Test ***	YS 234 psi	TS psi	E %	Impact Test ***	Ave 345	Tem	HT psi/Se	Threads EL	NP	B	V	F	D	D	N	
2	420726	KLB	44727	54540	32				2494/ 5			30	G	G	G	G	G	
2	420738	KLB	39088	56855	32				2494/ 5			30	G	G	G	G	G	
2	450960	KLB	44887	54741	33				2494/ 5			30	G	G	G	G	G	

APPENDIX B
SAMPLE LS-DYNA INPUT FILE

```
*KEYWORD
$$ HM_OUTPUT_DECK created 10:28:47 02-05-2005 by HyperMesh Version 6.0
$$ Ls-dyna Input Deck Generated by HyperMesh Version  : 6.0
$$ Generated using HyperMesh-Ls-dyna Template Version : 6.0
*CONTROL_TERMINATION
$$  ENDTIM    ENDCYC     DTMIN    ENDENG    ENDMAS
     0.25
*CONTROL_CONTACT
$$  SLSFAC    RWPNAL    ISLCHK    SHLTHK    PENOPT    THKCHG     ORIEN
ENMASS

$$  USRSTR    USRFRC     NSBCS    INTERM     XPENE     SSTHK      ECDT
TIEDPRJ

$$   SFRIC     DFRIC       EDC    INTVFC        TH     TH_SF  TIPEN_SF

$$  IGNORE    FRCENG
              1
*CONTROL_OUTPUT
$$   NPOPT    NEECHO    NREFUP    IACCOP     OPIFS    IPNINT    IKEDIT
       1         3                              1      1000         0
*CONTROL_ENERGY
$$    HGEN      RWEN    SLNTEN     RYLEN
       2
$$DATABASE_OPTION -- Control Cards for ASCII output
*DATABASE_NODOUT
5.0000E-04         1
*DATABASE_ELOUT
5.0000E-04         1
*DATABASE_GLSTAT
5.0000E-04         1
*DATABASE_MATSUM
5.0000E-04         1
*DATABASE_RCFORC
5.0000E-04         1
*DATABASE_ABSTAT
5.0000E-04         1
*DATABASE_NODFOR
5.0000E-04         1
*DATABASE_RBDOUT
5.0000E-04         1
*DATABASE_SLEOUT
5.0000E-04         1
*DATABASE_BINARY_D3PLOT
$$ DT/CYCL      LCDT      BEAM      NPLTC
    0.005
```

```
*DATABASE_BINARY_D3DUMP
$$ DT/CYCL
  30000.0
*DATABASE_BINARY_RUNRSF
$$ DT/CYCL
  75000.0
*DATABASE_BINARY_INTFOR
$$ DT/CYCL      LCID
    0.005
*DATABASE_EXTENT_BINARY
$$   NEIPH     NEIPS    MAXINT    STRFLG    SIGFLG    EPSFLG    RLTFLG
ENGFLG

$$  CMPFLG    IEVERP    BEAMIP     DCOMP      SHGE     STSSZ    N3THDT
              1
$$ NINTSLD

*NODE
  17301       4777.456159.085026285386278.847544964405
                                      ...
                              Omitted for brevity
                         ...
  72916       4472.656-101.29390336354 -30.19570579158
*MAT_RIGID
$HMNAME MATS       4Rigid Steel
       47.8600E-09  200000.0      0.29
     1.0         2         7

*MAT_RIGID
$HMNAME MATS       5Impactor
       59.2592E-09  200000.0      0.29
     1.0         5         7

*MAT_PIECEWISE_LINEAR_PLASTICITY
$HMNAME MATS       3Tubing
       37.8600E-09  200000.0      0.29     376.0

$$ HM Entries in Stress-Strain Curve =         8
      0.0    0.0237    0.0422      0.05    0.1409    0.2133    0.2496    0.2586
    336.0     336.7     401.2     434.3     537.2     589.6     675.0     677.0
*PART
$HMNAME COMPS       26.553 Thk Tube
$HMCOLOR COMPS       2      12
```

```
       2        1        3
$HMNAME COMPS       3Mandrel
$HMCOLOR COMPS       3       7

       3        2        4
$HMNAME COMPS       4Impactor
$HMCOLOR COMPS       4       7

       4        3        5
*SECTION_SHELL
$HMNAME PROPS       1Steel
       1       16                4
    7.62     7.62     7.62     7.62
$HMNAME PROPS       2Mandrel
       2       16
    12.7     12.7     12.7     12.7
*SECTION_SOLID
$HMNAME PROPS       3Impactor
       3        2
*CONTACT_AUTOMATIC_GENERAL_ID
$HMNAME GROUPS       1Tube Expand
$HMCOLOR GROUPS       1       1
$HMFLAG GROUPS SLAVE MASTER
       1
       0                0
    0.15     0.15

*ELEMENT_SHELL
  67683      2   72901   72902   72916   72915
                                    ...
                          Omitted for brevity
                     ...
  51123      3   54880   54878   54877   54879
*ELEMENT_SOLID
  16204      4   17301   17304   17303   17302   17305   17308   17307   17306
$$
$$ Sets Defined In HyperMesh
$$
*SET_PART_LIST
$HMSET
$HMNAME SETS      1SLAVE_RIGID_BODY_SET_PART_1
       1      0.0      0.0      0.0      0.0
       8
```

```
*SET_PART_LIST
$HMSET
$HMNAME SETS      2SLAVE_RIGID_BODY_SET_PART_1.1
       2       0.0       0.0       0.0       0.0
      12
*BOUNDARY_SPC_NODE
$HMNAME LOADCOLS       3Velocity
$HMCOLOR LOADCOLS       3       9
    72910         0         1         1         1         1         1         1
                                      ...
                                Omitted for brevity
                          ...
    72251         0         1         1         1         1         1         1
*INITIAL_VELOCITY_NODE
$HMNAME LOADCOLS       3Velocity
$HMCOLOR LOADCOLS       3       9
    17308   27777.0       0.0       0.0
    17307   27777.0       0.0       0.0
    17306   27777.0       0.0       0.0
    17305   27777.0       0.0       0.0
    17304   27777.0       0.0       0.0
    17303   27777.0       0.0       0.0
    17302   27777.0       0.0       0.0
    17301   27777.0       0.0       0.0
    54880   27770.0       0.0       0.0
    54877   27770.0       0.0       0.0
    54879   27770.0       0.0       0.0
    54878   27770.0       0.0       0.0
*CONSTRAINED_RIGID_BODIES
       3         4
*END
```

APPENDIX C

820 KG MASS EXPANDING TUBE SIMULATION RESULTS

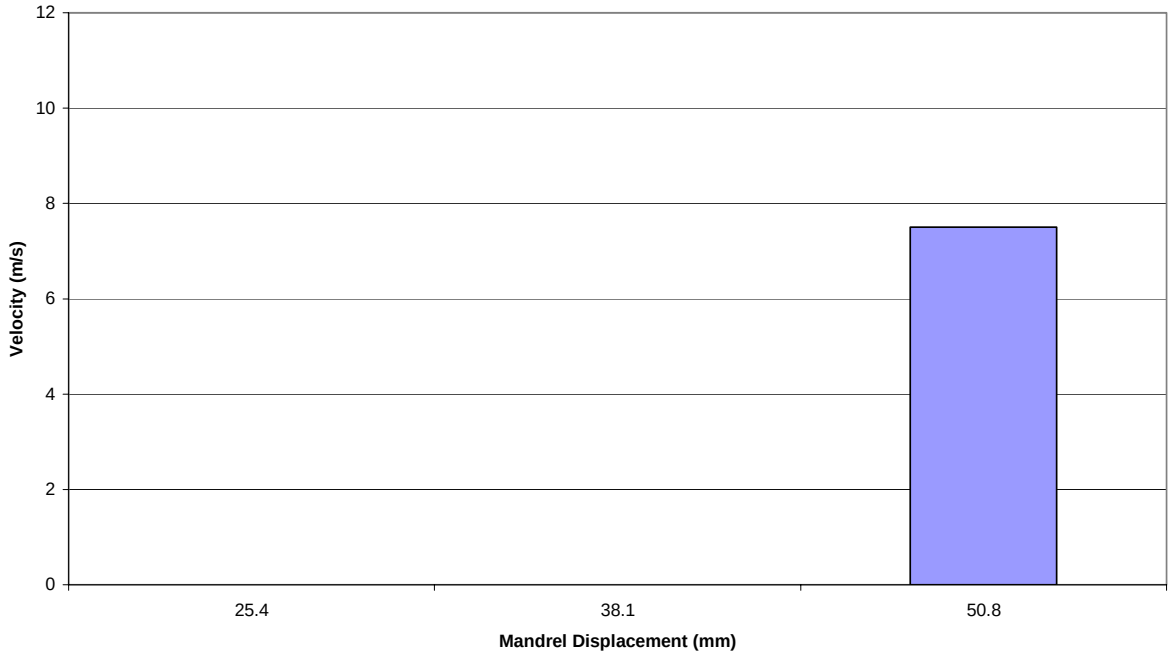

Figure 55. DN80 Occupant Impact Velocity vs. Mandrel Displacement for 820 kg Mass

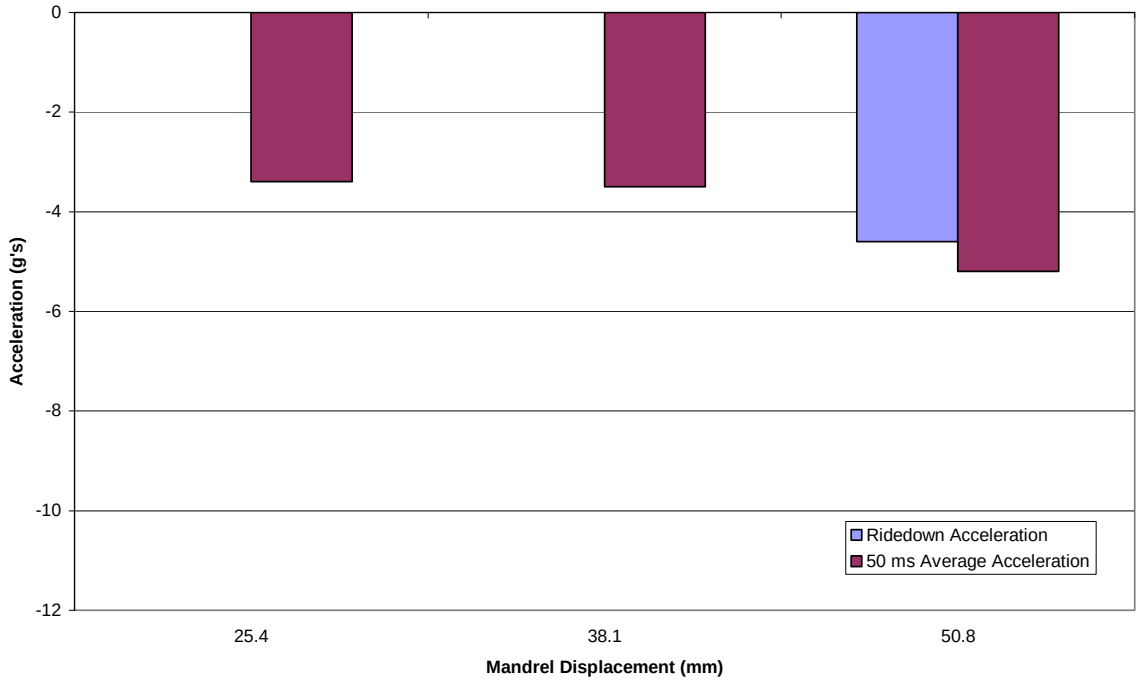

Figure 56. DN80 50 Ridedown Acceleration and Millisecond Average Acceleration vs. Mandrel Displacement for 820 kg Mass

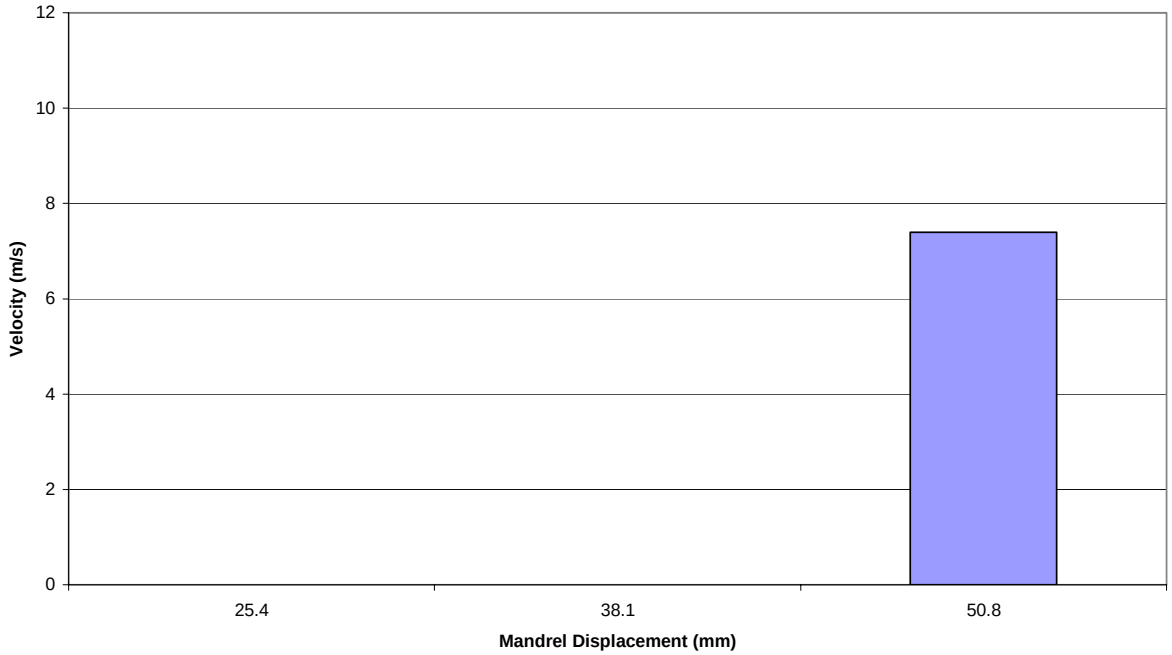

Figure 57. DN90 Occupant Impact Velocity vs. Mandrel Displacement for 820 kg Mass

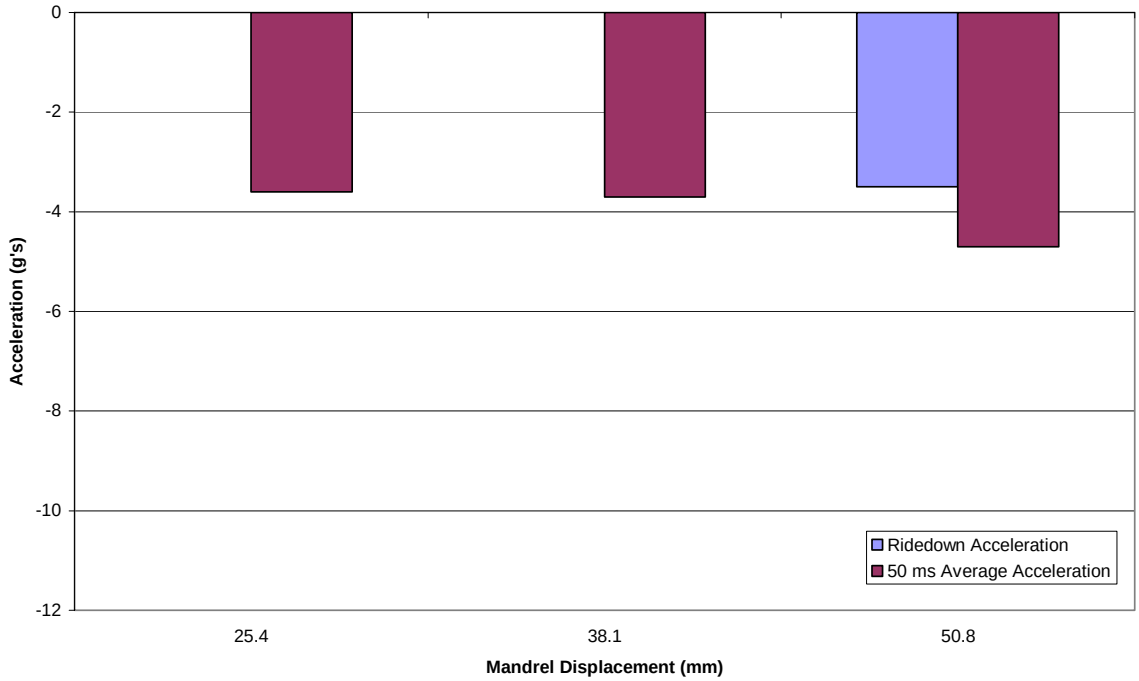

Figure 58. DN90 Ridedown Acceleration and 50 Millisecond Average Acceleration vs. Mandrel Displacement for 820 kg Mass

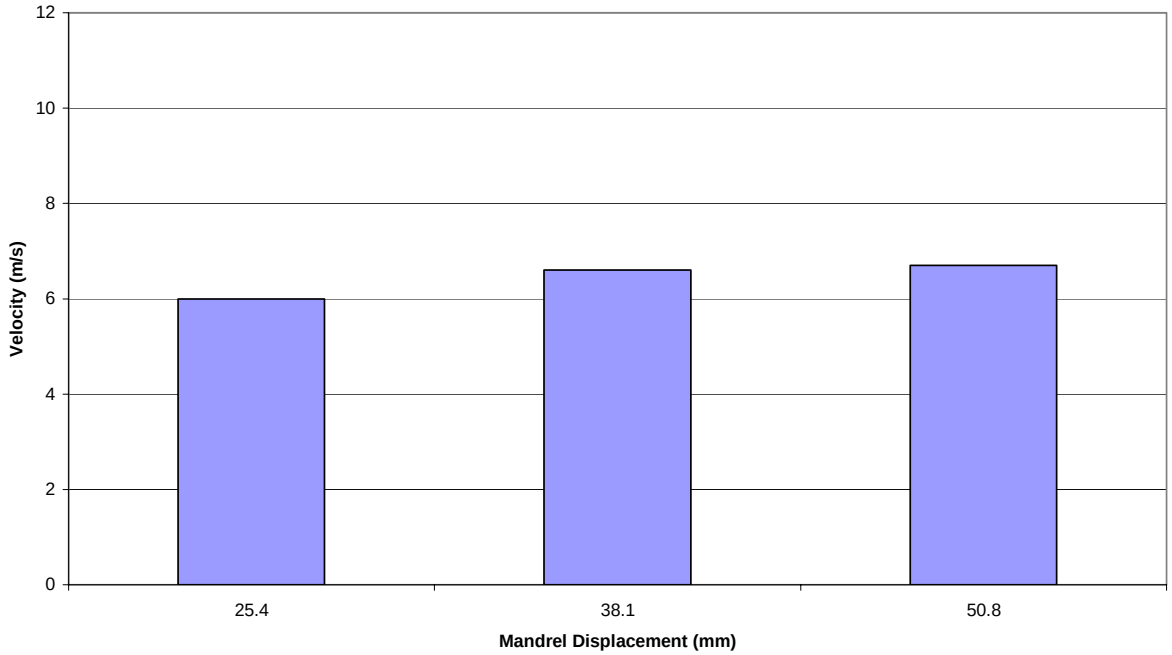

Figure 59. DN100 Occupant Impact Velocity vs. Mandrel Displacement for 820 kg Mass

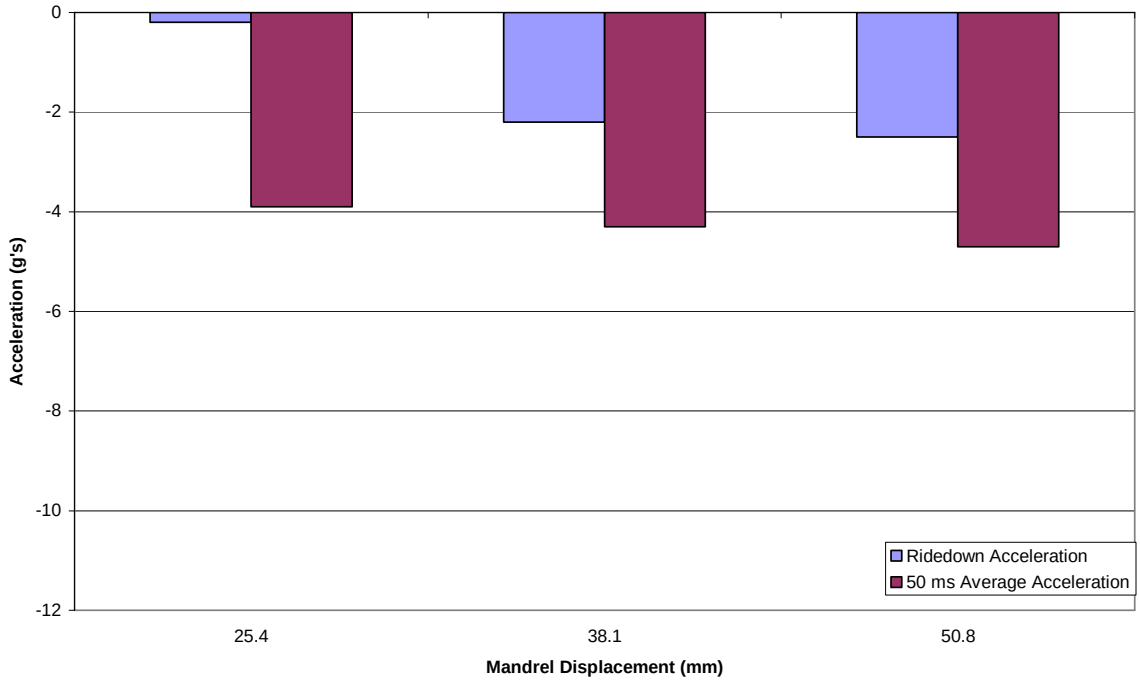

Figure 60. DN100 Ridedown Acceleration and 50 ms Average Acceleration vs. Mandrel Displacement for 820 kg Mass

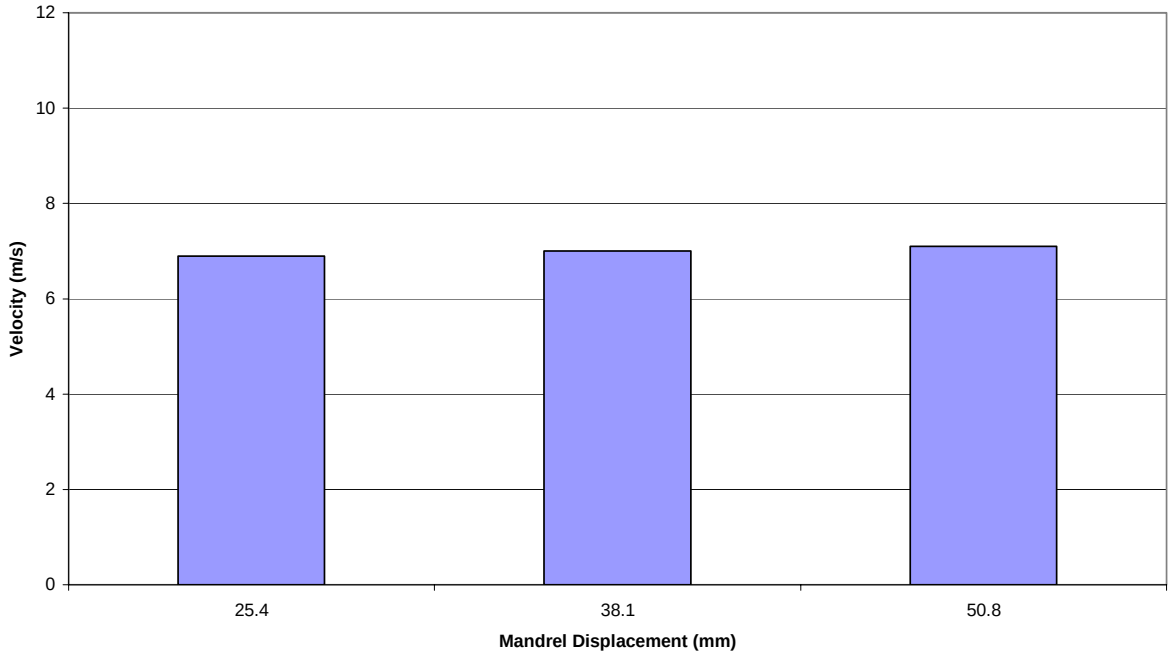

Figure 61. DN125 Occupant Impact Velocity vs. Mandrel Displacement for 820 kg Mass

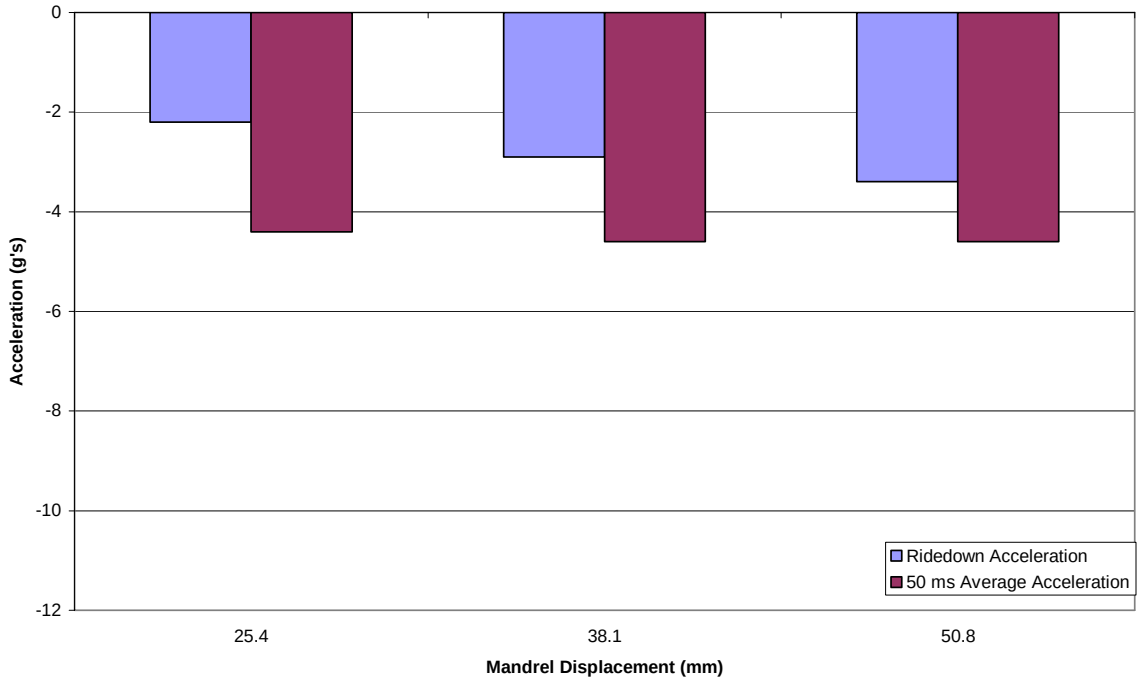

Figure 62. DN125 Ridedown Acceleration and 50 Millisecond Average Acceleration vs. Mandrel Displacement for 820 kg Mass

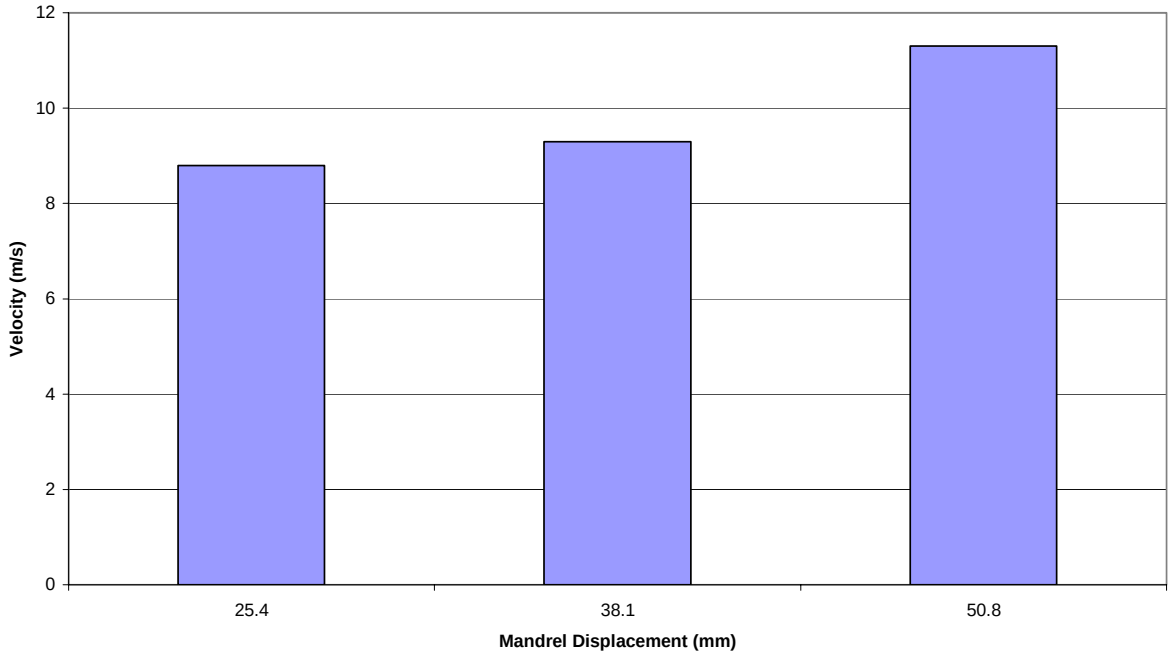

Figure 63. DNX80 Occupant Impact Velocity vs. Mandrel Displacement for 820 kg Mass

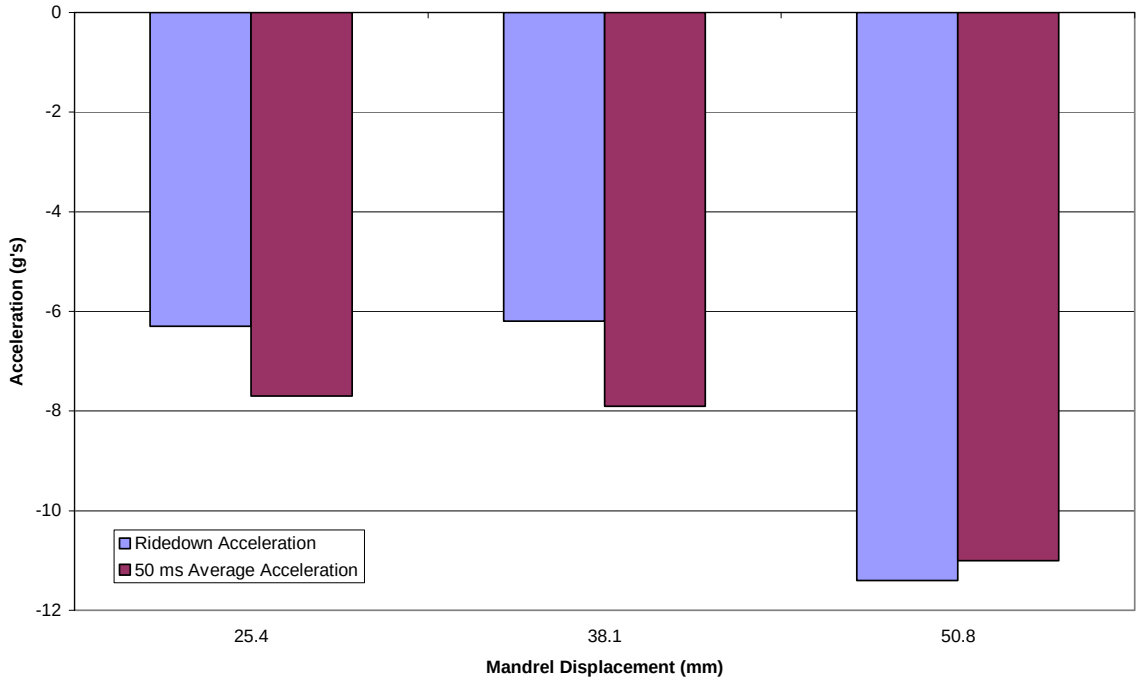

Figure 64. DNX80 Ridedown Acceleration and 50 Millisecond Average Acceleration vs. Mandrel Displacement for 820 kg Mass

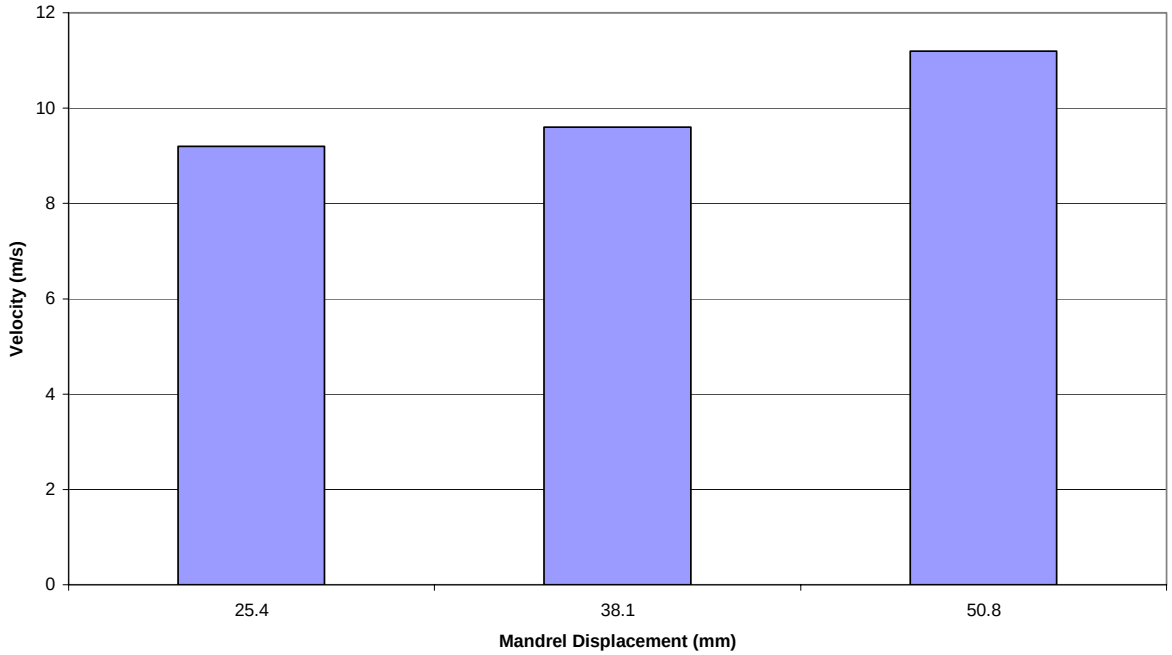

Figure 65. DNX90 Occupant Impact Velocity vs. Mandrel Displacement for 820 kg Mass

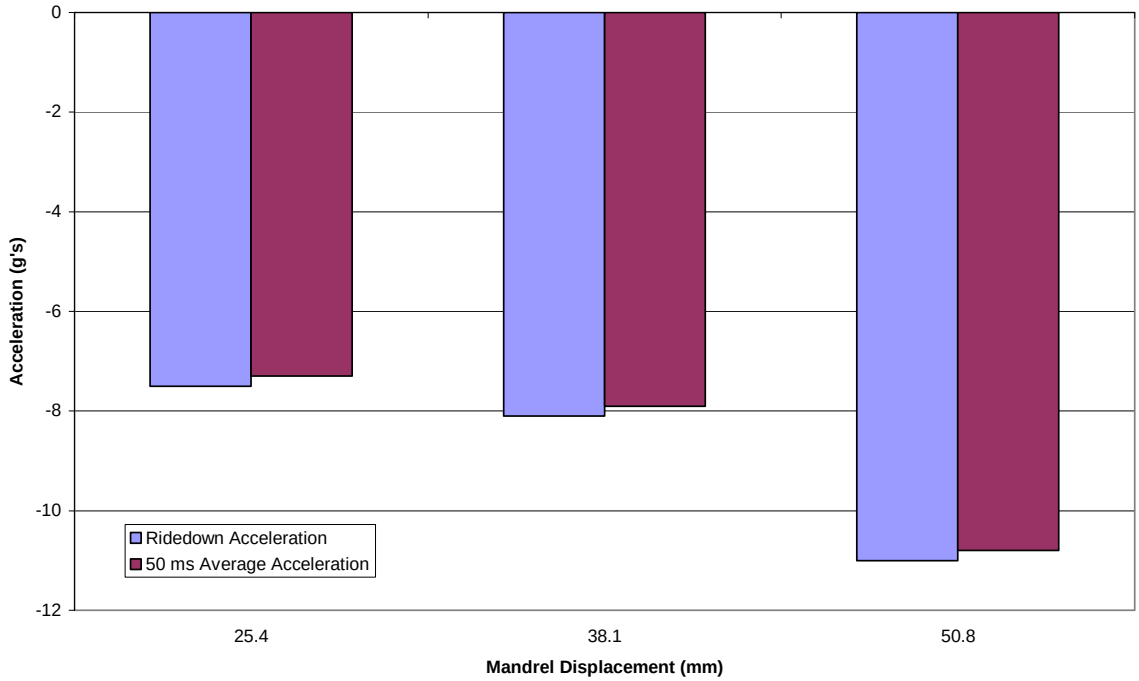

Figure 66. DNX90 Ridedown Acceleration and 50 Millisecond Average Acceleration vs. Mandrel Displacement for 820 kg Mass

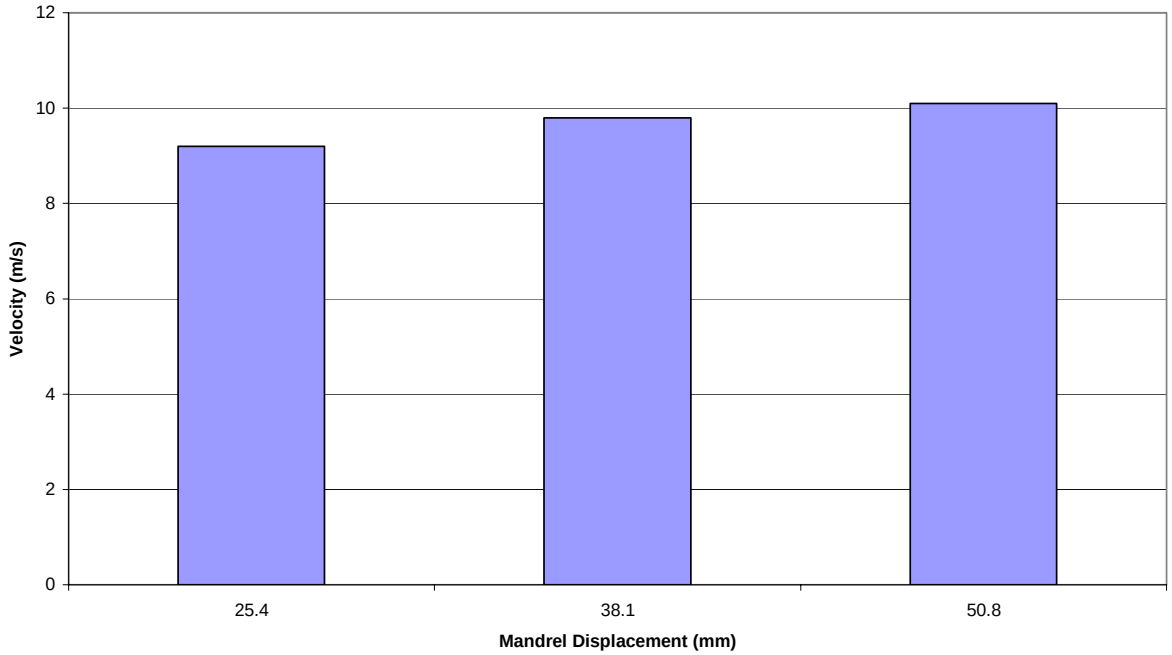

Figure 67. DNX100 Occupant Impact Velocity vs. Mandrel Displacement for 820 kg Mass

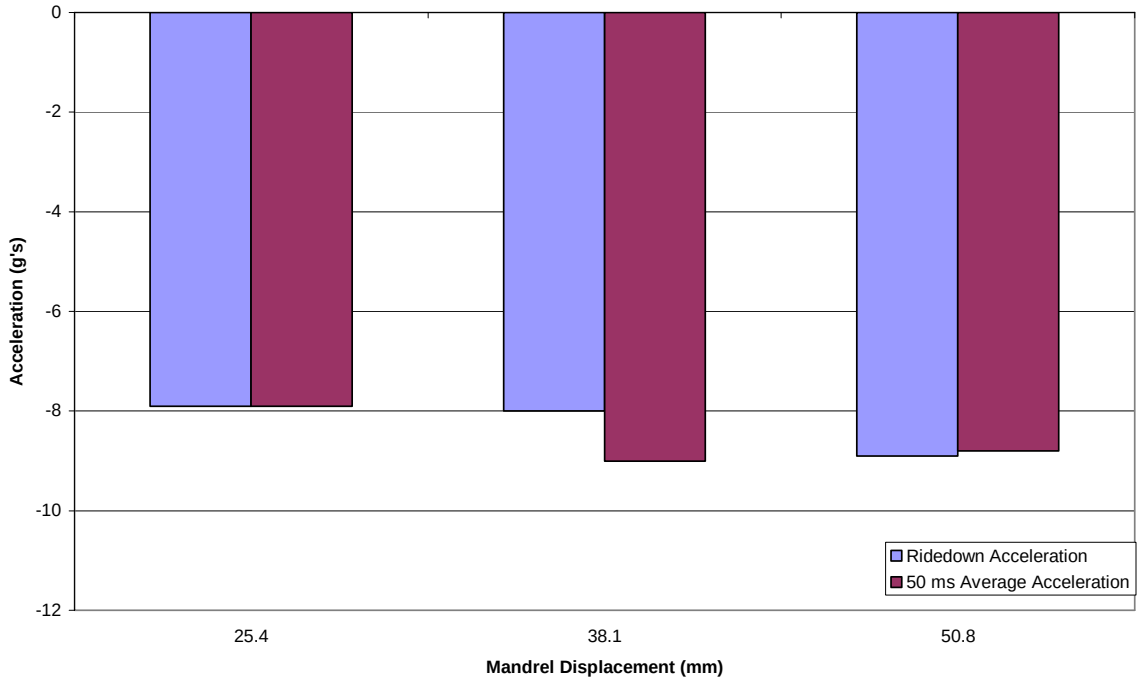

Figure 68. DNX100 Ridedown Acceleration and 50 Millisecond Average Acceleration vs. Mandrel Displacement for 820 kg Mass

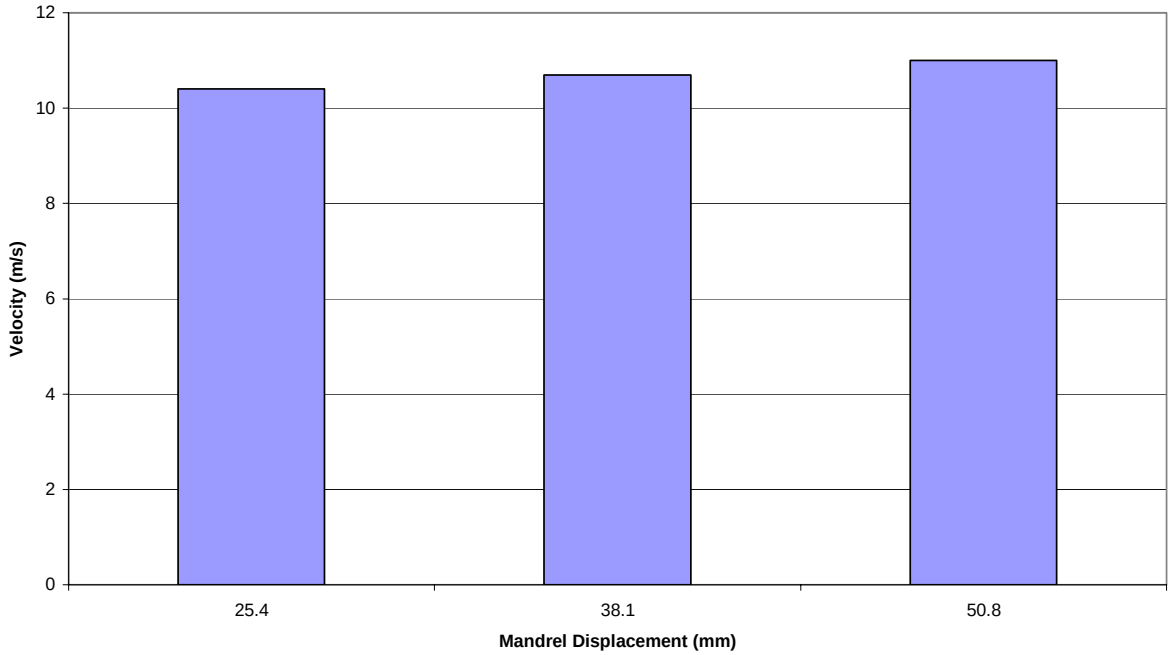

Figure 69. DNX125 Occupant Impact Velocity vs. Mandrel Displacement for 820 kg Mass

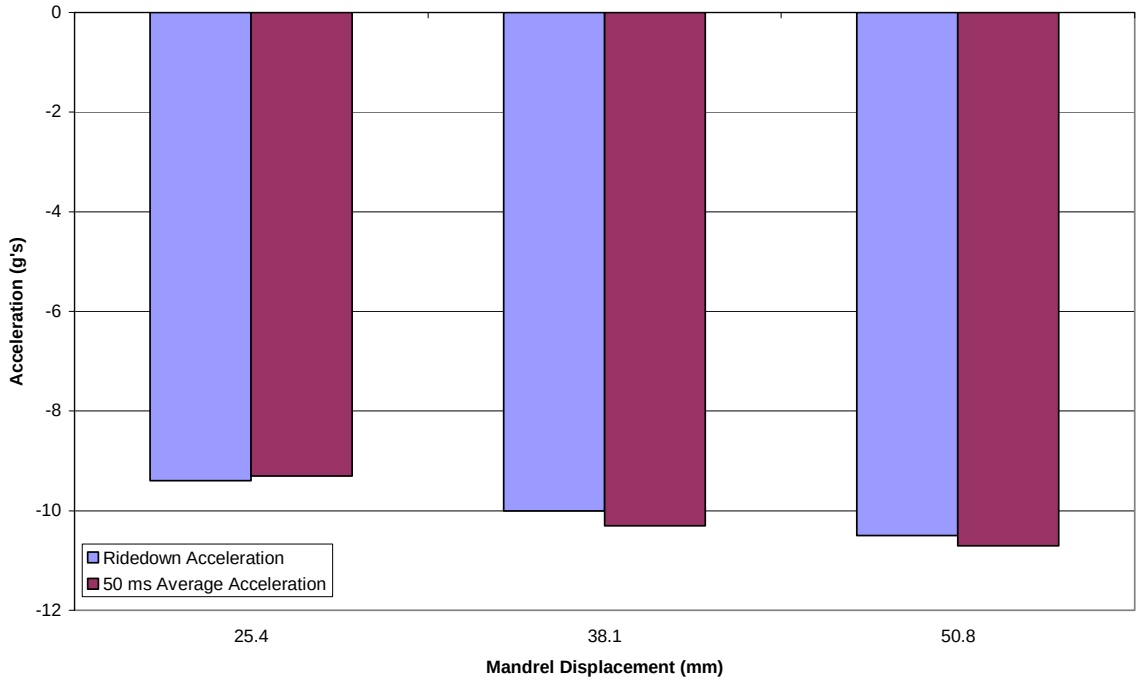

Figure 70. DNX125 Ridedown Acceleration and 50 Millisecond Average Acceleration vs. Mandrel Displacement for 820 kg Mass

APPENDIX D

2000 kg MASS EXPANDING TUBE SIMULATION RESULTS

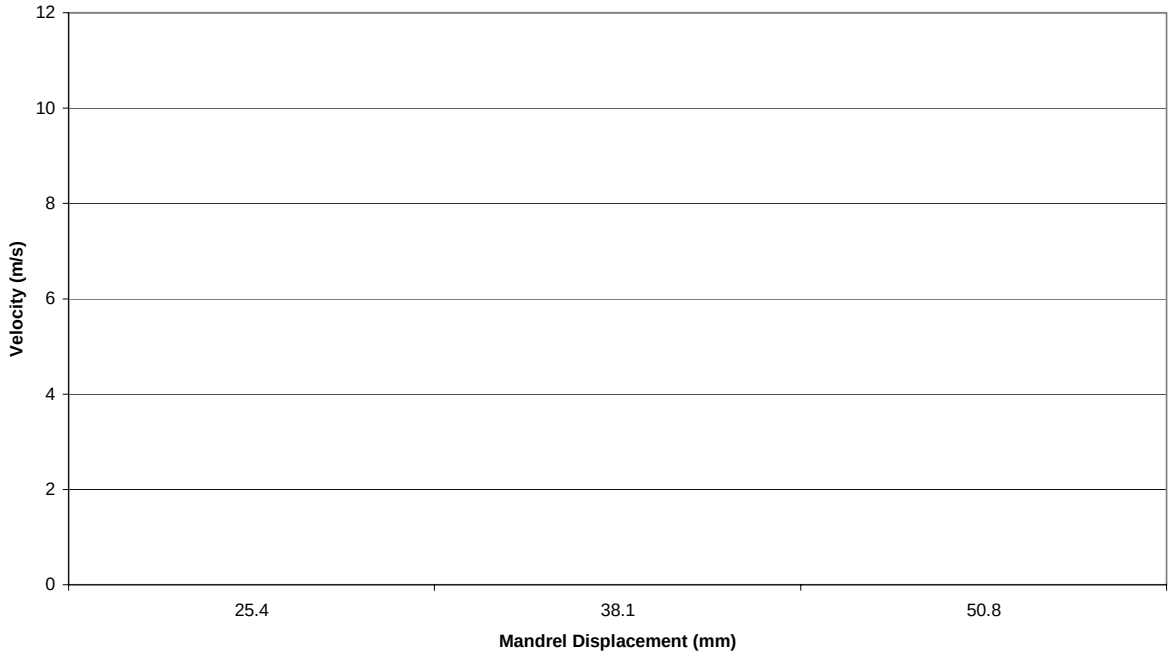

Figure 71. DN80 Occupant Impact Velocity vs. Mandrel Displacement for 2000 kg Mass

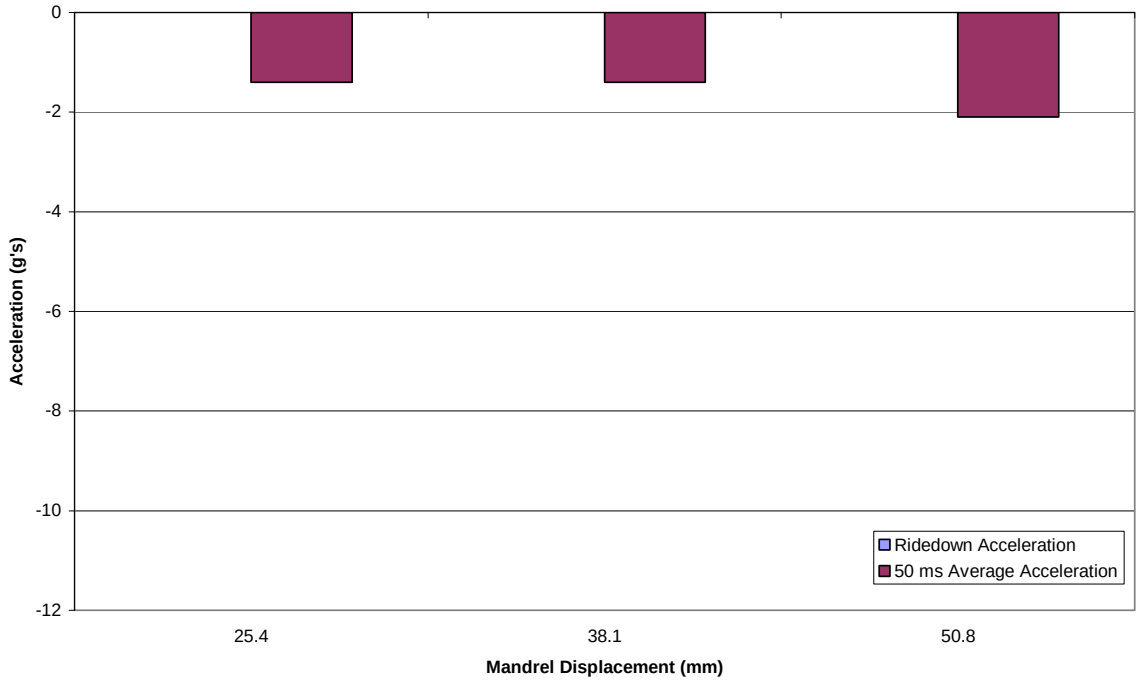

Figure 72. DN80 Ridedown Acceleration and 50 Millisecond Average Acceleration vs. Mandrel Displacement for 2000 kg Mass

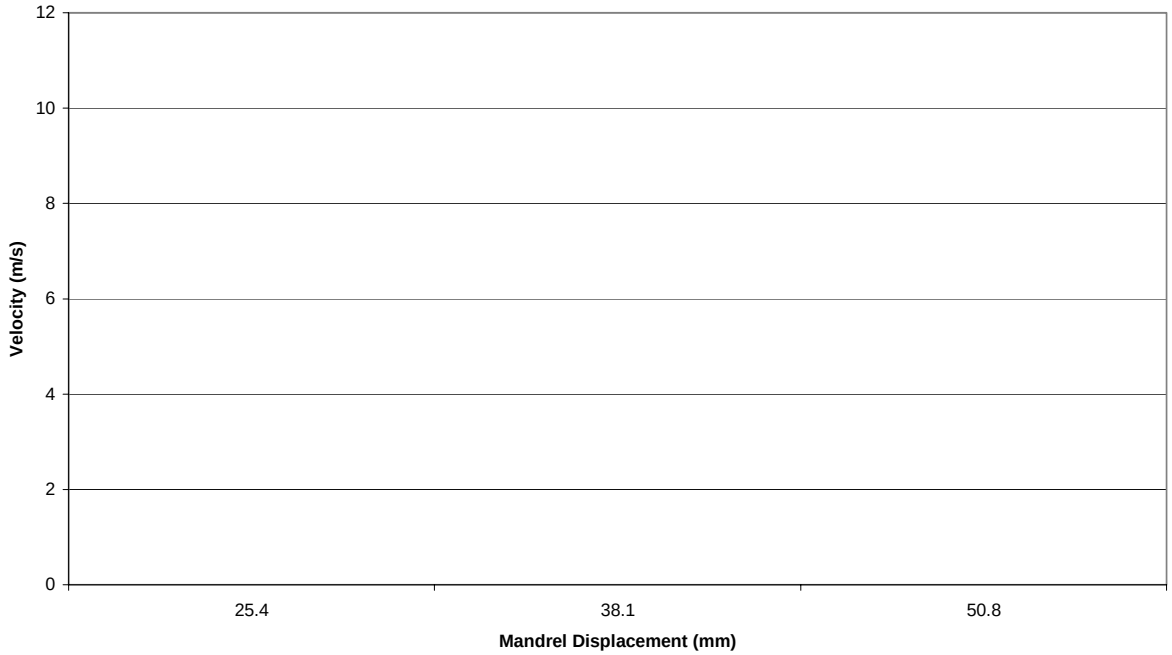

Figure 73. DN90 Occupant Impact Velocity vs. Mandrel Displacement for 2000 kg Mass

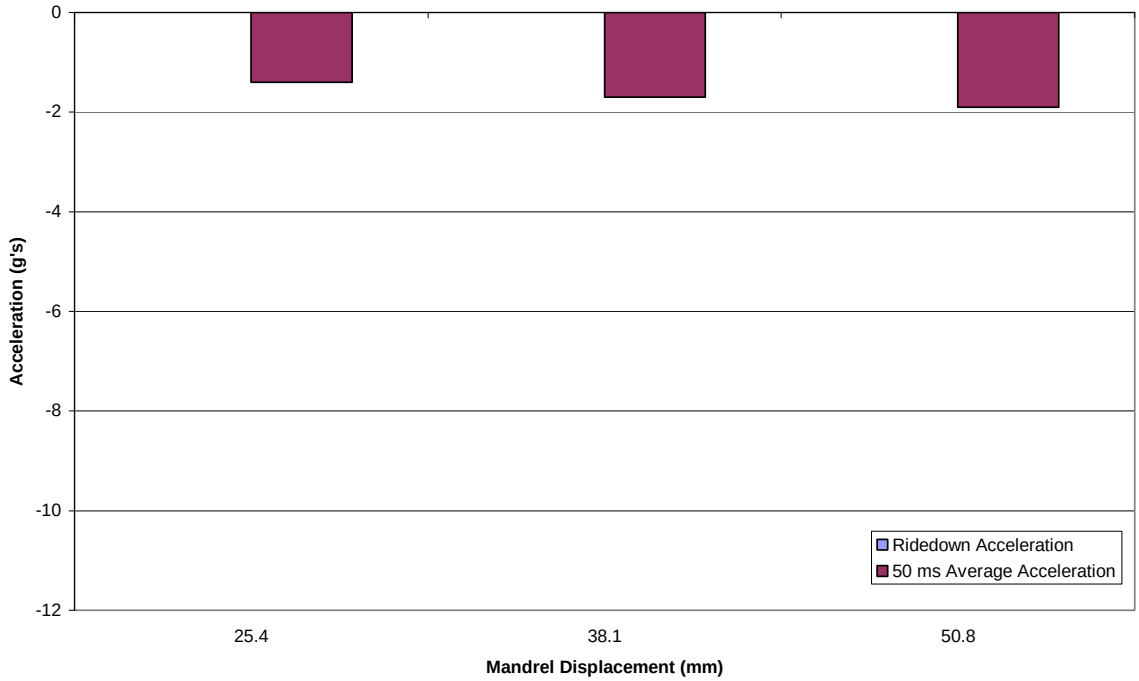

Figure 74. DN90 Ridedown Acceleration and 50 Millisecond Average Acceleration vs. Mandrel Displacement for 2000 kg Mass

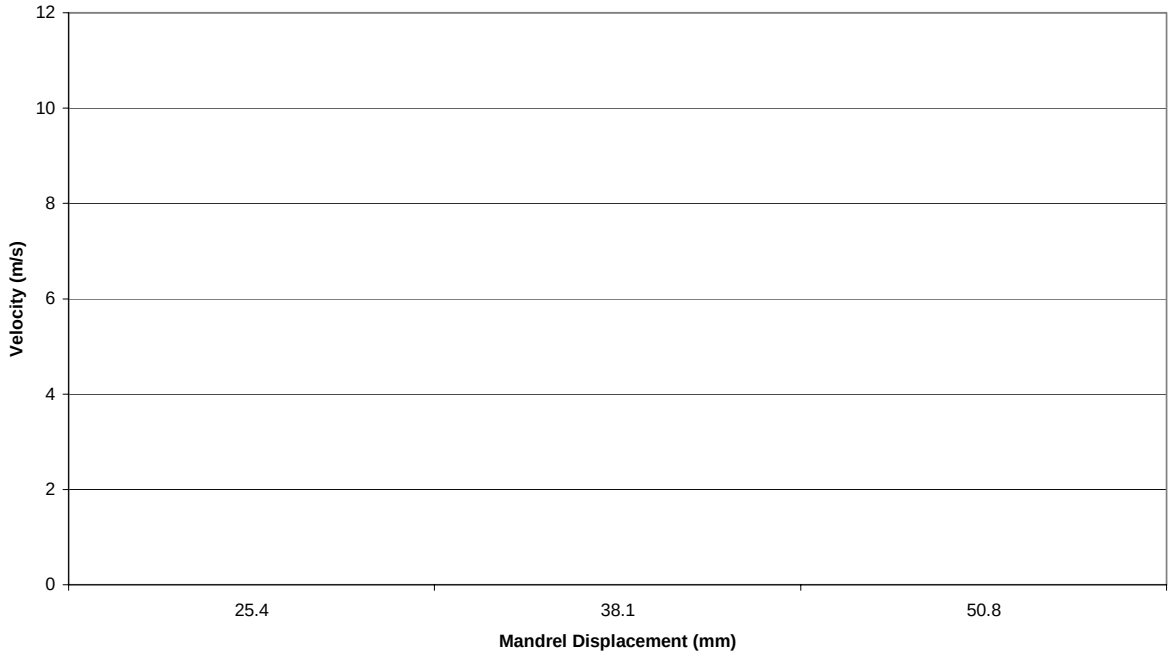

Figure 75. DN100 Occupant Impact Velocity vs. Mandrel Displacement for 2000 kg Mass

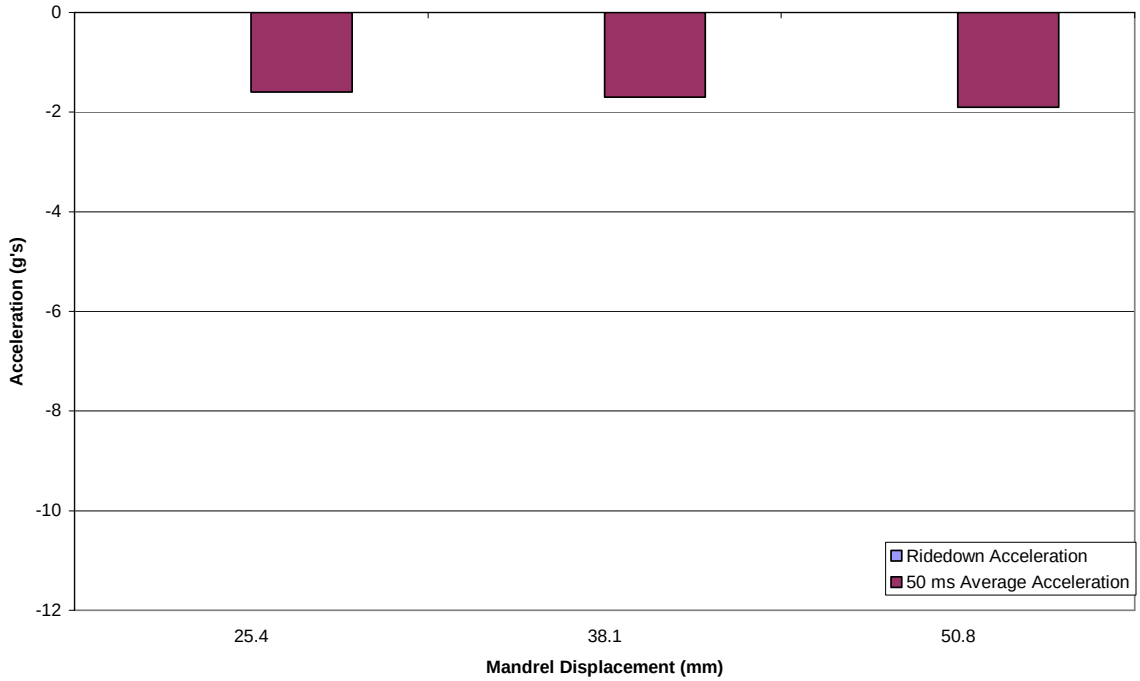

Figure 76. DN100 Ridedown Acceleration and 50 Millisecond Average Acceleration vs. Mandrel Displacement for 2000 kg Mass

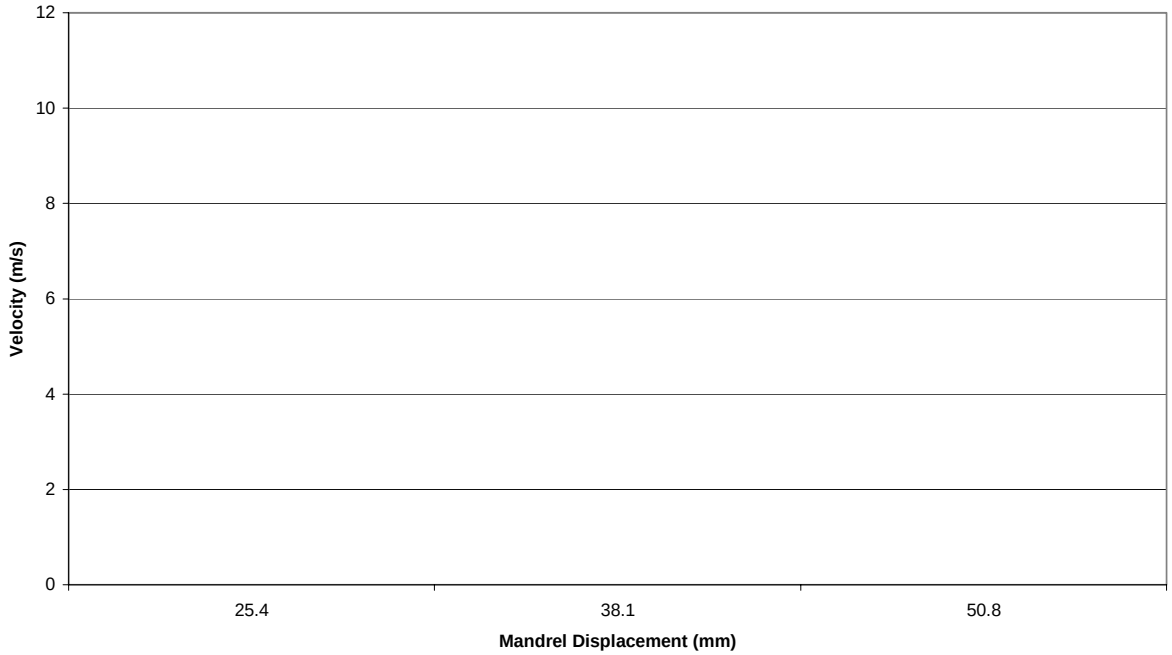

Figure 77. DN125 Occupant Impact Velocity vs. Mandrel Displacement for 2000 kg Mass

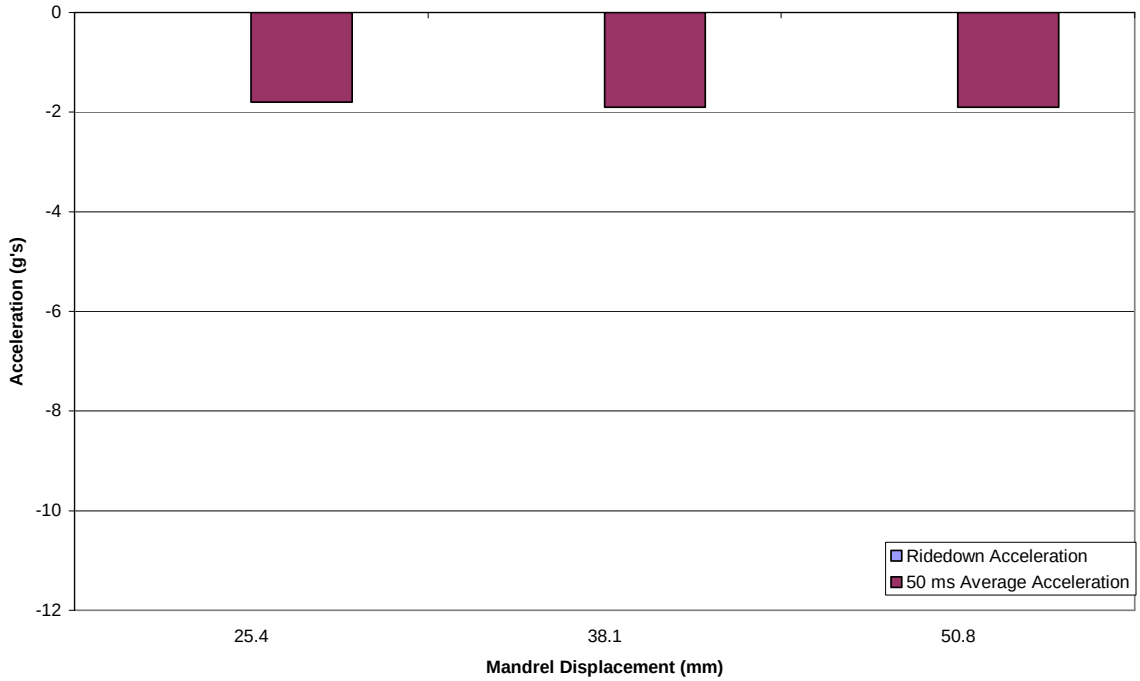

Figure 78. DN125 Ridedown Acceleration and 50 Millisecond Average Acceleration vs. Mandrel Displacement for 2000 kg Mass

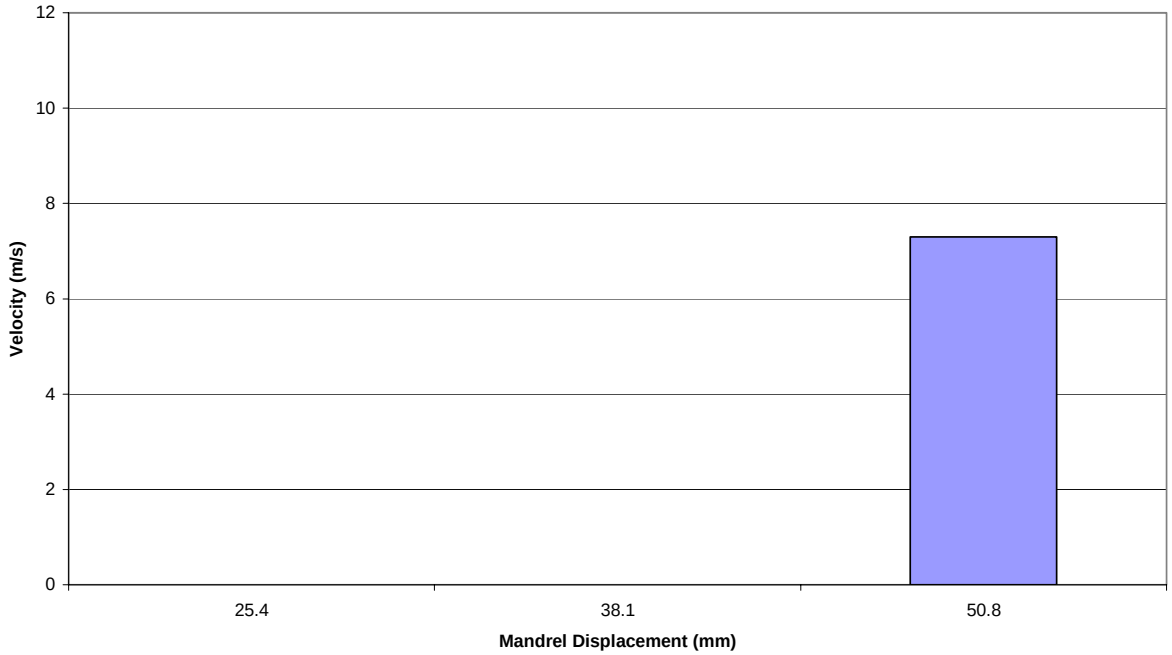

Figure 79. DNX80 Occupant Impact Velocity vs. Mandrel Displacement for 2000 kg Mass

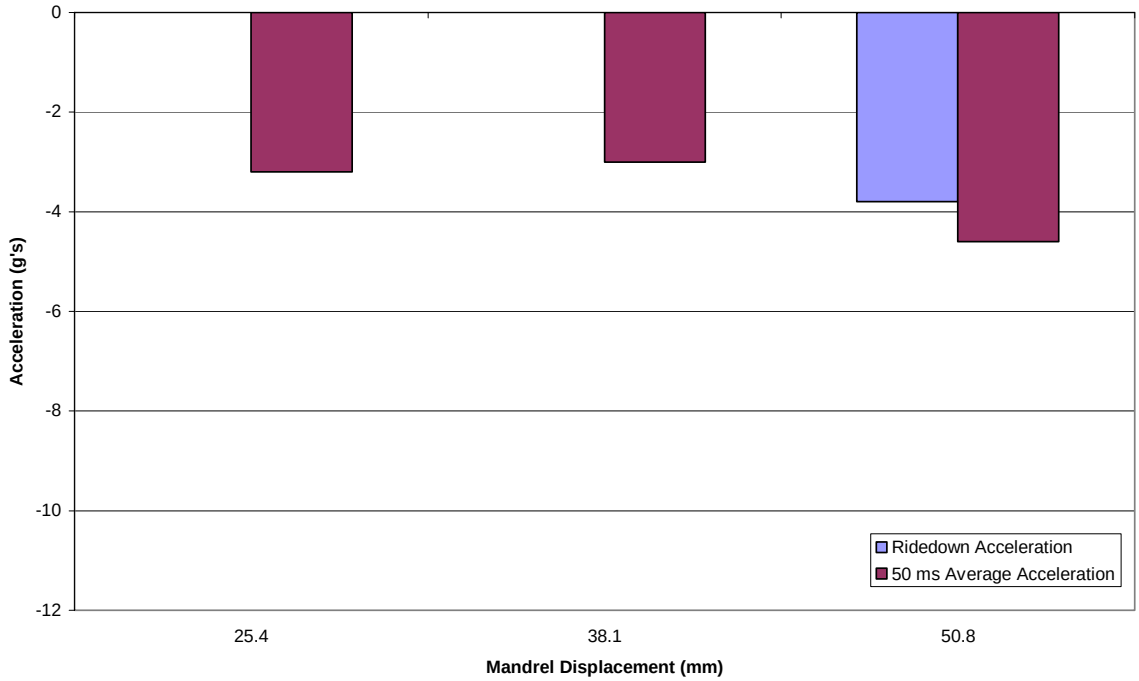

Figure 80. DNX80 Ridedown Acceleration and 50 Millisecond Average Acceleration vs. Mandrel Displacement for 2000 kg Mass

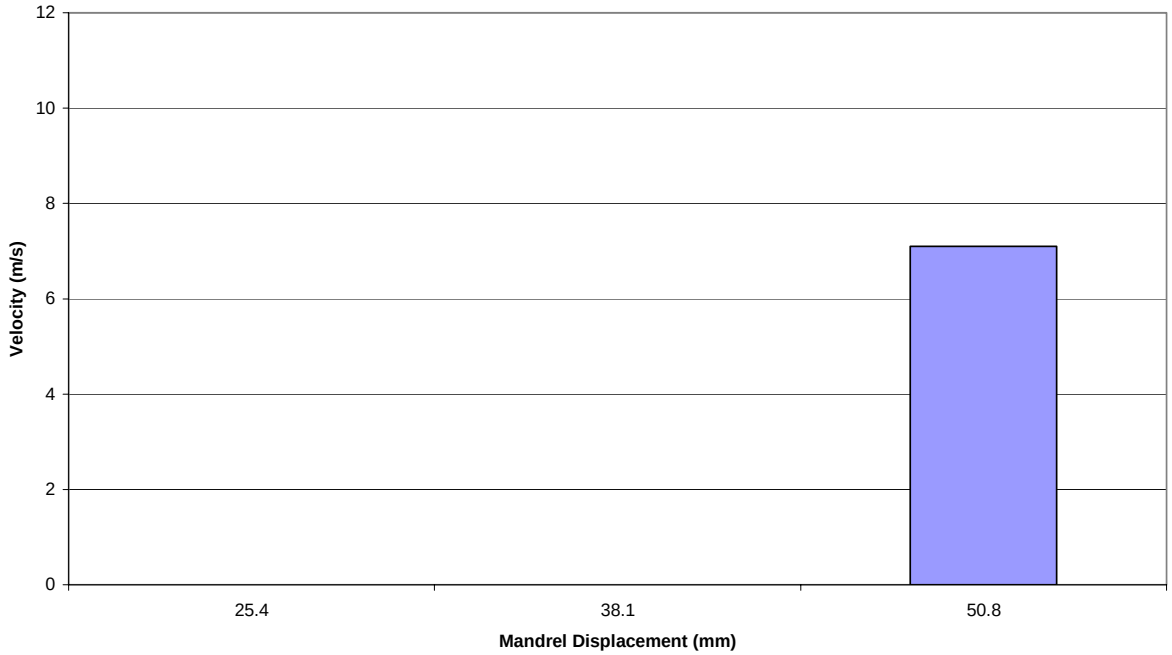

Figure 81. DNX90 Occupant Impact Velocity vs. Mandrel Displacement for 2000 kg Mass

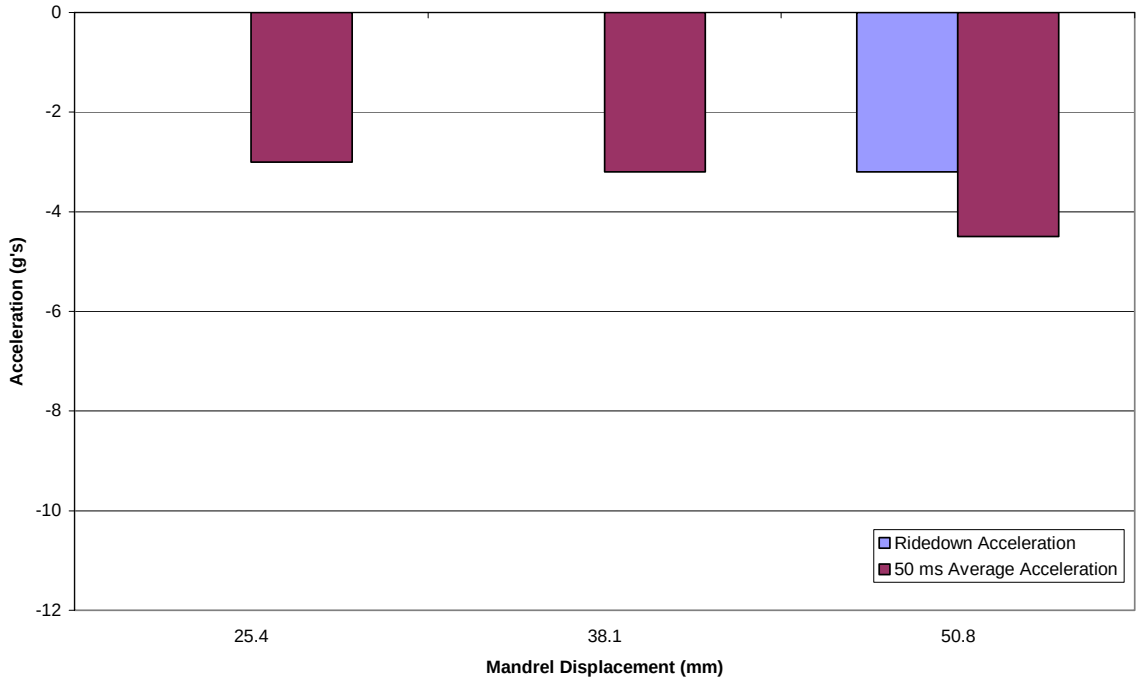

Figure 82. DNX90 Ridedown Acceleration and 50 Millisecond Average Acceleration vs. Mandrel Displacement for 2000 kg Mass

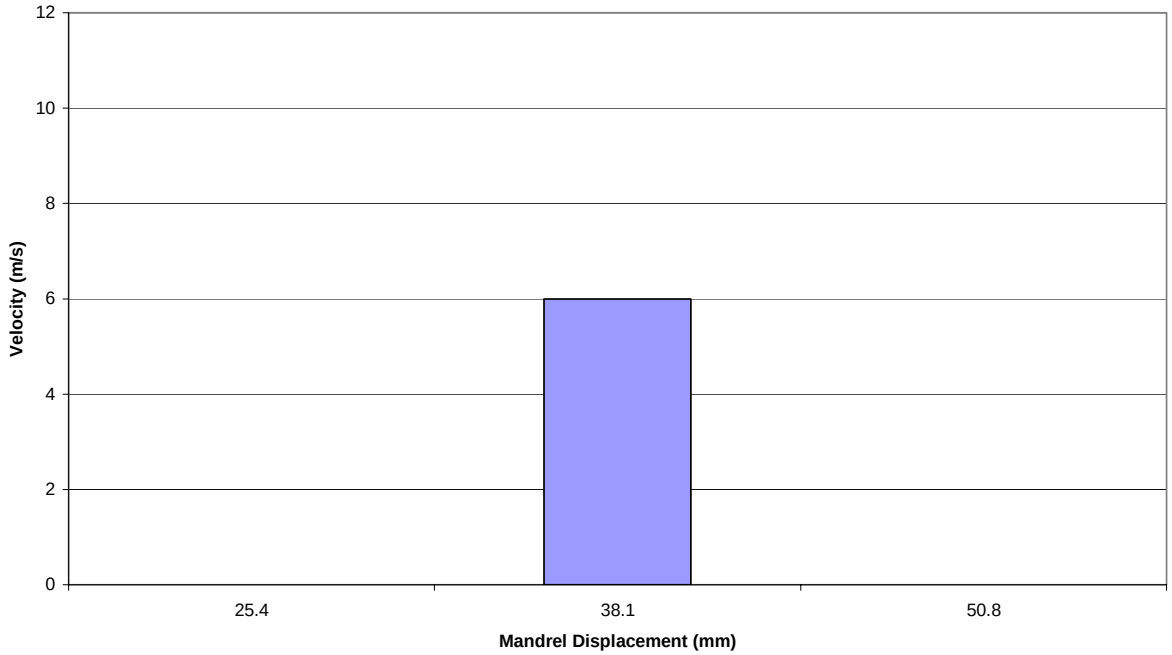

Figure 83. DNX100 Occupant Impact Velocity vs. Mandrel Displacement for 2000 kg Mass

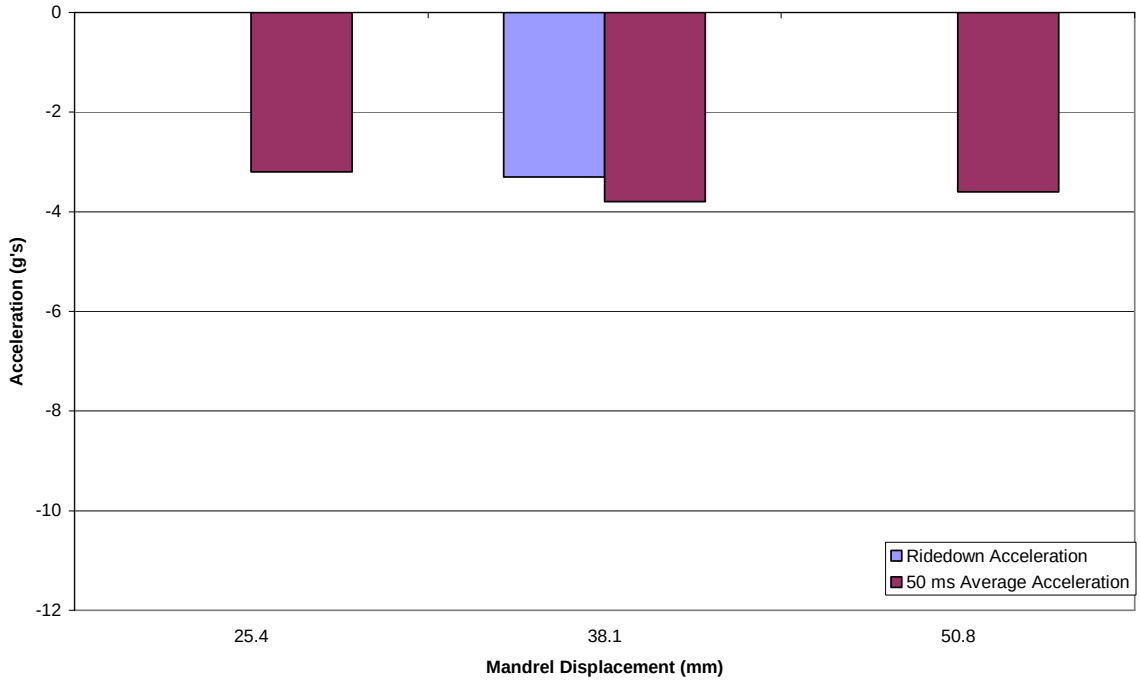

Figure 84. DNX100 Ridedown Acceleration and 50 Millisecond Average Acceleration vs. Mandrel Displacement for 2000 kg Mass

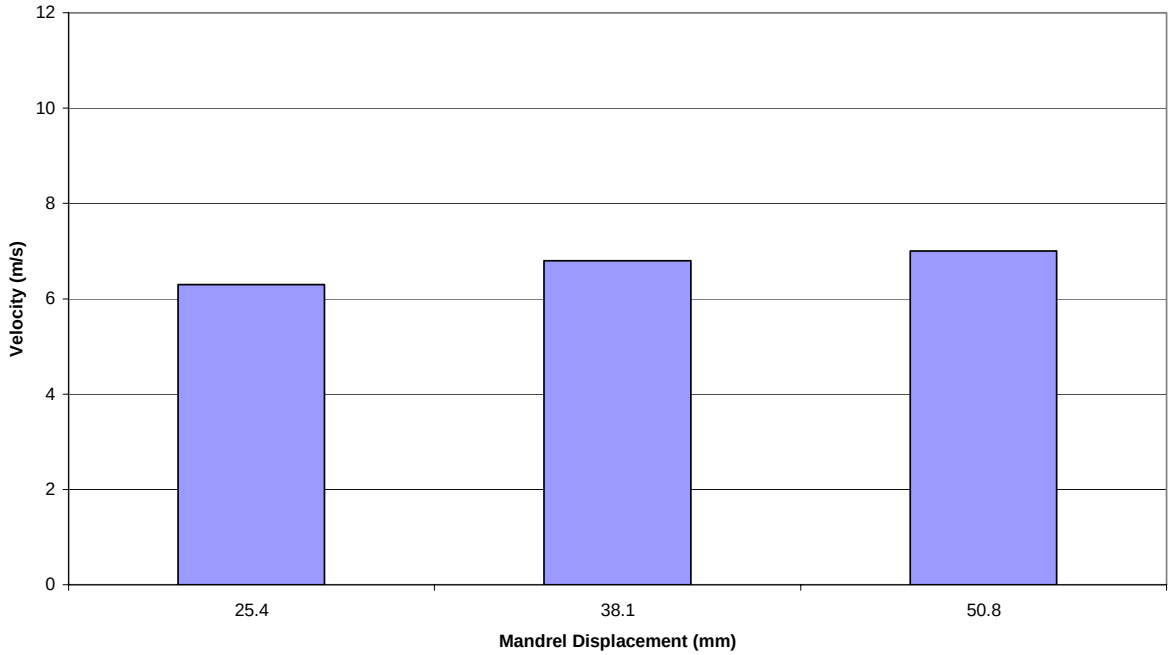

Figure 85. DNX125 Occupant Impact Velocity vs. Mandrel Displacement for 2000 kg Mass

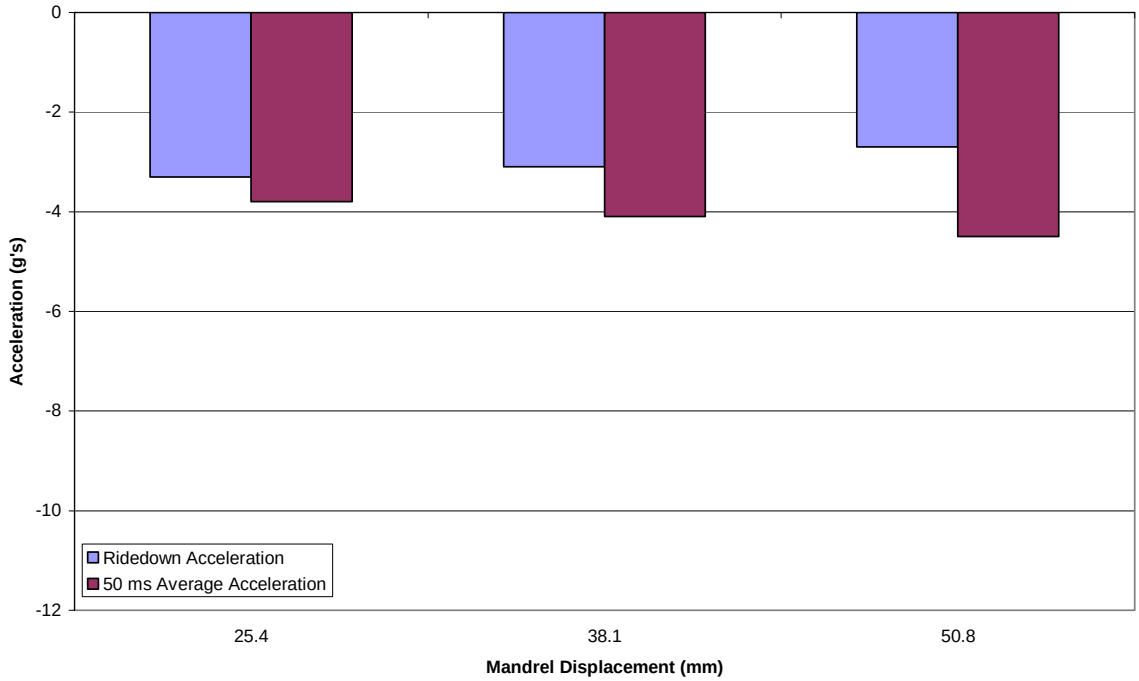

Figure 86. DNX125 Ridedown Acceleration and 50 Millisecond Average Acceleration vs. Mandrel Displacement for 2000 kg Mass

APPENDIX E

DEFORMING AN+GLE SIMULATION RESULTS

Table 6. Deforming Angle Simulation Table

Test No.	Vehicle Mass (kg)	Angle Thk (mm)	Arm Length (mm)	Bend Disp (mm)	Edge Dist (mm)	Moment Arm (mm)
1	2000	9.525	88.9	19.05	15.875	63.5
2	2000	9.525	88.9	19.05	19.05	60.3
3	2000	9.525	88.9	19.05	25.4	54.0
4	2000	9.525	88.9	19.05	31.75	47.6
5	2000	9.525	88.9	19.05	38.1	41.3
6	2000	9.525	88.9	25.4	12.7	66.7
7	2000	9.525	88.9	25.4	19.05	60.3
8	2000	9.525	88.9	38.1	38.1	41.3
9	2000	9.525	88.9	41.275	31.75	47.6
10	2000	9.525	88.9	44.45	31.75	47.6
11	2000	12.7	88.9	44.45	31.75	44.5
12	2000	9.525	88.9	50.8	12.7	66.7
13	2000	9.525	88.9	50.8	19.05	60.3
14	2000	9.525	88.9	50.8	25.4	54.0
15	2000	9.525	88.9	50.8	31.75	47.6
16	2000	9.525	88.9	50.8	38.1	41.3
17	2000	6.35	88.9	50.8	31.75	50.8
18	2000	6.35	88.9	50.8	38.1	44.5
19	820	9.525	88.9	19.05	25.4	54.0
20	820	6.35	88.9	41.275	31.75	50.8
21	820	9.525	88.9	41.275	31.75	47.6
22	820	6.35	88.9	44.45	31.75	50.8
23	820	9.525	88.9	44.45	31.75	47.6
24	820	7.9375	88.9	44.45	31.75	49.2
25	820	9.525	88.9	50.8	31.75	47.6
26	820	6.35	88.9	50.8	31.75	50.8

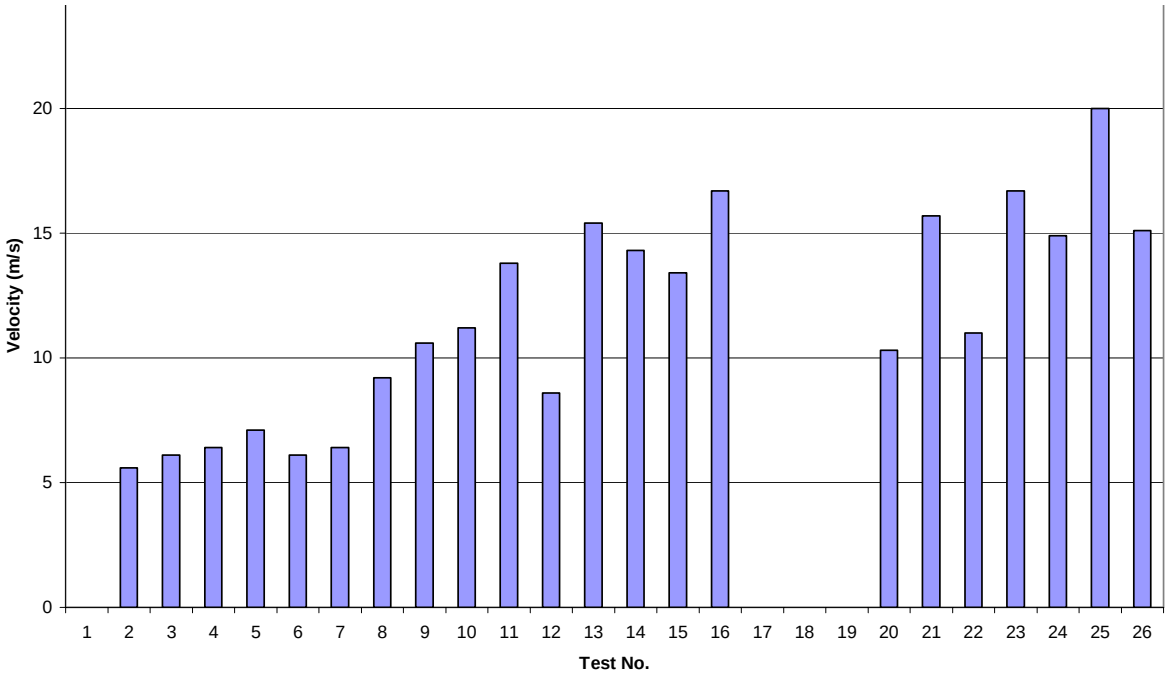

Figure 87. Occupant Impact Velocity for Deforming Angle Simulations

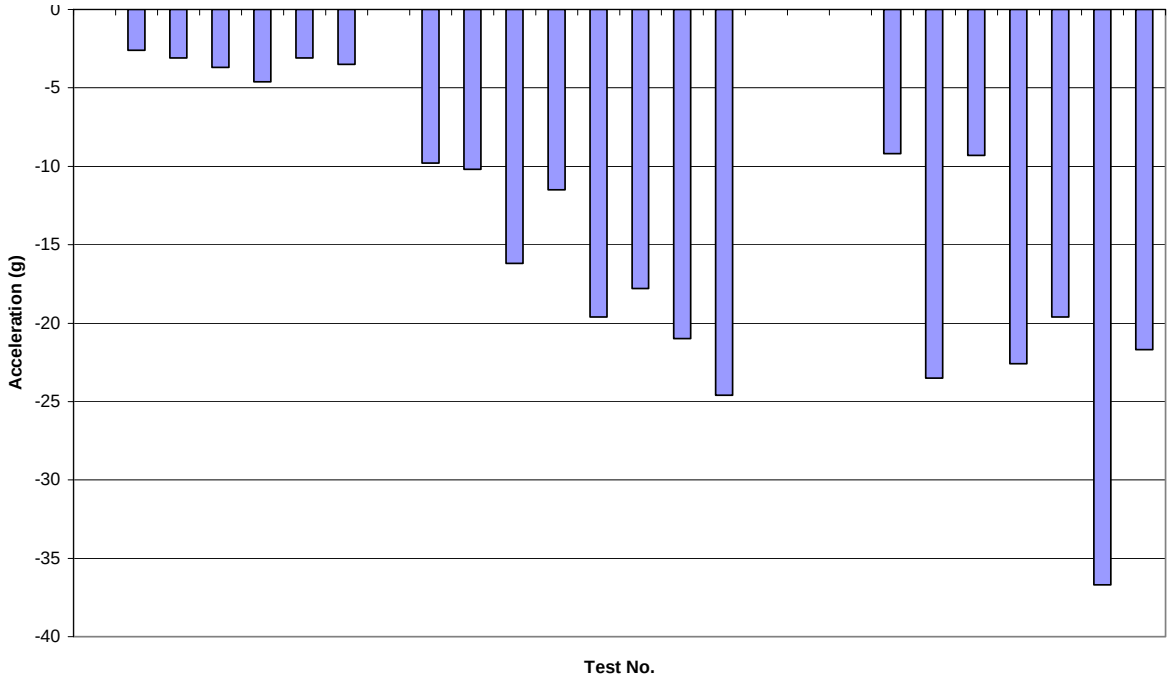

Figure 88. Ridedown Accelerations for Deforming Angle Simulations

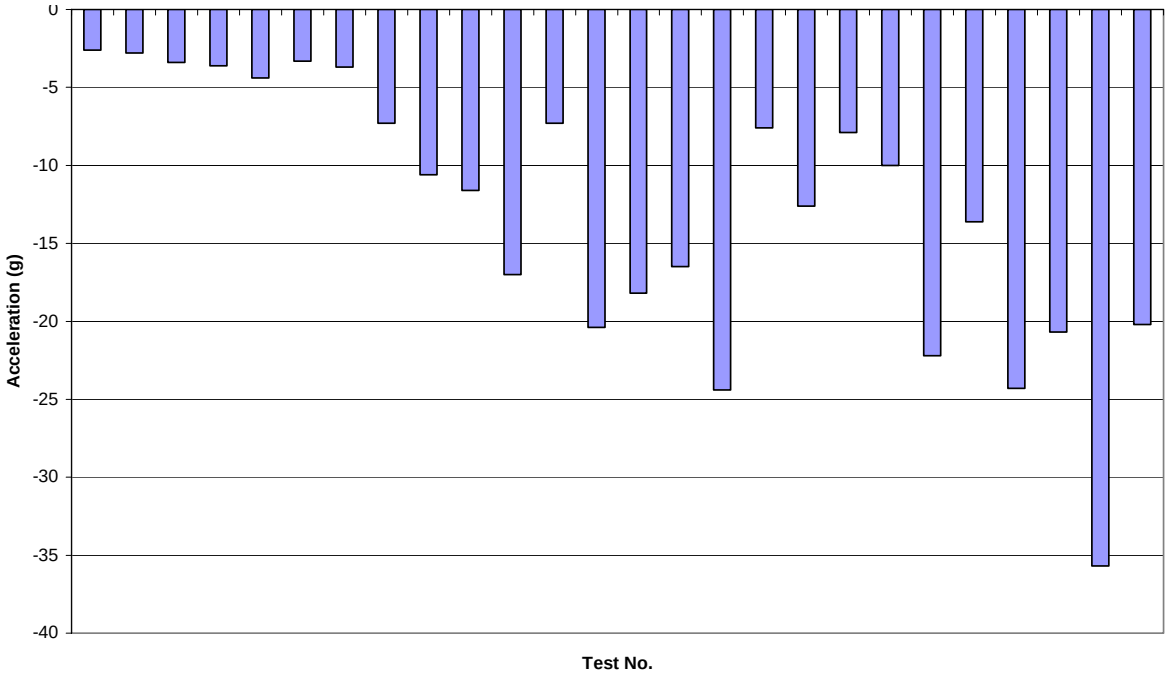

Figure 89. 50 Millisecond Average Acceleration for Deforming Angle Simulations

APPENDIX F

DEFORMING PLATE 820 kg MASS SIMULATION RESULTS

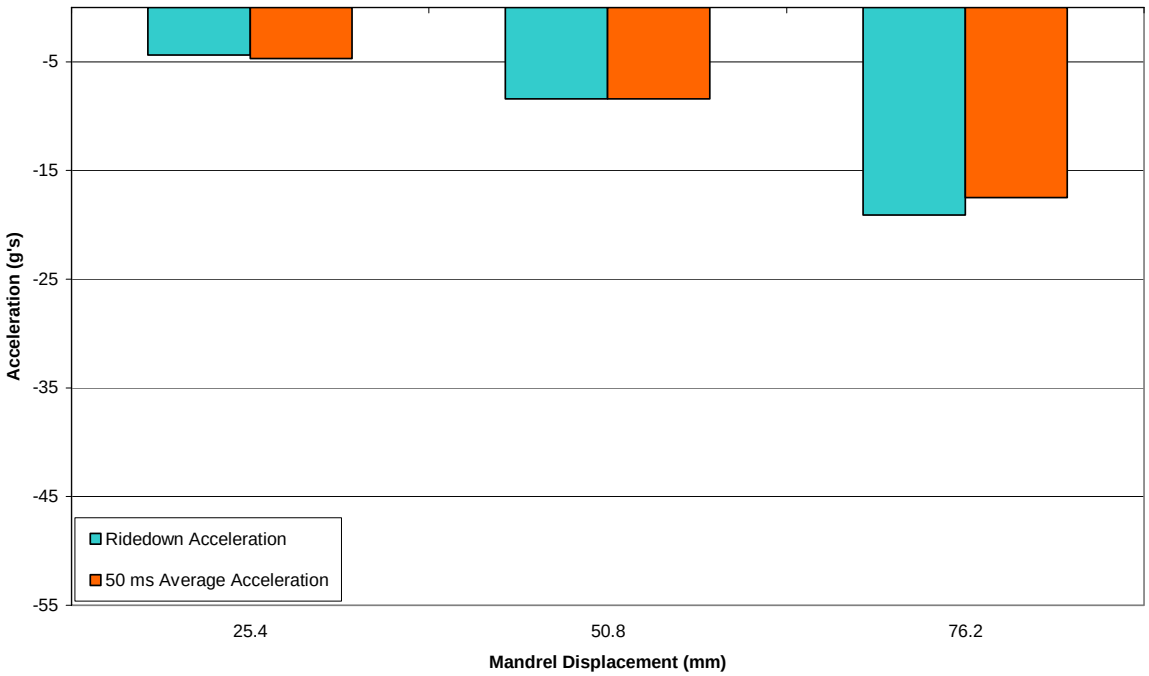

Figure 90. 6.35 mm Thick Deforming Plate with 50.8 mm Moment Arm Ridedown Acceleration and 50 Millisecond Average Acceleration vs. Mandrel Displacement for 820 kg Mass

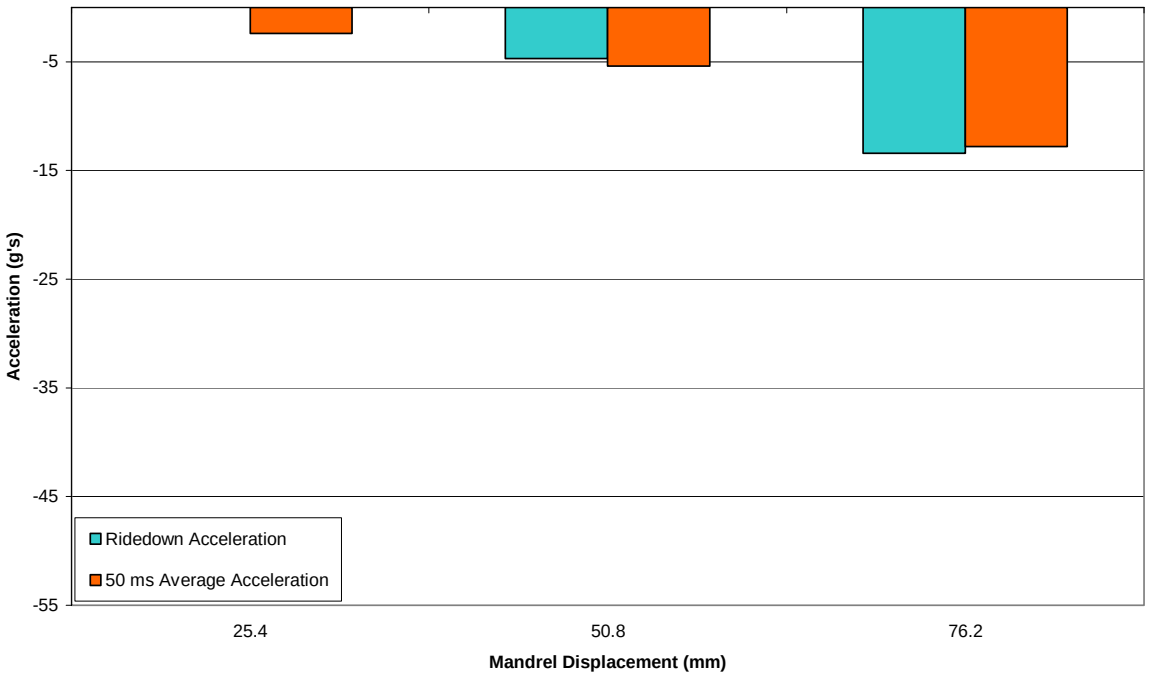

Figure 91. 6.35 mm Thick Deforming Plate with 76.2 mm Moment Arm Ridedown Acceleration and 50 Millisecond Average Acceleration vs. Mandrel Displacement for 820 kg Mass

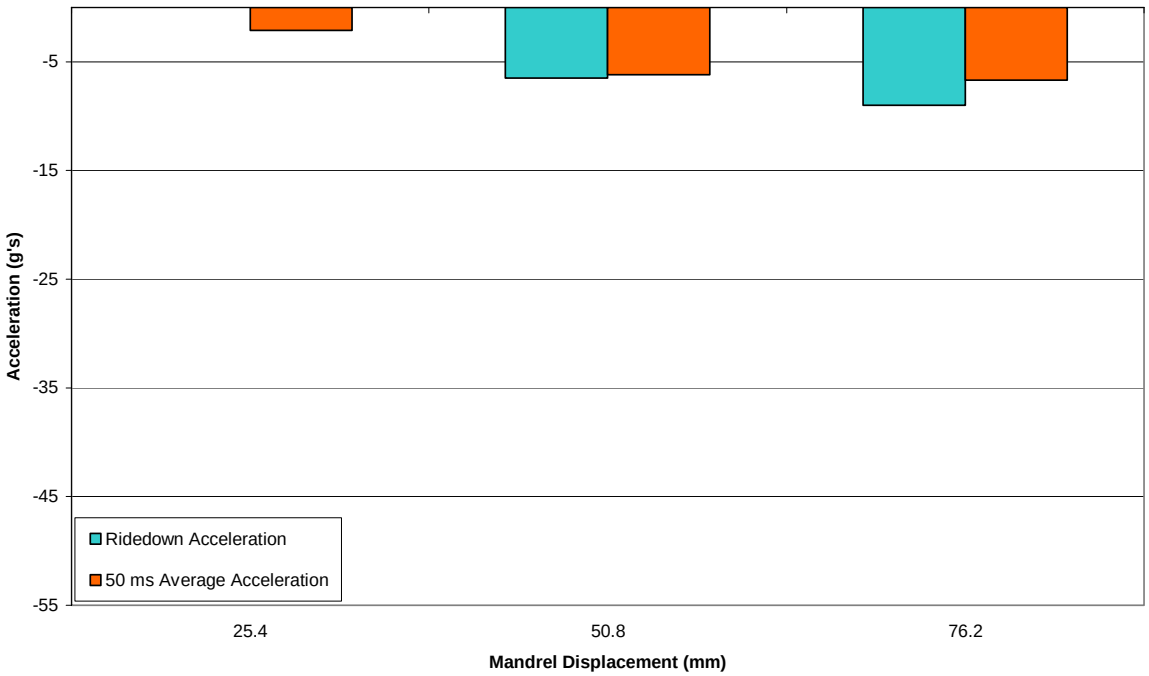

Figure 92. 6.35 mm Thick Deforming Plate with 101.6 mm Moment Arm Ridedown Acceleration and 50 Millisecond Average Acceleration vs. Mandrel Displacement for 820 kg Mass

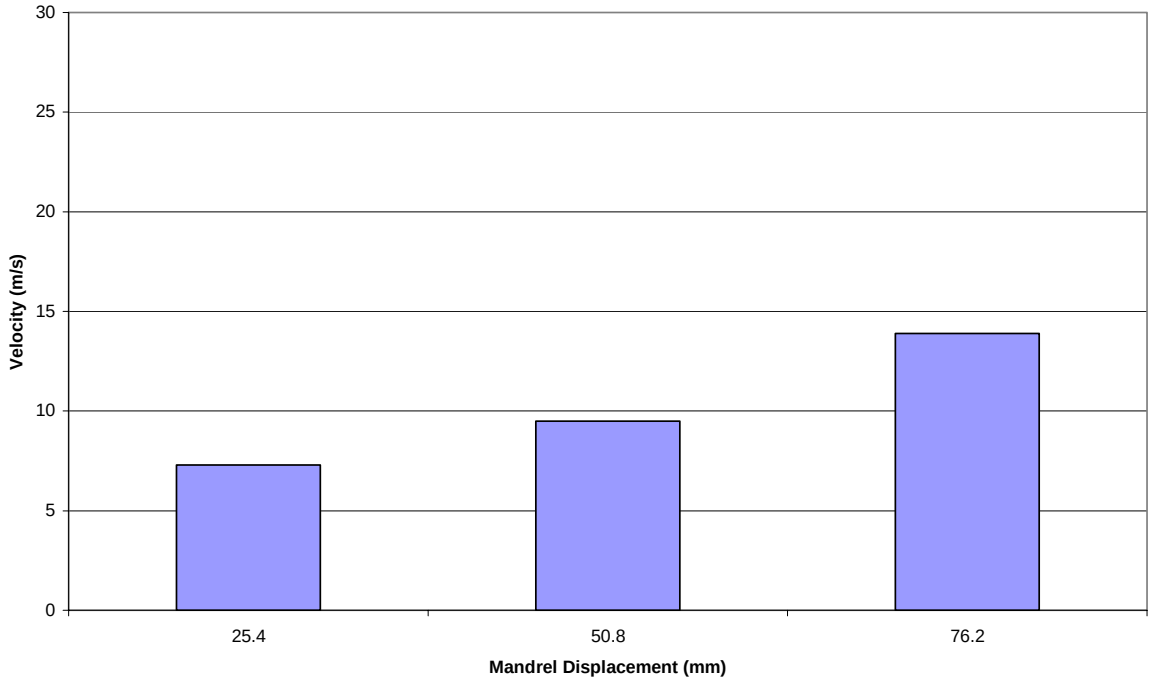

Figure 93. 6.35 mm Thick Deforming Plate with 50.8 mm Moment Arm Occupant Impact Velocity vs. Mandrel Displacement for 820 kg Mass

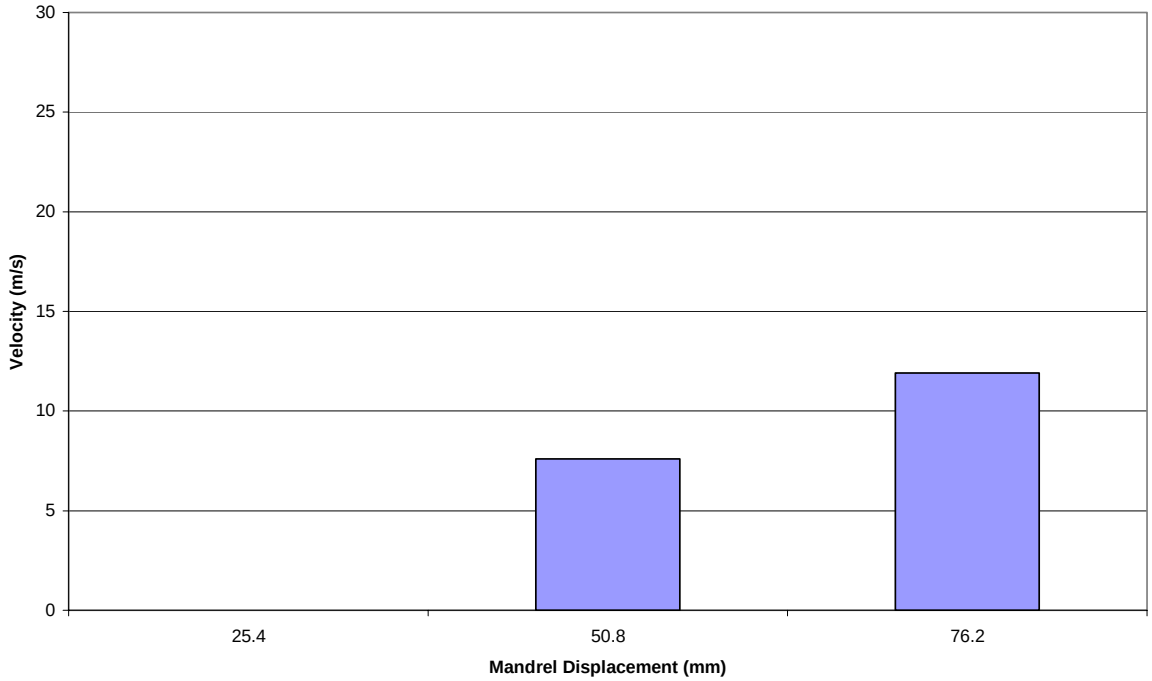

Figure 94. 6.35 mm Thick Deforming Plate with 76.2 mm Moment Arm Occupant Impact Velocity vs. Mandrel Displacement for 820 kg Mass

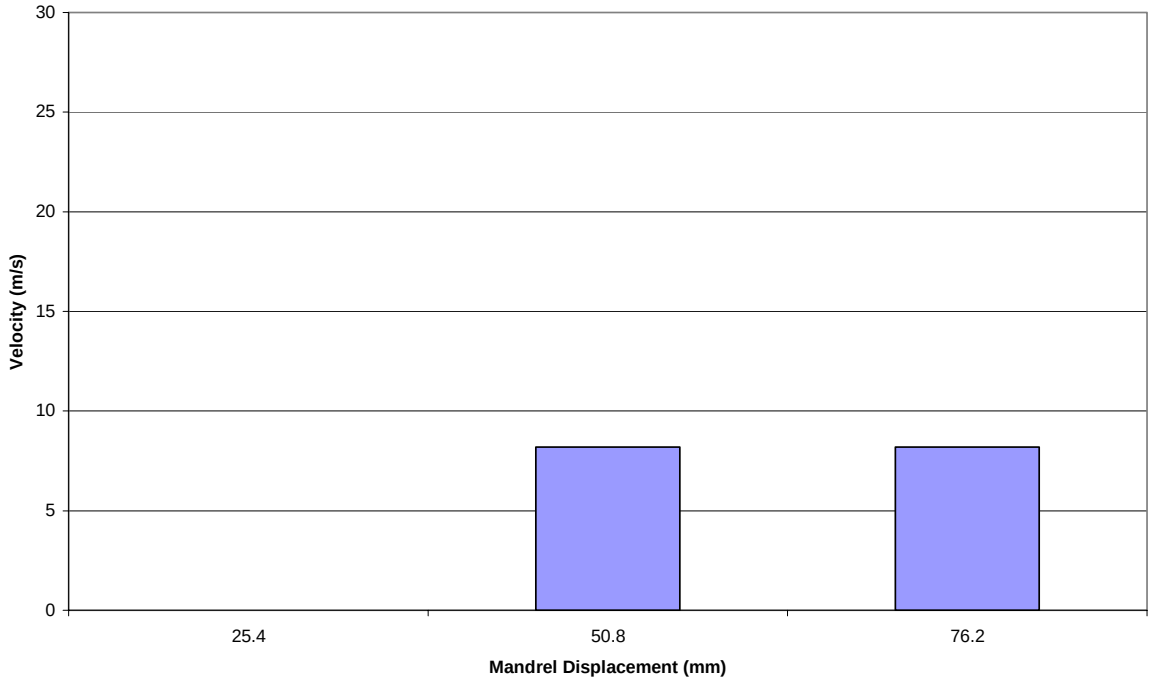

Figure 95. 6.35 mm Thick Deforming Plate with 101.6 mm Moment Arm Occupant Impact Velocity vs. Mandrel Displacement for 820 kg Mass

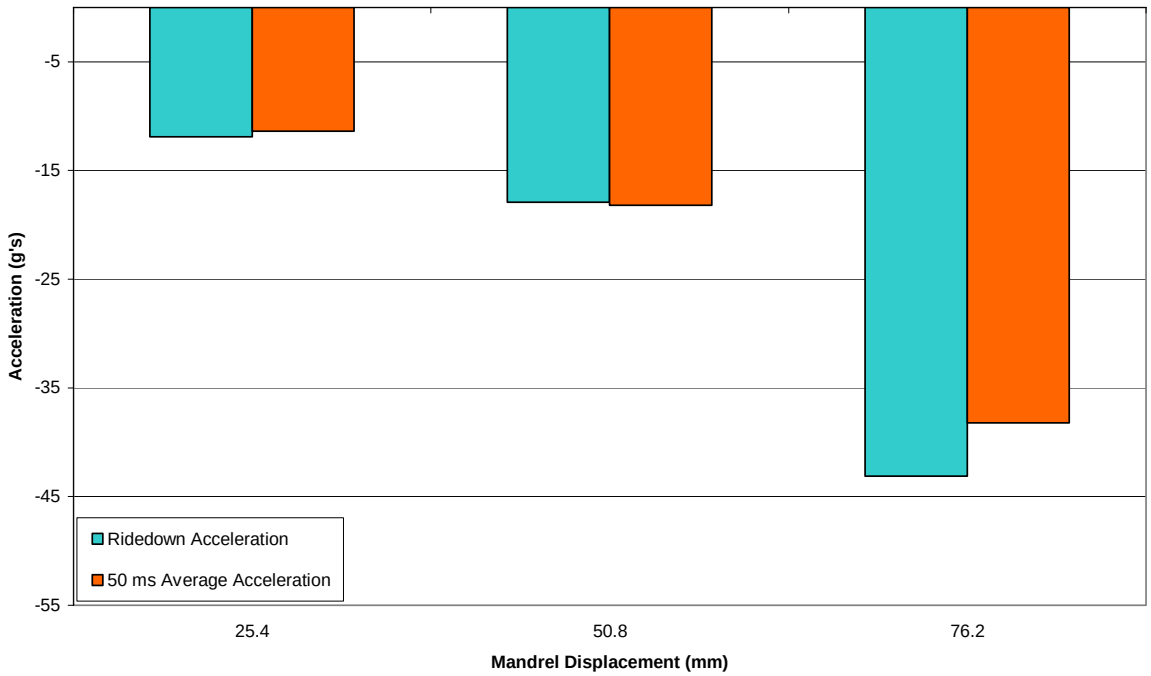

Figure 96. 9.53 mm Thick Deforming Plate with 50.8 mm Moment Arm Ridedown Acceleration and 50 Millisecond Average Acceleration vs. Mandrel Displacement for 820 kg Mass

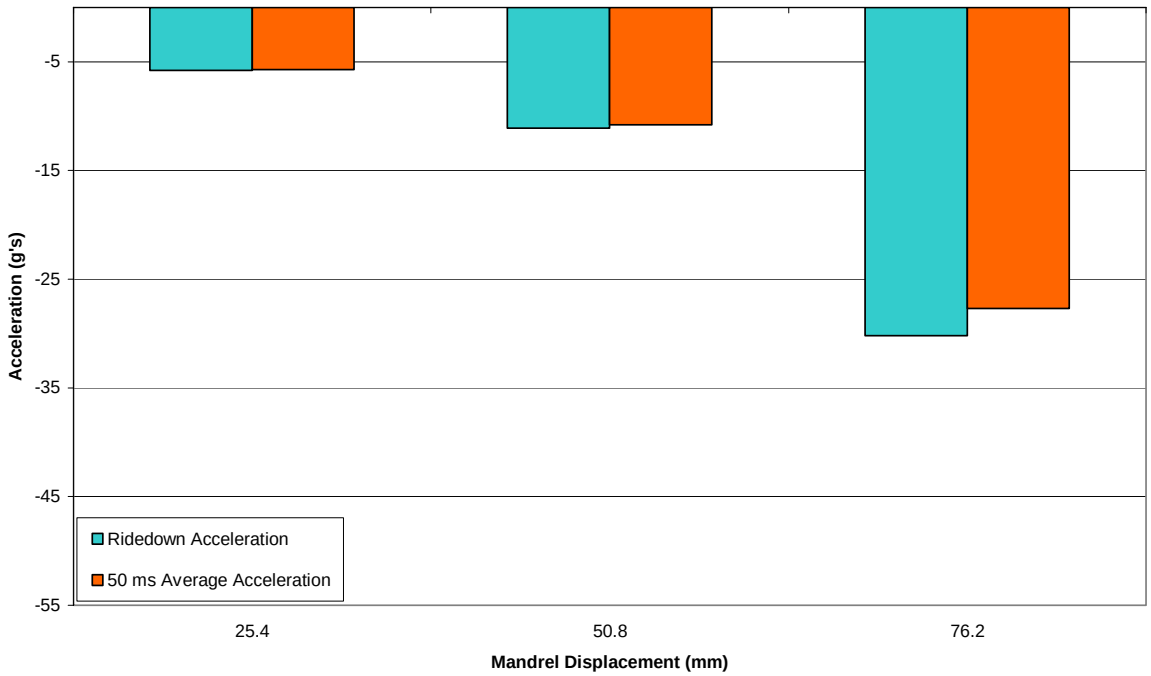

Figure 97. 9.53 mm Thick Deforming Plate with 76.2 mm Moment Arm Ridedown Acceleration and 50 Millisecond Average Acceleration vs. Mandrel Displacement for 820 kg Mass

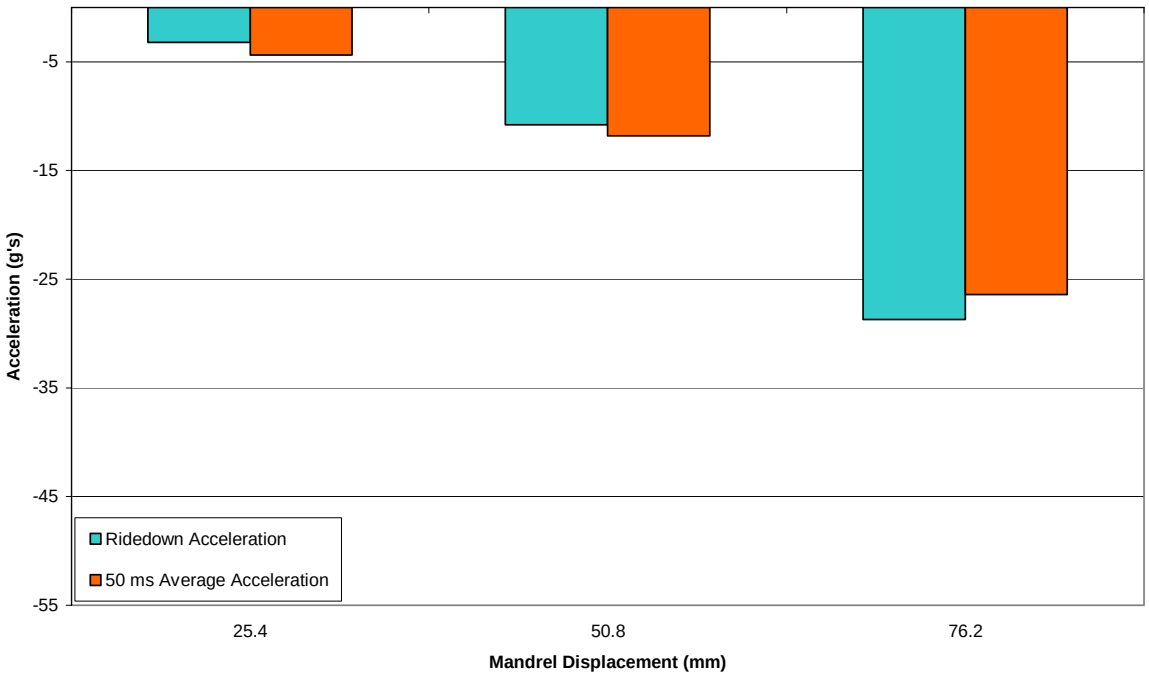

Figure 98. 9.53 mm Thick Deforming Plate with 101.5 mm Moment Arm Ridedown Acceleration and 50 Millisecond Average Acceleration vs. Mandrel Displacement for 820 kg Mass

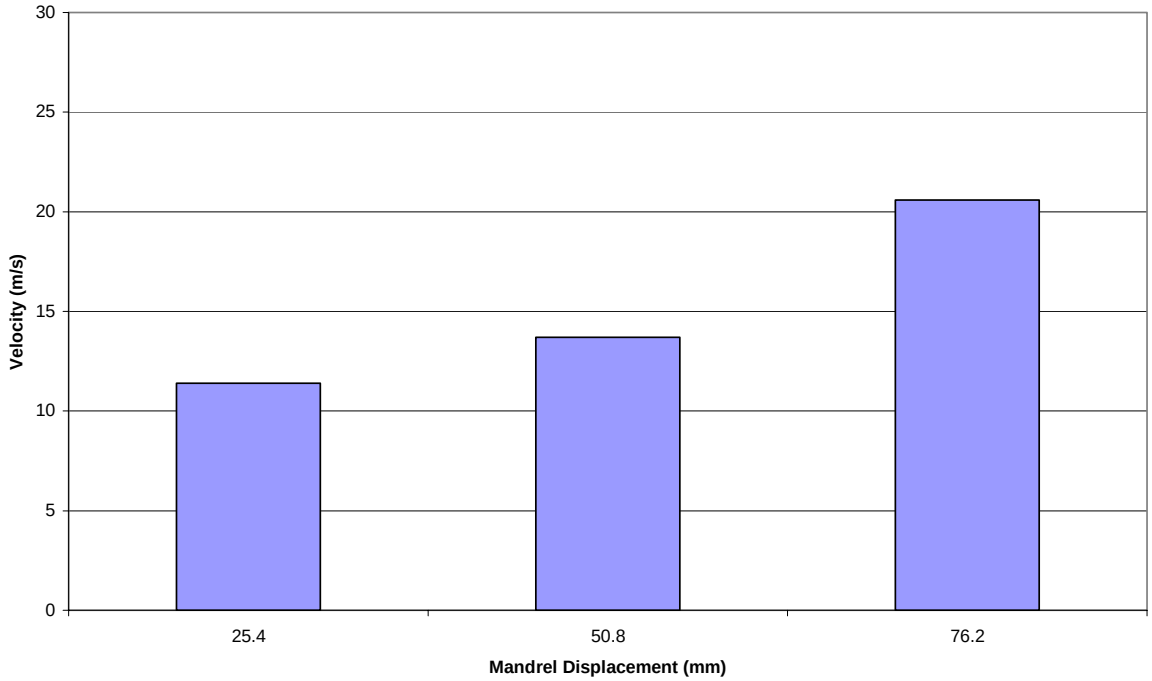

Figure 99. 9.53 mm Thick Deforming Plate with 50.8 mm Moment Arm Occupant Impact Velocity vs. Mandrel Displacement for 820 kg Mass

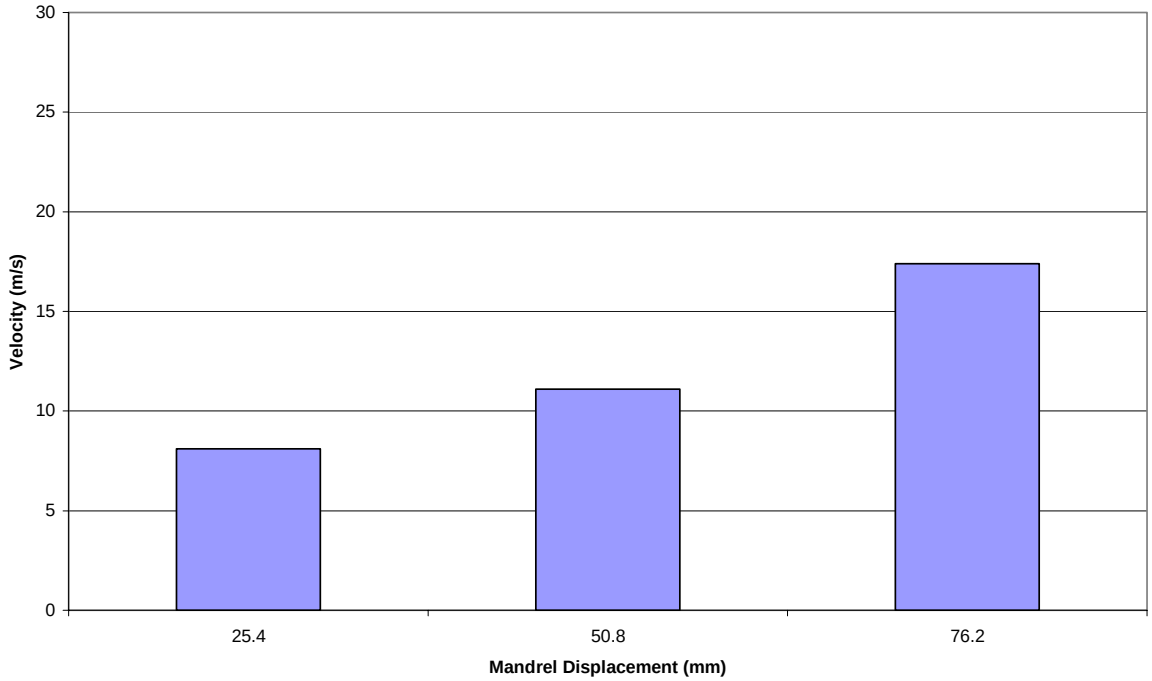

Figure 100. 9.53 mm Thick Deforming Plate with 76.2 mm Moment Arm Occupant Impact Velocity vs. Mandrel Displacement for 820 kg Mass

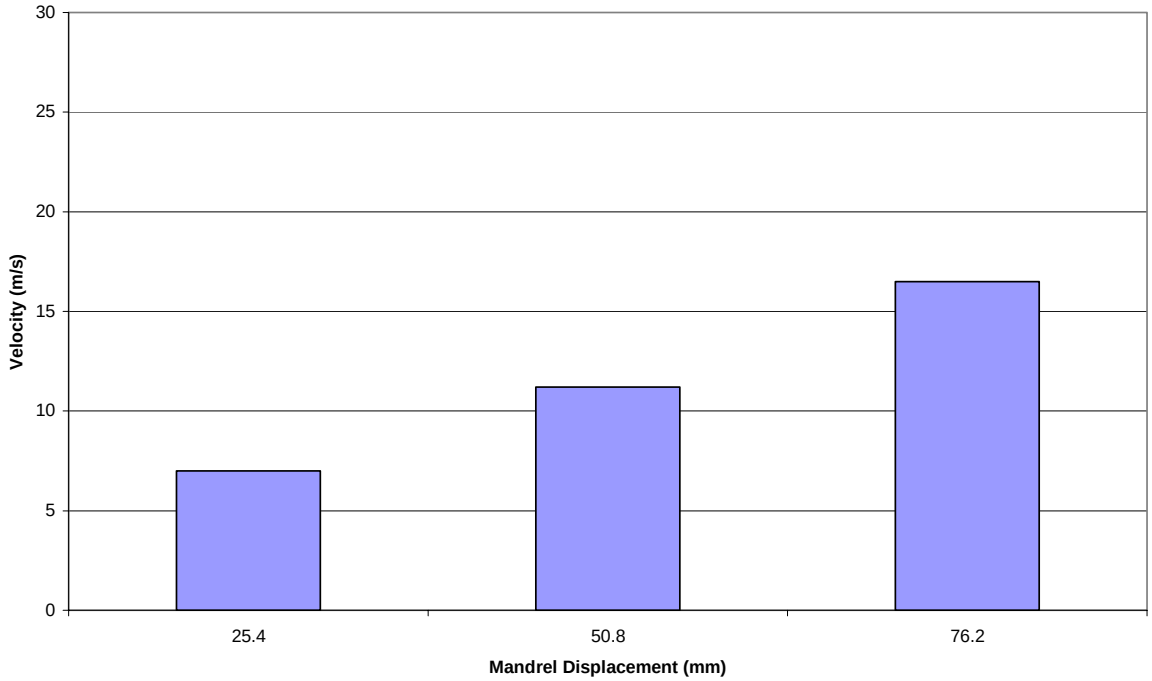

Figure 101. 9.53 mm Thick Deforming Plate with 101.6 mm Moment Arm Occupant Impact Velocity vs. Mandrel Displacement for 820 kg Mass

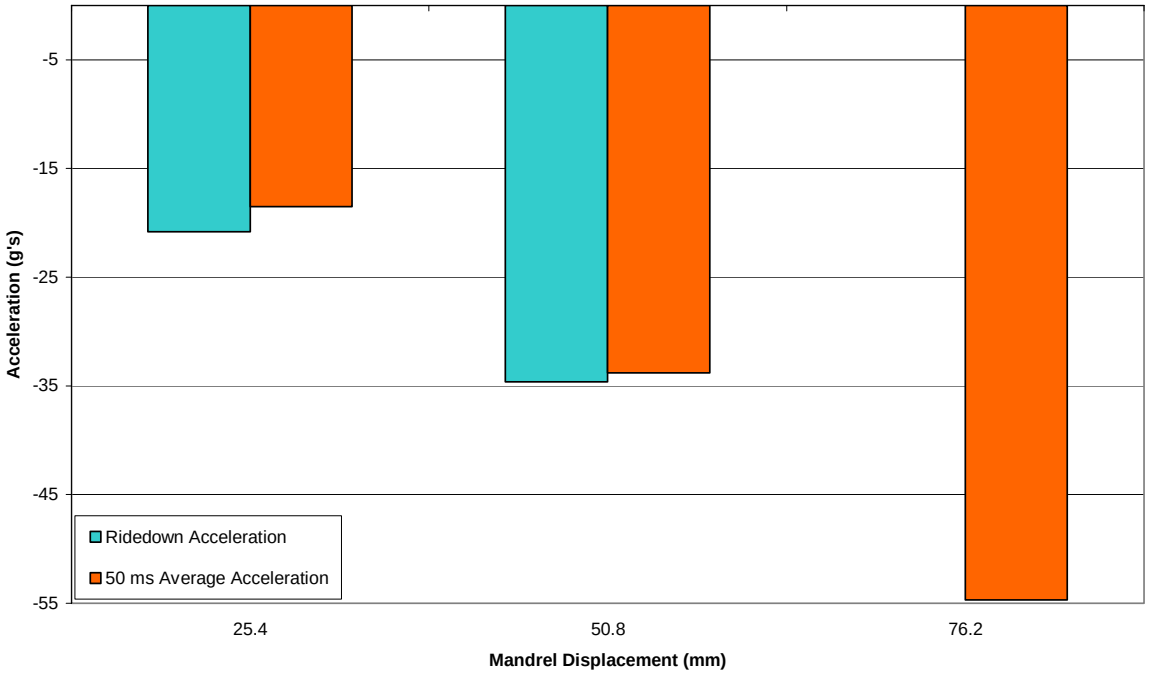

Figure 102. 12.7 mm Thick Deforming Plate with 50.8 mm Moment Arm Ridedown Acceleration and 50 Millisecond Average Acceleration vs. Mandrel Displacement for 820 kg Mass

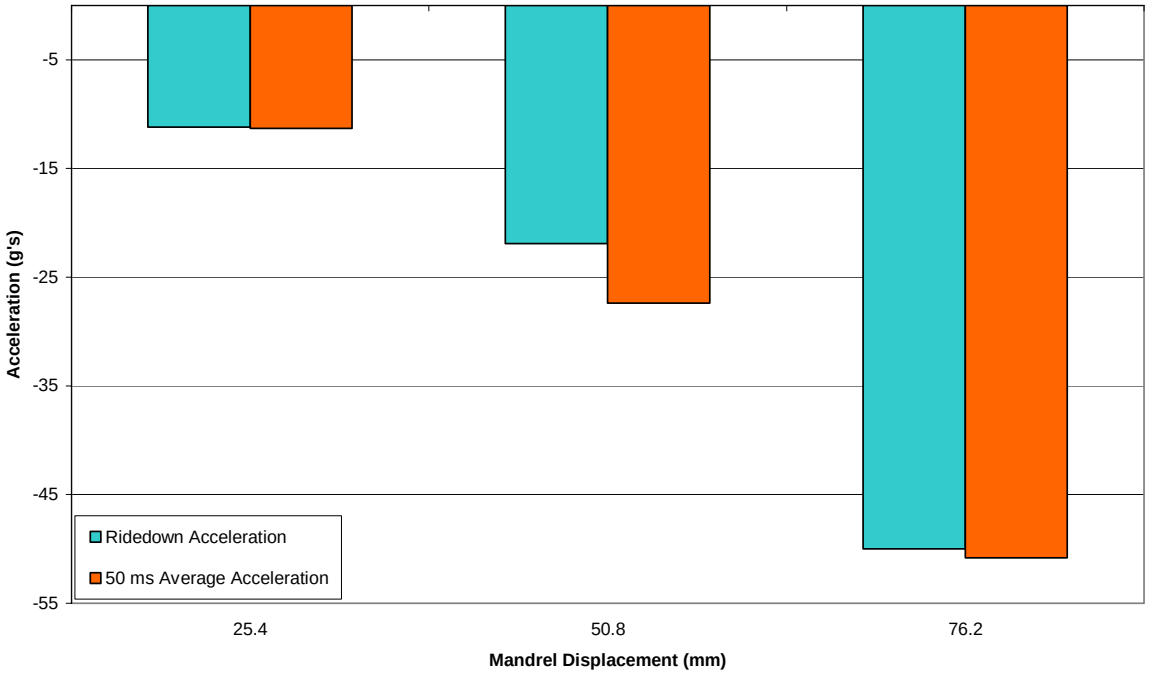

Figure 103. 12.7 mm Thick Deforming Plate with 76.2 mm Moment Arm Ridedown Acceleration and 50 Millisecond Average Acceleration vs. Mandrel Displacement for 820 kg Mass

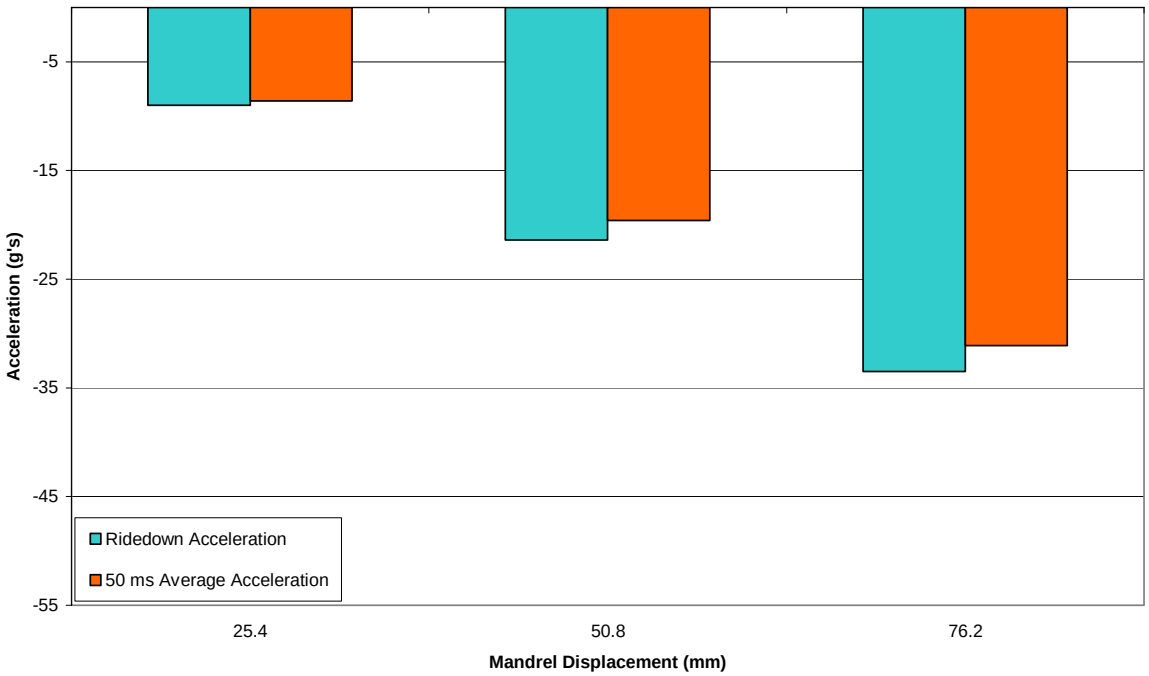

Figure 104. 12.7 mm Thick Deforming Plate with 101.6 mm Moment Arm Ridedown Acceleration and 50 Millisecond Average Acceleration vs. Mandrel Displacement for 820 kg Mass

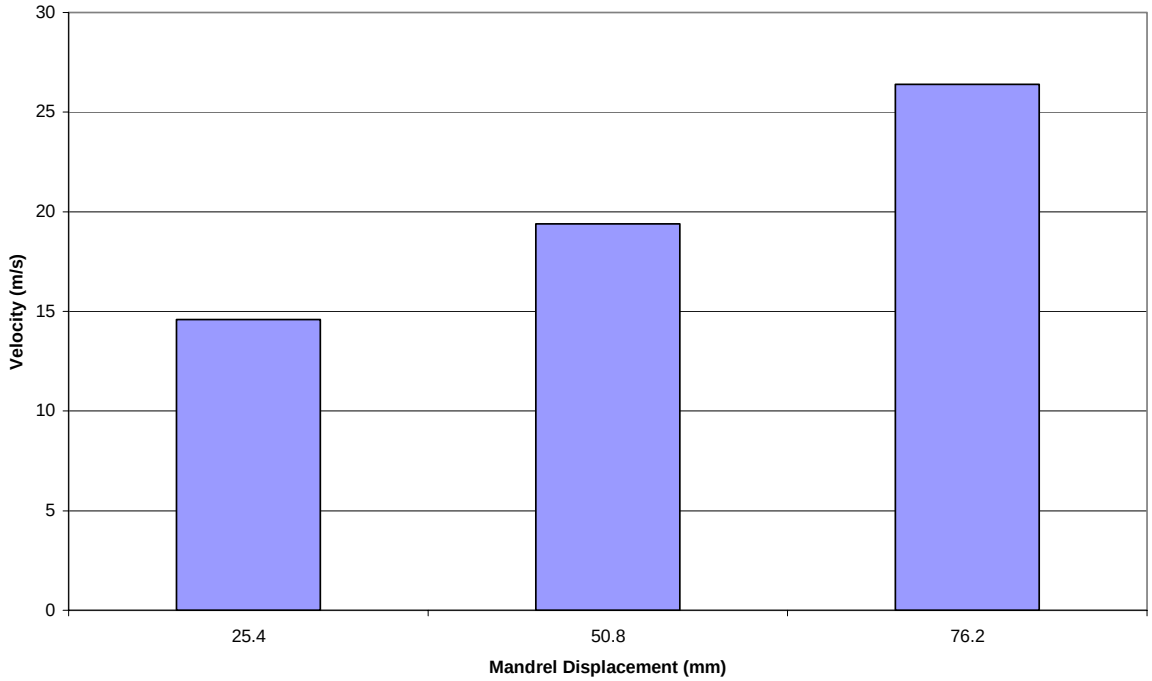

Figure 105. 12.7 mm Thick Deforming Plate with 50.8 mm Moment Arm Occupant Impact Velocity vs. Mandrel Displacement for 820 kg Mass

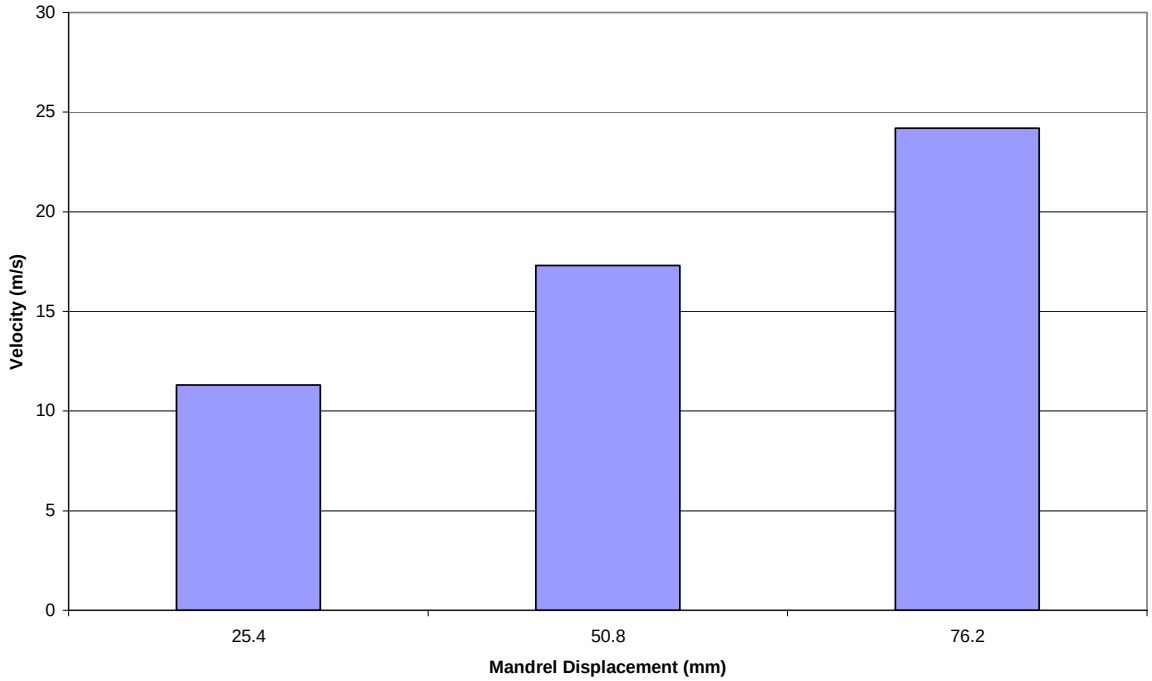

Figure 106. 12.7 mm Thick Deforming Plate with 76.2 mm Moment Arm Occupant Impact Velocity vs. Mandrel Displacement for 820 kg Mass

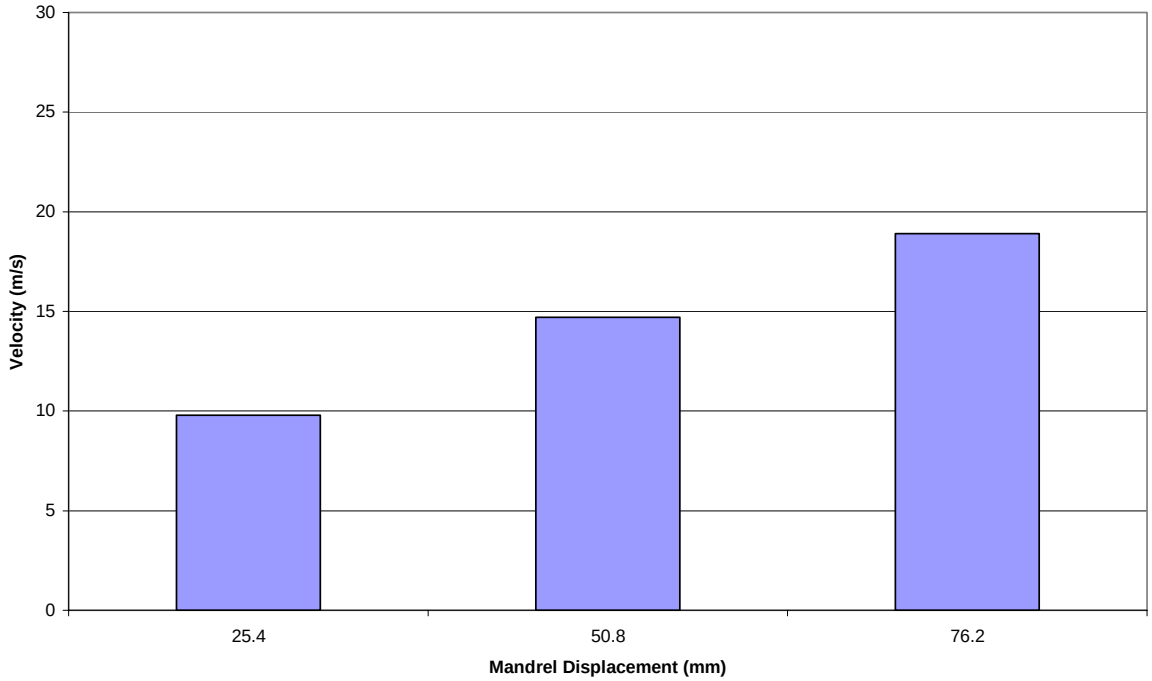

Figure 107. 12.7 mm Thick Deforming Plate with 101.6 mm Moment Arm Occupant Impact Velocity vs. Mandrel Displacement for 820 kg Mass

APPENDIX G

DEFORMING PLATE 2000 kg MASS SIMULATION RESULTS

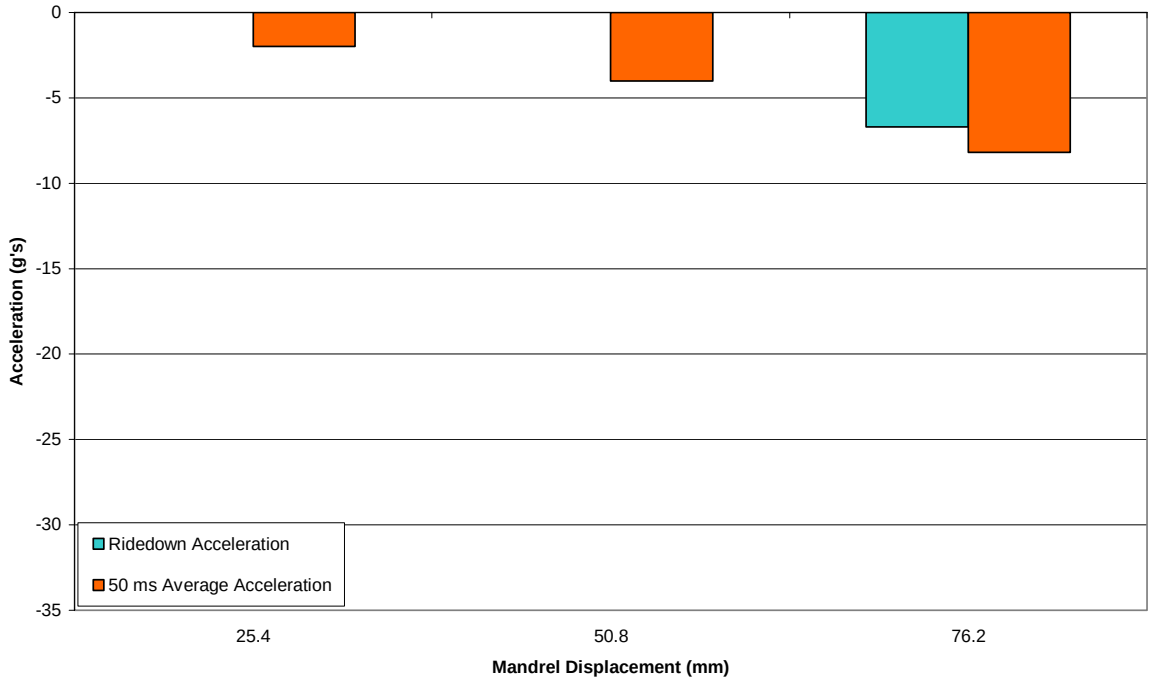

Figure 108. 6.35 mm Thick Deforming Plate with 50.8 mm Moment Arm Ridedown Acceleration and 50 Millisecond Average Acceleration vs. Mandrel Displacement for 2000 kg Mass

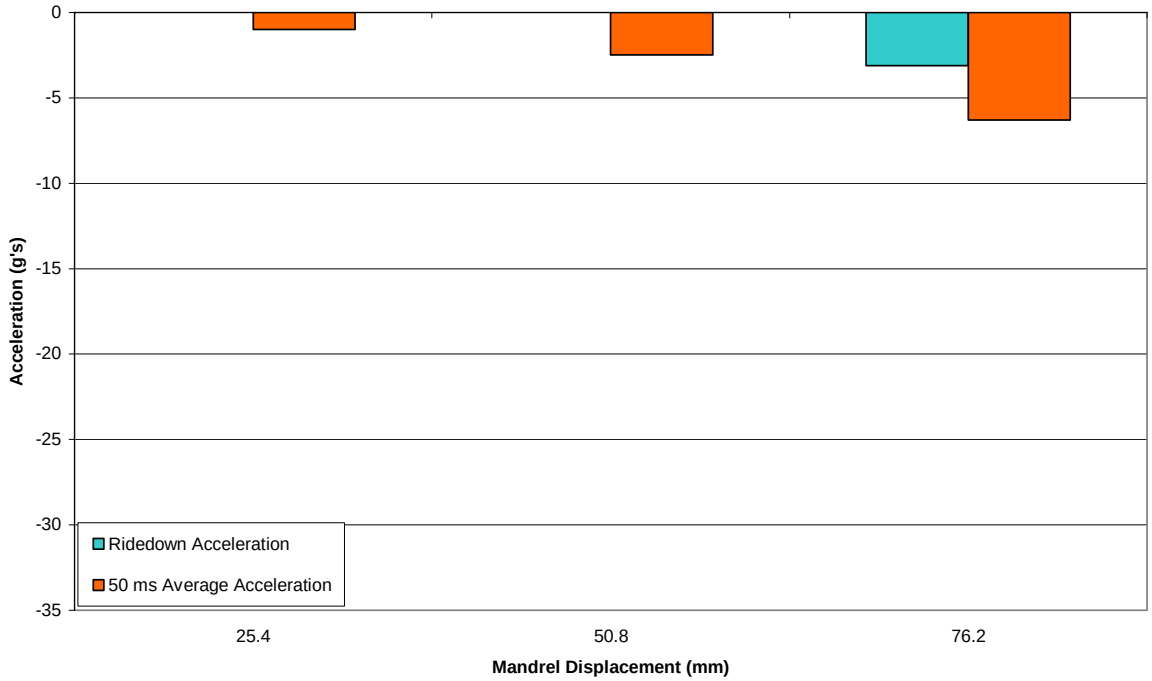

Figure 109. 6.35 mm Thick Deforming Plate with 76.2 mm Moment Arm Ridedown Acceleration and 50 Millisecond Average Acceleration vs. Mandrel Displacement for 2000 kg Mass

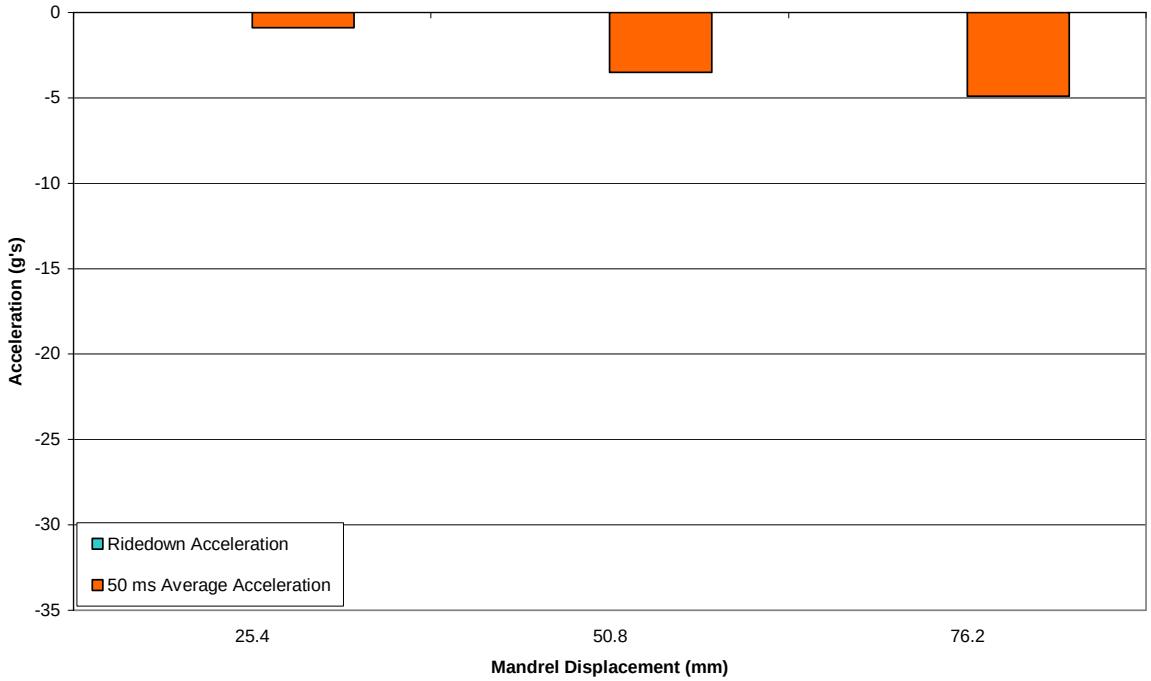

Figure 110. 6.35 mm Thick Deforming Plate with 101.6 mm Moment Arm Ridedown Acceleration and 50 Millisecond Average Acceleration vs. Mandrel Displacement for 2000 kg Mass

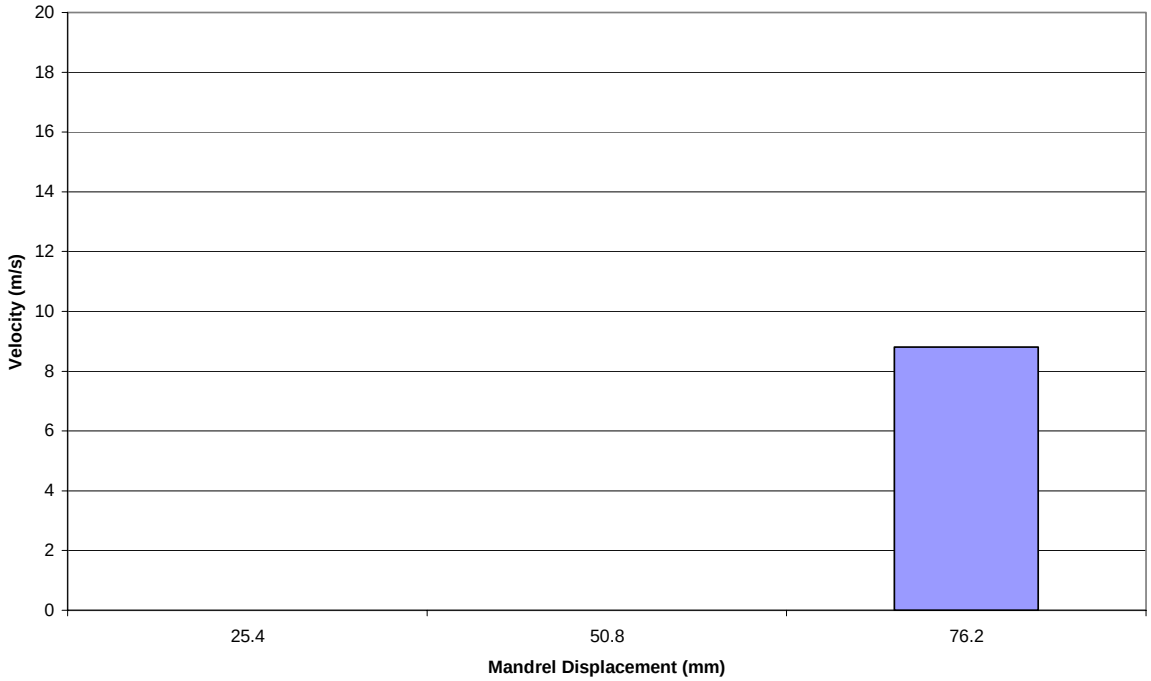

Figure 111. 6.35 mm Thick Deforming Plate with 50.8 mm Moment Arm Occupant Impact Velocity vs. Mandrel Displacement for 2000 kg Mass

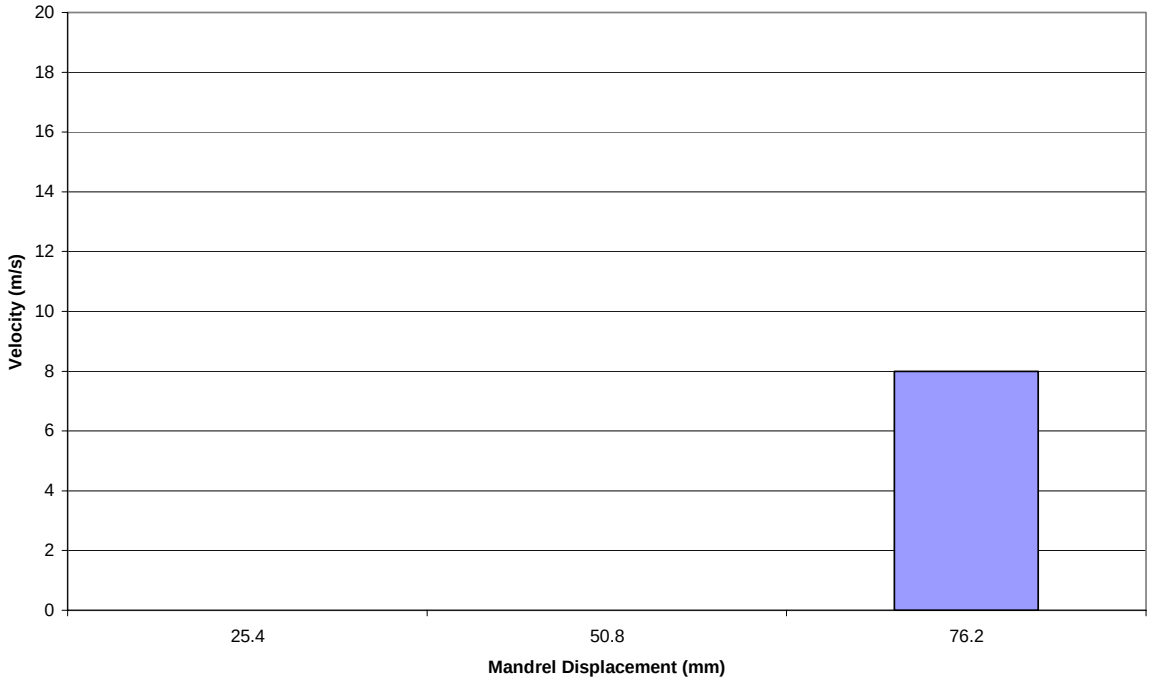

Figure 112. 6.35 mm Thick Deforming Plate with 76.2 mm Moment Arm Occupant Impact Velocity vs. Mandrel Displacement for 2000 kg Mass

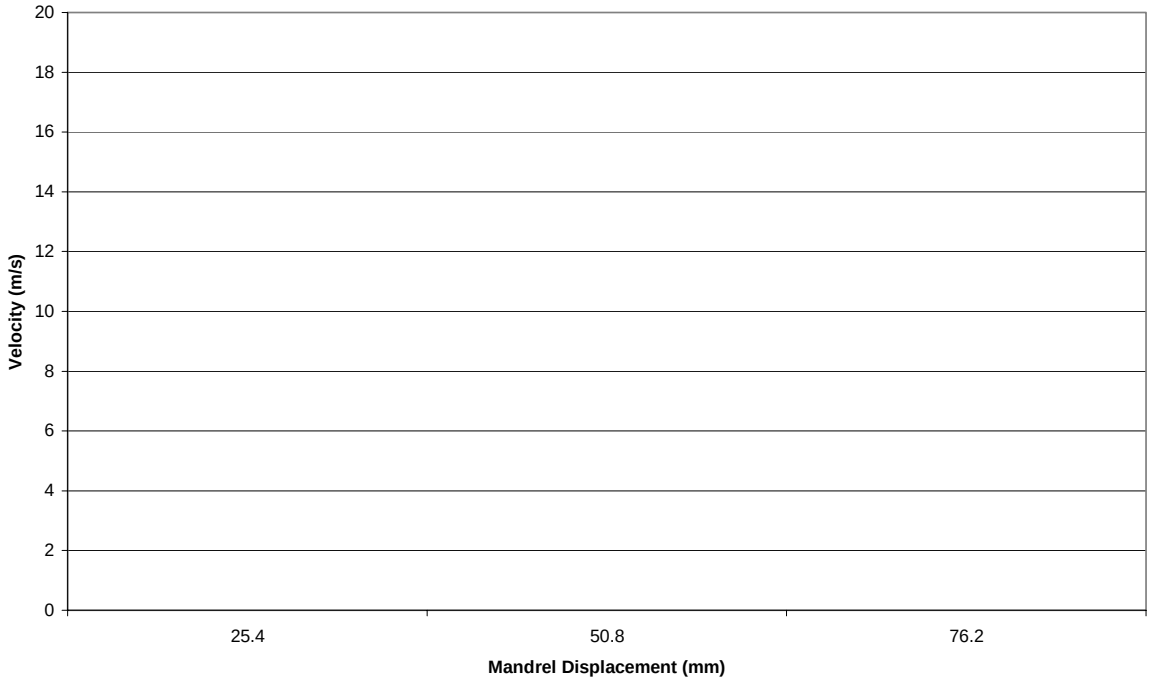

Figure 113. 6.35 mm Thick Deforming Plate with 101.6 mm Moment Arm Occupant Impact Velocity vs. Mandrel Displacement for 2000 kg Mass

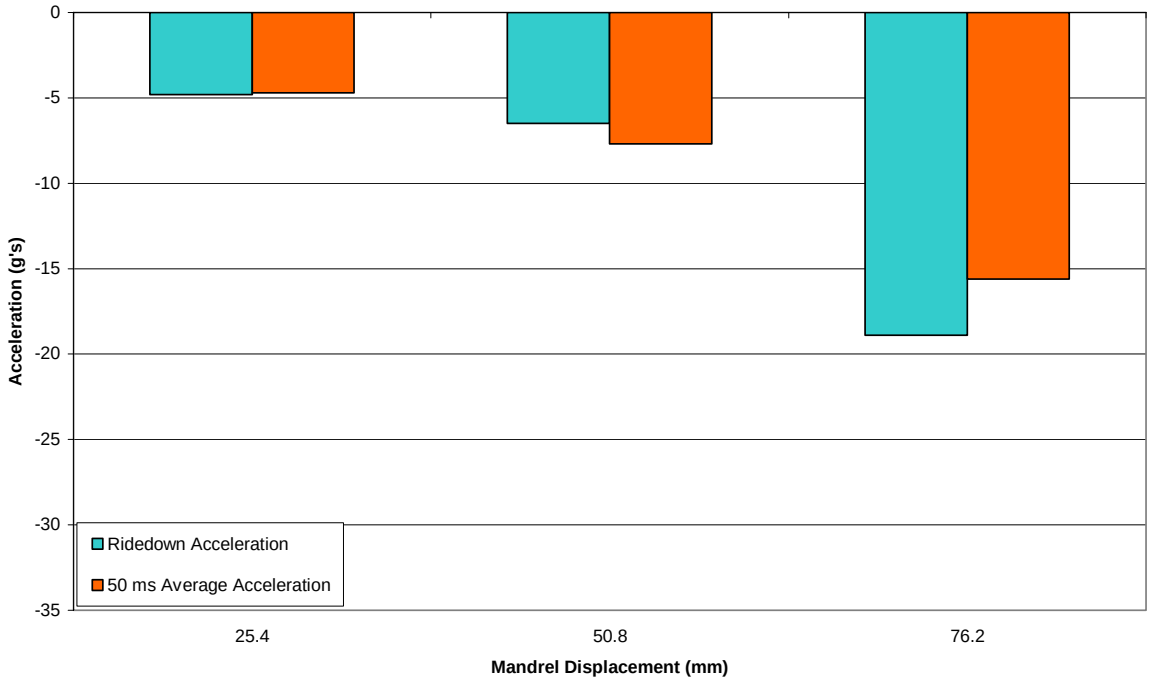

Figure 114. 9.53 mm Thick Deforming Plate with 50.8 mm Moment Arm Ridedown Acceleration and 50 Millisecond Average Acceleration vs. Mandrel Displacement for 2000 kg Mass

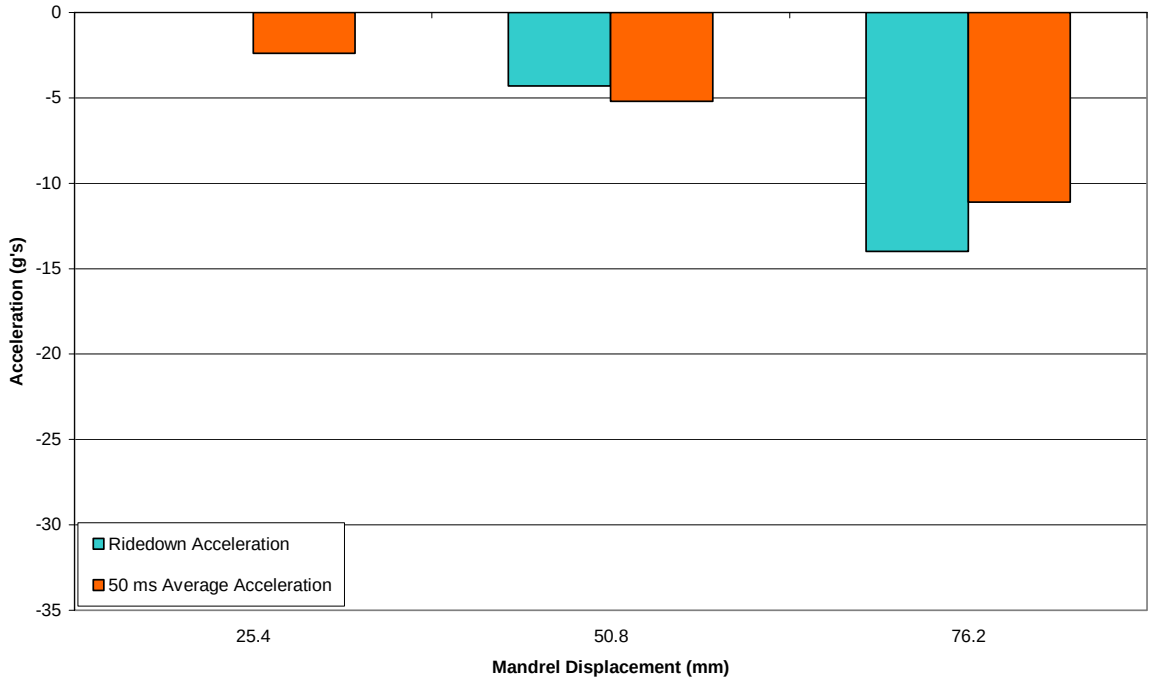

Figure 115. 9.53 mm Thick Deforming Plate with 76.2 mm Moment Arm Ridedown Acceleration and 50 Millisecond Average Acceleration vs. Mandrel Displacement for 2000 kg Mass

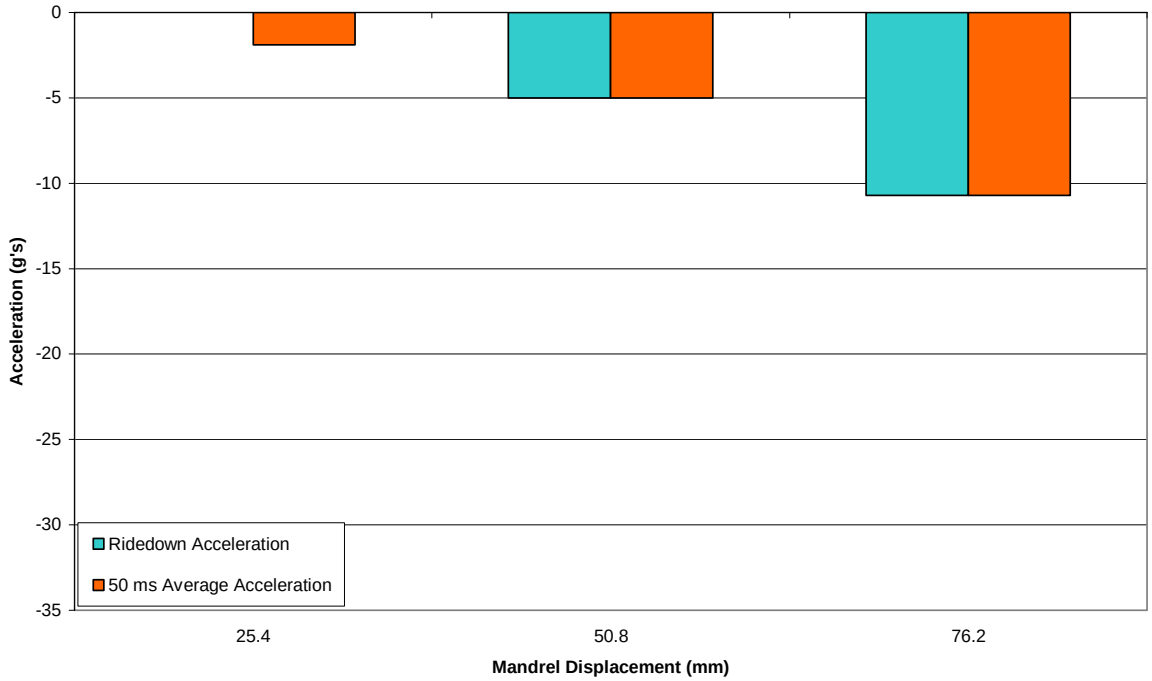

Figure 116. 9.53 mm Thick Deforming Plate with 101.6 mm Moment Arm Ridedown Acceleration and 50 Millisecond Average Acceleration vs. Mandrel Displacement for 2000 kg Mass

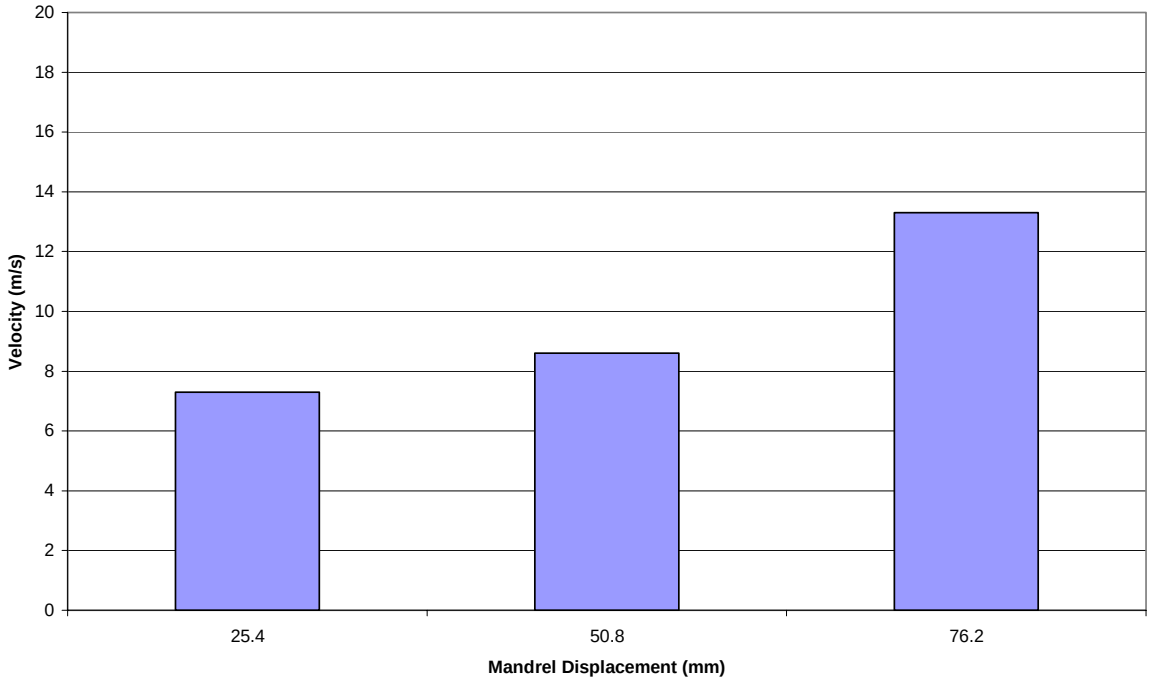

Figure 117. 9.53 mm Thick Deforming Plate with 50.8 mm Moment Arm Occupant Impact Velocity vs. Mandrel Displacement for 2000 kg Mass

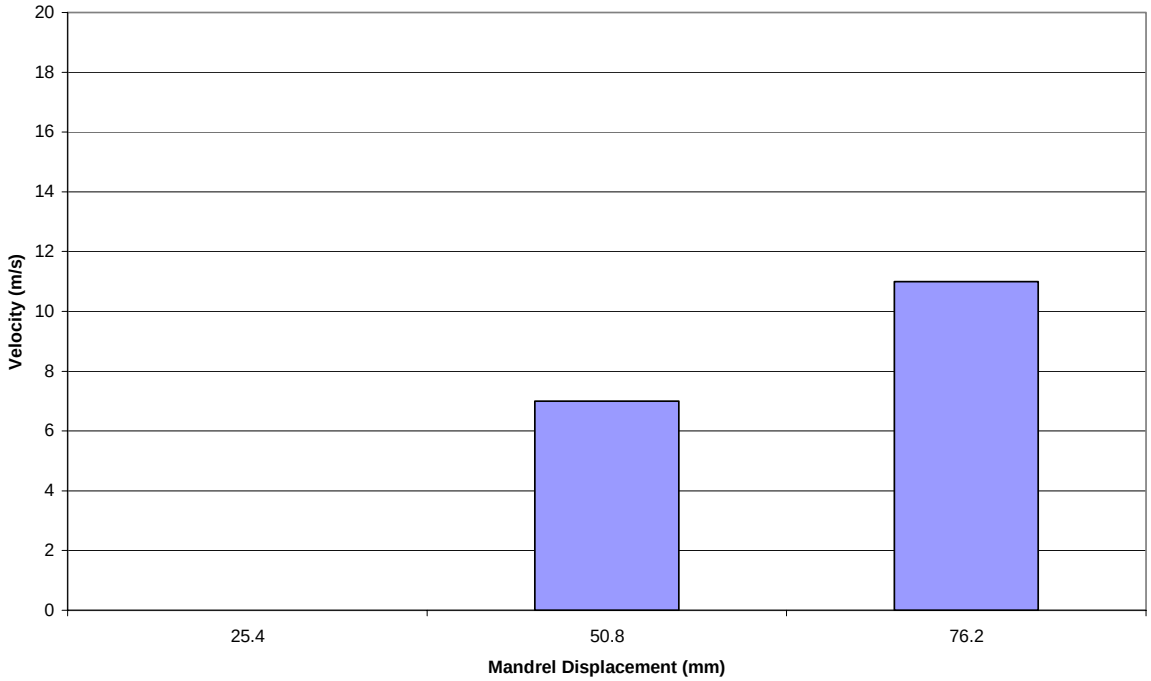

Figure 118. 9.53 mm Thick Deforming Plate with 76.2 mm Moment Arm Occupant Impact Velocity vs. Mandrel Displacement for 2000 kg Mass

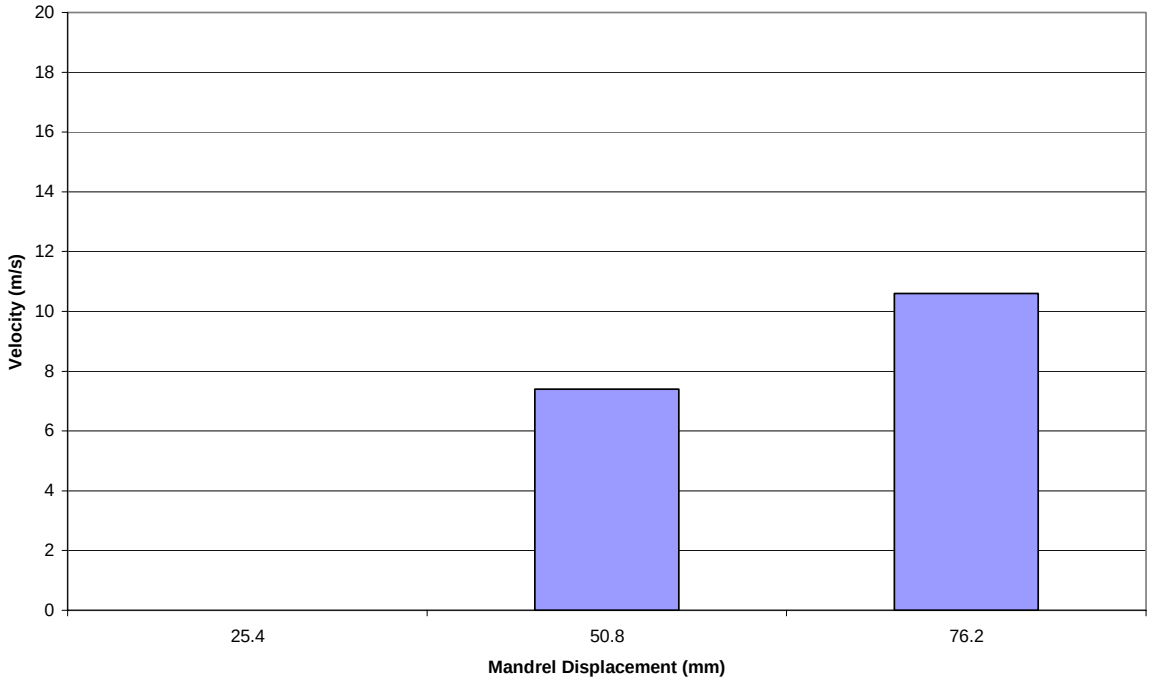

Figure 119. 9.53 mm Thick Deforming Plate with 101.6 mm Moment Arm Occupant Impact Velocity vs. Mandrel Displacement for 2000 kg Mass

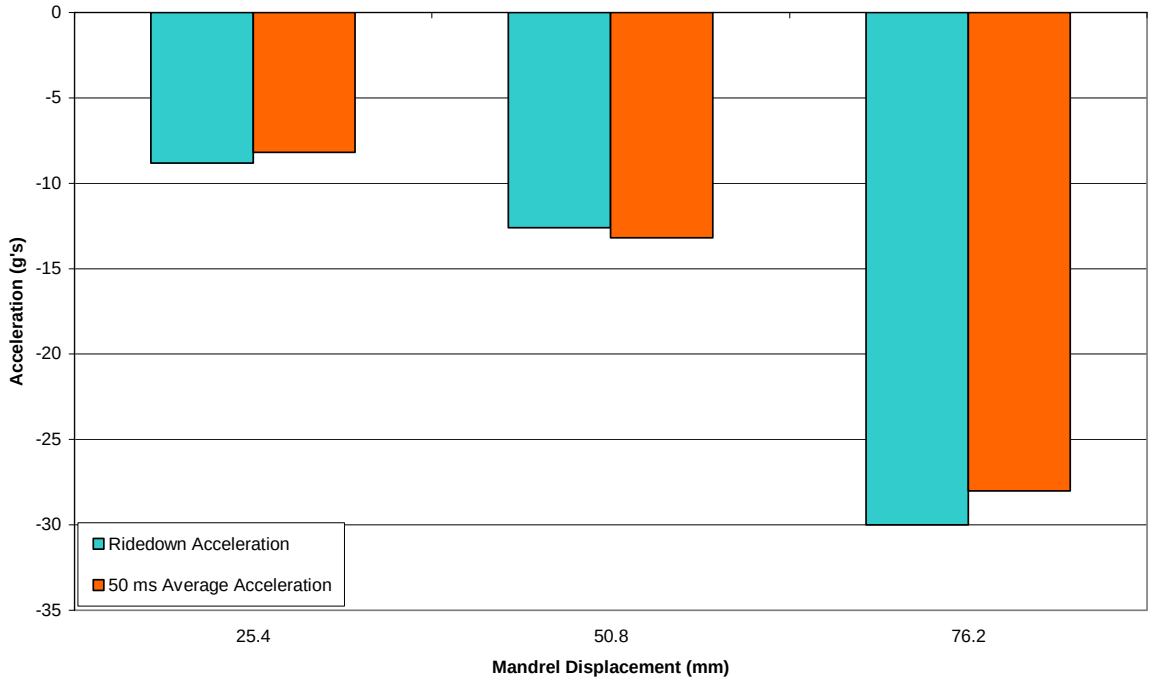

Figure 120. 12.7 mm Thick Deforming Plate with 50.8 mm Moment Arm Ridedown Acceleration and 50 Millisecond Average Acceleration vs. Mandrel Displacement for 2000 kg Mass

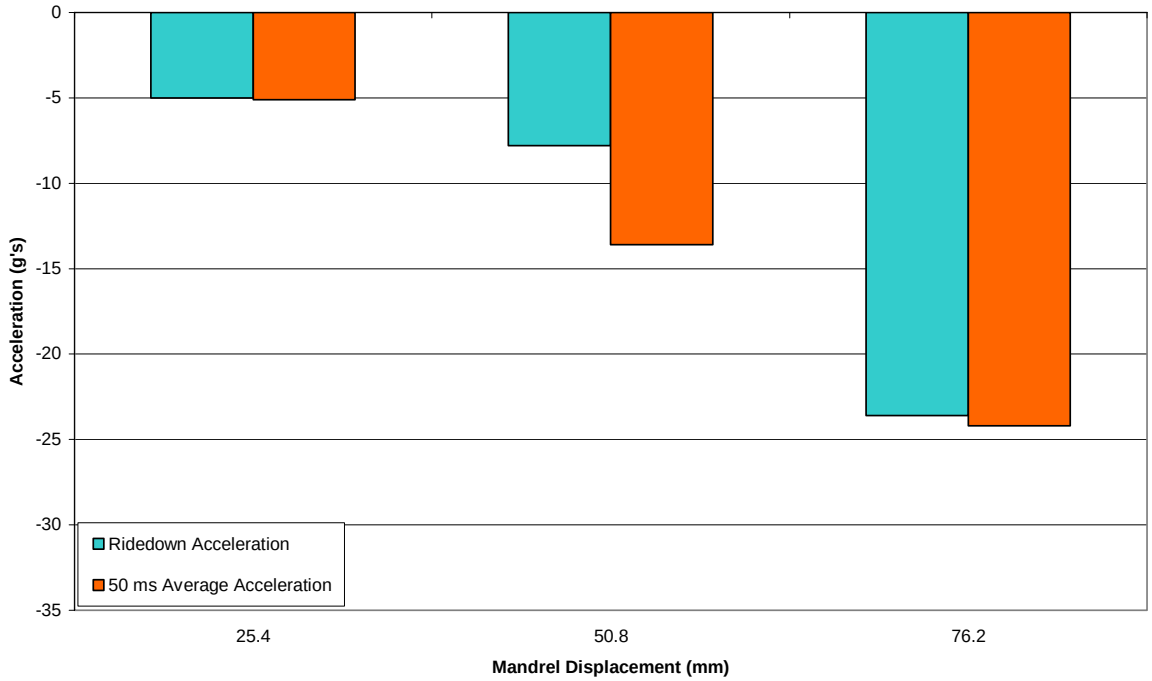

Figure 121. 12.7 mm Thick Deforming Plate with 76.2 mm Moment Arm Ridedown Acceleration and 50 Millisecond Average Acceleration vs. Mandrel Displacement for 2000 kg Mass

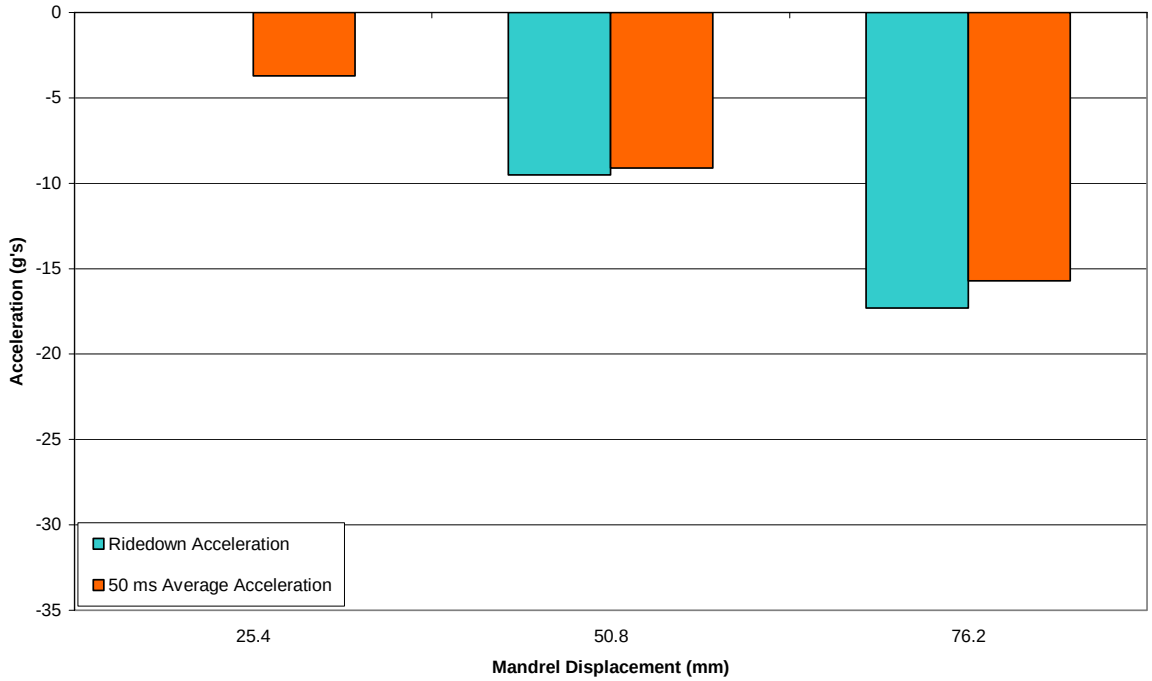

Figure 122. 12.7 mm Thick Deforming Plate with 101.6 mm Moment Arm Ridedown Acceleration and 50 Millisecond Average Acceleration vs. Mandrel Displacement for 2000 kg Mass

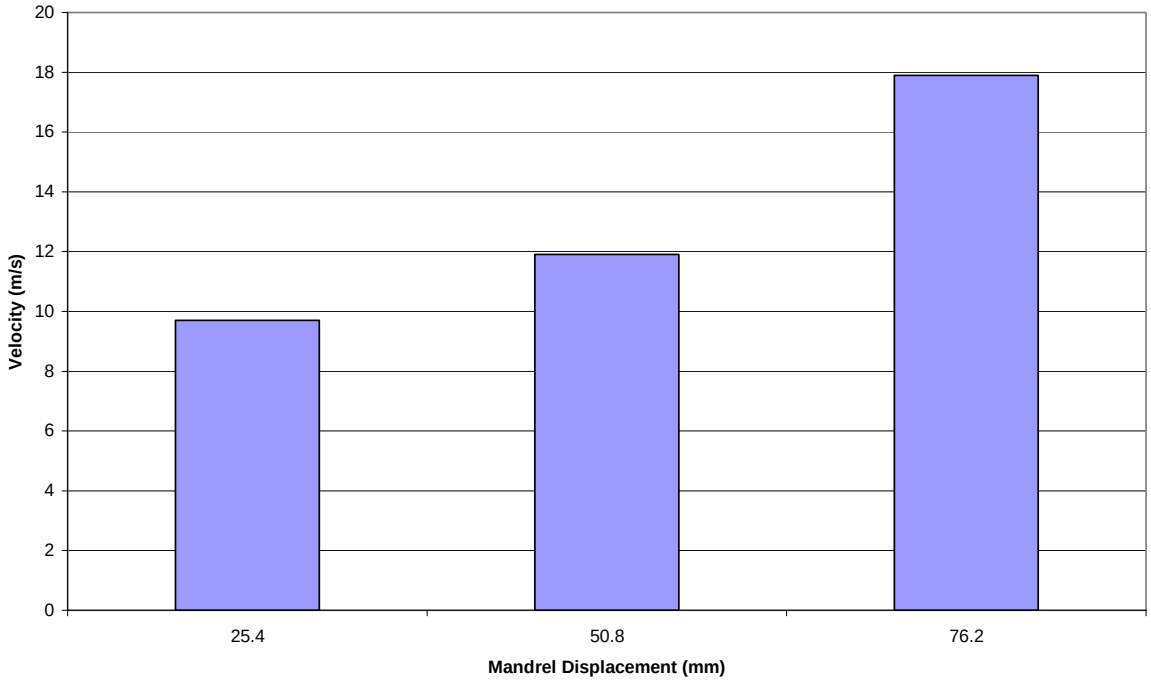

Figure 123. 12.7 mm Thick Deforming Plate with 50.8 mm Moment Arm Occupant Impact Velocity vs. Mandrel Displacement for 2000 kg Mass

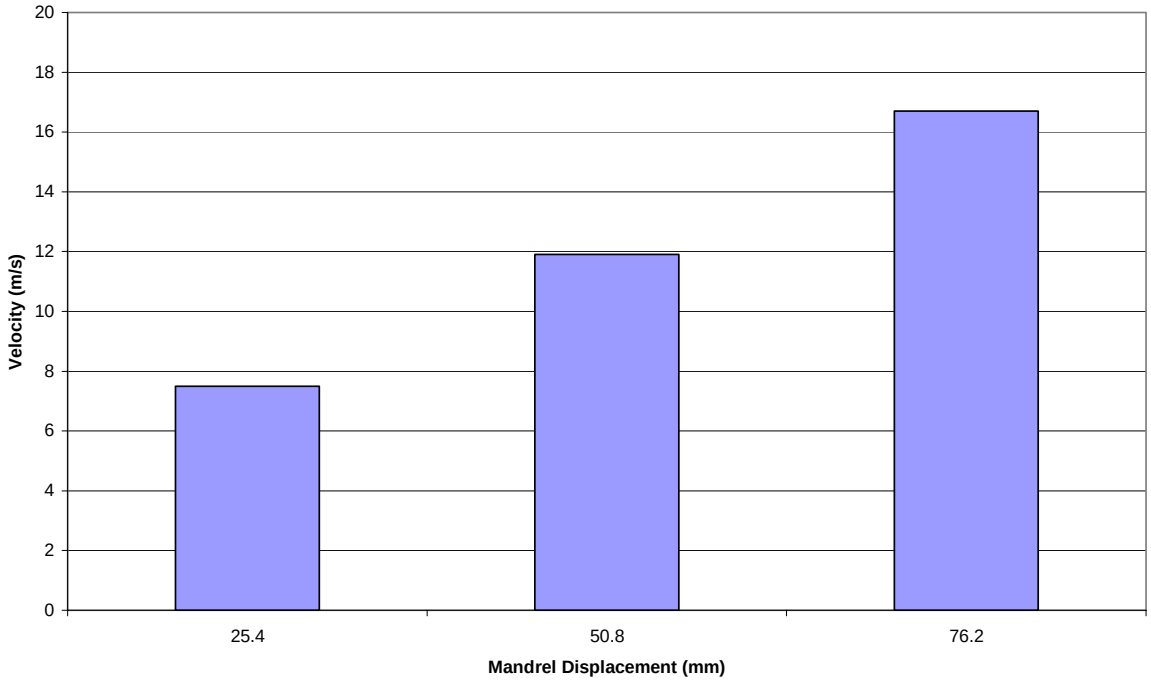

Figure 124. 12.7 mm Thick Deforming Plate with 76.2 mm Moment Arm Occupant Impact Velocity vs. Mandrel Displacement for 2000 kg Mass

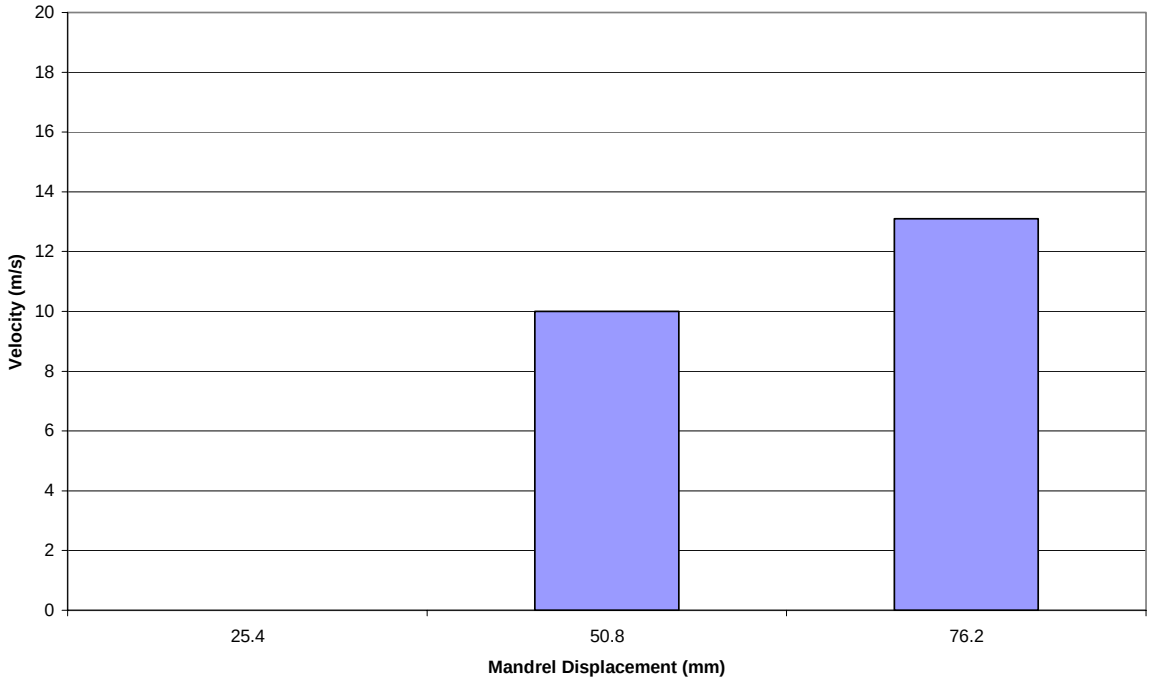

Figure 125. 12.7 mm Thick Deforming Plate with 101.6 mm Moment Arm Occupant Impact Velocity vs. Mandrel Displacement for 2000 kg Mass

VITA

Christopher Ryan Michalec
11112 Javalin Tr.
Helotes, TX 78023

Christopher Ryan Michalec received his B.S. degree in mechanical engineering from Texas A&M University in December 2003. Immediately after graduating, he began work at Texas A&M University towards a M.S. degree in mechanical engineering. He worked for Texas Transportation Institute through the duration of his undergraduate and graduate education. While employed with TTI, a majority of his time was spent as a draftsman developing construction drawings of current highway safety devices. Along with drafting, he participated in the design process, construction, and crash analysis of these safety devices. Upon completion of the M.S. degree, Mr. Michalec will be employed with Schlumberger in Rosharon, Texas. He will be designing mechanical components that aid in the oil extraction process.